USING THE δ^{18}O-SALINITY RELATIONSHIP TO IDENTIFY FRESHWATER INPUTS TO A NORTH ATLANTIC ESTUARY

by

Elizabeth Kerrigan

Submitted in partial fulfillment of the requirements
for the degree of Master of Science

at

Dalhousie University
Halifax, Nova Scotia
March 2015

To my family, my friends, and my love;

I am forever grateful for your support.

Thank you for following me down this long and winding road.

TABLE OF CONTENTS

List of Tables . . . . . **v**

List of Figures . . . . . **vii**

Abstract . . . . . **xi**

List of Abbreviations and Symbols Used . . . . . **xii**

Acknowledgements . . . . . **xiii**

Chapter 1 Introduction **1**

1.1 Motivation 1

1.2 Water Mass Analysis 2
1.2.1 Introduction to Stable Isotopes 2
1.2.2 Isotope Fractionation in Water 3
1.2.3 Tracing ^{18}O through the Hydrological Cycle 6
1.2.4 δ^{18}O-Salinity Relationship 8

1.3 Oceanographic Setting of Halifax Harbour and its Approaches 10
1.3.1 Halifax Harbour 10
1.3.2 Scotian Shelf 19

1.4 Objectives 21

Chapter 2 Methods **23**

2.1 Field Sites 23
2.1.1 Halifax Harbour 23
2.1.2 Scotian Shelf 25

2.2 Halifax Harbour Water Sampling 26
2.2.1 Bedford Basin 26
2.2.2 Sackville River 27
2.2.3 Halifax Harbour 27
2.2.4 Northwest Arm 27
2.2.5 Wastewater 28
2.2.6 Sampling Uncertainty 28

2.3 Offshore Water Sampling 31
2.3.1 Glider and Station 2 31
2.3.2 Atlantic Zone Monitoring Program (AZMP) Stations 31

2.4 Precipitation Sampling . . . 31
2.4.1 Rainfall Sampling . . . 31
2.4.2 Snow Sampling . . . 38
2.4.3 Amount Weighting of Precipitation . . . 40

2.5 δ^{18}O and δ^{2}H Measurements . . . 41
2.5.1 Cavity Ring-Down Spectroscopy . . . 42
2.5.2 Analyzing Water Samples . . . 46
2.5.3 Defining Working Standards . . . 48
2.5.4 Calibrating Sample Run Measurements . . . 50
2.5.5 Memory Effect . . . 52
2.5.6 Drift Effect . . . 55

2.6 Salinity Measurements . . . 56

Chapter 3 Sources & Variability . . . 58

3.1 Freshwater Inputs . . . 58
3.1.1 Precipitation . . . 58
3.1.2 Sackville River . . . 69
3.1.3 Wastewater . . . 72
3.1.4 Defining Freshwater End Members . . . 74

3.2 Offshore Inputs . . . 77
3.2.1 Scotian Shelf . . . 77
3.2.2 Defining an Offshore End Member . . . 82

Chapter 4 Mass Balance . . . 89

4.1 Mass Balance with Potential Offshore End Members . . . 90
4.1.1 Error Associated with Offshore End Member Selection . . . 90
4.1.2 Selection of the Offshore End Member . . . 94

4.2 Mass Balance in Bedford Basin . . . 101
4.2.1 Surface Water . . . 104
4.2.2 Deep Water . . . 117

Chapter 5 Conclusions . . . 133

Bibliography . . . 136

LIST OF TABLES

1.1	Meteoric Water Line of Truro, NS (*Fritz et al.*, 1987)	7
1.2	Fluvial and effluent discharges in Halifax Harbour (*Buckley and Winters*, 1992)	13
1.3	Scotian Shelf End Members proposed by *Khatiwala et al.* (1999)	20
2.1	Halifax Harbour sampling locations	24
2.2	GPS coordinate replacement for HL-3	26
2.3	"Intake Line" vs. "Grab" samples for the Northwest Arm	28
2.4	δ^{18}O/δ^{2}H variability of 4 L (1 & 60 m) Bedford Basin water samples	29
2.5	Samples collected in Niskin vs. collection bottles	30
2.6	Evaporation test results for 60 and 250 ml water samples	34
2.7	Calculated δ^{18}O/δ^{2}H enrichment in samples after 72 hours	37
2.8	Variability in δ^{18}O/δ^{2}H during a snowfall event	39
2.9	IAEA Reference Materials	48
2.10	δ^{18}O of Working Standards using IAEA Reference Materials	50
2.11	Working Standard reference values for this study	51
2.12	Memory effect of the Picarro L2301-i water isotope analyzer	54
2.13	Memory coefficients before and after vapourizer cleaning	55
2.14	Precision and drift tests for the Picarro L2301-i water isotope analyzer	56
3.1	δ^{18}O of single rainfall events over two days	60
3.2	P values for groupings of average yearly δ^{18}O of precipitation	64
3.3	Amount-weighted monthly averages in δ^{18}O of precipitation	67
3.4	P values for δ^{18}O of precipitation for a month over two sample years	68
3.5	Monthly variability in δ^{18}O of Sackville River surface samples	70
3.6	δ^{18}O of wastewater outfalls and Sackville River on April 3, 2014	72
3.7	Halifax Harbour freshwater and potential offshore end members	88

4.1 Percentage of negative mass fraction results calculated using different offshore end members 95

4.2 Final Bedford Basin end members for this study 100

LIST OF FIGURES

1.1 Global Meteoric Water Line (*Craig*, 1961) 7

1.2 Isotopic fractionation of δ^{18}O and δ^{2}H in the hydrological cycle . . 8

1.3 Schematic of δ^{18}O-S relationship with potential end members . . . 9

1.4 Geographic divisions of Halifax Harbour (*Fader and Miller*, 2008) 11

1.5 Water and wastewater services around the HRM (*Halifax Water*, 2012) 14

1.6 Sackville River water level and daily precipitation over a year . . . 15

1.7 Horizontal circulation of water in Halifax Harbour (*Huntsman*, 1924; *Shan et al.*, 2011) 17

1.8 Schematic of water circulation in Halifax Harbour (*Fader and Miller*, 2008) 18

1.9 Movement of water masses along the Scotian Shelf 19

1.10 δ^{18}O-S relationship in the Scotian Slope & Labrador Sea (*Fairbanks*, 1982) 21

2.1 Halifax Harbour sampling locations 23

2.2 Halifax Line AZMP sample sites in Oct 2008 & Apr 2009 25

2.3 Precipitation collection bottle used in this study 32

2.4 Change in the residual fraction of water with time, due to evaporation 35

2.5 Change in δ^{18}O and δ^{2}H due to evaporation 36

2.6 Calculated vs. averaged amount-weighted monthly δ^{18}O of precipitation 41

2.7 Picarro L2301-i WS-CRDS isotopic water analyzer 42

2.8 Schematic of cavity ring-down spectroscopy in the Picarro L2301-i isotopic water analyzer 43

2.9 Differences in average δ^{18}O of saltwater calculated in different labs (*Walker et al.*, in prep.) 45

2.10 Flow chart outlining the Picarro L2301-i isotopic liquid analyzer calibration 47

2.11 Calibration of IAEA Reference Materials GISP and VSMOW2 . . 49

2.12 Measured δ^{18}O compared with δ^{18}O reference values of Working Standards 51

3.1 Variability in δ^{18}O with amount of rainfall 59

3.2 Variability in δ^{18}O of precipitation with surface air temperature and time 61

3.3 Yearly fluctuation in δ^{18}O of precipitation 62

3.4 Variability in δ^{18}O with type of precipitation collected between the first and last snowfall of winter/spring 2013 63

3.5 Annual variability in δ^{18}O of precipitation 64

3.6 Yearly amount-weighted averages for δ^{18}O of precipitation with different yearly combinations 65

3.7 Year-to-year variability in monthly amount-weighted δ^{18}O averages 67

3.8 Amount-weighted monthly δ^{18}O of precipitation 68

3.9 Change in δ^{18}O of Sackville River surface water with time and water level 69

3.10 Monthly change in δ^{18}O of Sackville River over a year 71

3.11 Water and wastewater service districts in Halifax, adapted from *Halifax Water* (2012) 73

3.12 Yearly change in δ^{18}O of Sackville River (May 2012 - Apr 2014) and precipitation (July 2012 - June 2013) 74

3.13 Average amount-weighted δ^{18}O of summer end member groupings 77

3.14 Halifax Line AZMP δ^{18}O, salinity, and temperature data measured in October 2008 and April 2009 79

3.15 Temperature-Salinity plots with depth for Halifax Line samples . . 81

3.16 δ^{18}O-S relationship for Halifax Line samples 82

3.17 Halifax Line AZMP δ^{18}O and salinity data (Oct 2008 & Apr 2009) with added Halifax Harbour samples (Oct 2012 & Apr 2013) . . . 83

3.18 δ^{18}O-S relationship for Halifax Line samples (Apr & Sept 2008) (*Shadwick and Thomas*, 2011) 84

3.19 δ^{18}O-S relationship for Halifax Line samples (Oct 2008 & Apr 2009) and Halifax Harbour samples (Oct 2012 & Apr 2013) 84

3.20 δ^{18}O-S relationship for Halifax Line samples (Oct 2008 & Apr 2009) 86

3.21 Bedford Basin end members 87

4.1 Average mass fractions for Bedford Basin (1 & 60 m) samples (June 2012 - Oct 2013) using five offshore end members 91

4.2 Average mass fractions for Bedford Basin (1 & 60 m) samples in summer 2012, winter 2012/2013, and summer 2013 using three offshore end members 93

4.3 Schematic of a potential mass balance relationship 96

4.4 Bedford Basin samples against five δ^{18}O-S mixing triangles 97

4.5 Bedford Basin samples with mixing triangles and end members . . 98

4.6 Intersect of Halifax Line (Oct 2008 & Apr 2009) and Halifax Harbour samples and its fit as an end member 99

4.7 δ^{18}O-Salinity plots for Bedford Basin (1, 5, 10, & 60 m) 102

4.8 Vertical salinity profiles in Bedford Basin 103

4.9 Vertical salinity profiles for the fall of 2012 in Bedford Basin . . . 104

4.10 Bedford Basin 1 m mass fraction results for the total averaged and seasonal groupings of samples 105

4.11 δ^{18}O-S relationship for Bedford Basin samples (1 m), with BB end members included 107

4.12 δ^{18}O-S relationship for Bedford Basin 1 m data with BB end members, grouped seasonally 108

4.13 δ^{18}O-S relationship for Bedford Basin samples (1 m) in summer "2012" and "2013" 109

4.14 Zero-Salinity intercept calculated for seasonal groupings of δ^{18}O-S in Bedford Basin 1 m 110

4.15 (a) Mixing triangle for Bedford Basin 1 m samples, and (b) vertical salinity profiles in August and September of 2012 113

4.16 The ratio of observed δ^{18}O and δ^{18}O normalized to salinity, using the δ^{18}O-S relationship of Bedford Basin 1 m water 115

4.17 Monthly and seasonally grouped box-plot results for δ^{18}O normalized to salinity, using δ^{18}O-S of Bedford Basin surface waters . . . 116

4.18 Circulation schematic of water flow in Bedford Basin (1 & 60 m) . 118

4.19 Bedford Basin 60 m mass fraction results for the total averaged, and seasonal groupings of samples 119

4.20 δ^{18}O-S relationship for Bedford Basin (60 m) samples, with BB end members included 120

4.21 δ^{18}O-S relationship for Bedford Basin (60 m) samples with BB end members, grouped seasonally 122

4.22 Mixing triangle for Bedford Basin (60 m) samples 123

4.23 Change in δ^{18}O and salinity with time in Bedford Basin (1 & 60 m) 126

4.24 Ratio of observed δ^{18}O and δ^{18}O normalized to salinity, using the δ^{18}O-S relationship of Bedford Basin 60 m water 127

4.25 Bedford Basin (60 m) total averaged mass fraction results using Scotian Shelf end members (LShW, WSW, & SLEW) 128

4.26 Bedford Basin (60 m) δ^{18}O-S relationship and the fit of these samples to BB and SS mixing triangles 129

4.27 Scotian Shelf and Bedford Basin mixing triangles grouped into three categories to look at Bedford Basin (60 m) samples 130

ABSTRACT

The δ^{18}O-Salinity relationship allows us to define distinct end members in Bedford Basin, a system supplied by the North Atlantic Ocean. An isotopic analysis was performed on water in and around Bedford Basin to resolve contributions of offshore water, river water, and precipitation throughout the year. All freshwater inputs were found to co-vary when an annual cycle was defined, however there is a significant seasonal difference between the δ^{18}O of winter and summer freshwater inputs, leading to their selection as end members. Bedford Basin surface (1 m) samples confirm a dominant input of offshore water ($\sim$88%) and minimal freshwater input, dominated by "summer" precipitation, while deep samples (60 m) show even less freshwater from land ($<$3%). At 60 m, the zero-salinity intercept of the δ^{18}O-S relationship suggests that offshore freshwater dominates stable bottom waters (-15.55‰), and only bottom waters mixed with Bedford Basin surface water show freshwater from land (-7‰).

LIST OF ABBREVIATIONS AND SYMBOLS USED

Abbreviation	Description
AZMP	Atlantic Zone Monitoring Program
BBMP	Bedford Basin Monitoring Program
BIO	Bedford Institute of Oceanography
CCGS	Canadian Coast Guard Ship
CRDS	Cavity Ring-Down Spectroscopy
GISP	Greenland Ice Sheet Precipitation
GMWL	Global Mean Water Line
HL	Halifax Line
HRM	Halifax Regional Municipality
IAEA	International Atomic Energy Agency
IRMS	Isotope Ratio Mass Spectrometry
LSW	Labrador Slope Water
LShW	Labrador Shelf Water
OTN	Ocean Tracking Network
SLEW	St. Lawrence Estuary Water
SLRW	St. Lawrence River Water
WSW	Warm Slope Water
WWTF	Wastewater Treatment Facility
VSMOW2	Vienna Standard Mean Ocean Water 2

Symbol	Description	Units
T	Temperature	°C
δ	isotope ratio	‰
S	Salinity	psu
δ^{18}O	change in ratio of oxygen isotopes (^{18}O :^{16}O), relative to a standard	‰
δ^{2}H	change in ratio of hydrogen isotopes (^{2}H :^{1}H), relative to a standard	‰

ACKNOWLEDGEMENTS

First and foremost I would like to thank my two supervisors, Markus Kienast and Doug Wallace, for invaluable advice, guidance, and support throughout this project and my time at Dalhousie. In addition, I would like to thank John Cullen for all the guidance and advice, and Dan Kelley for coding, statistical, and equation help (in addition to more I'm sure!). Your counsel was greatly appreciated throughout this process.

I would like to thank Claire Normandeau, who helped me with everything lab-related. Thank you for collecting samples, teaching me how to use the instrument, setting up standards, analyzing data, cleaning the instrument, etc. I would not have much of a project if it were not for your support. In addition, thanks to Emily Chua and Robert Sanderson for helping me with lab work, running samples, and collecting rainwater. Thank you to Sally Walker for wonderful advice and guidance on mass balance and mixing - your expertise and knowledge has been incredibly helpful.

I would like to thank Adam Comeau, Richard Davis, Jon Pye, Christena MacDonald, and countless wonderful co-op students for all of your help with sample collection in Halifax Harbour, collecting water samples on nice, not-so-nice, and terrible days. In addition, thank you to all of the sea-going staff at the Bedford Institute of Oceanography (BIO) for sample collection and analysis in the monitoring programs of the Bedford Basin and Scotian Shelf. In particular thank you to the crew of the CCGS *Sigma-T* and the CCGS *Hudson* over the time of this study. Also at BIO, thank you to Rick Boyce and Bob Ryan for helping me to analyze salinity samples. Thank you to Halifax Water for letting me collect wastewater samples across the Halifax Regional Municipality. Thanks to Helmuth Thomas and his lab for providing the AZMP data used in this study.

In addition, to everyone who I ever came running to with a Kaleidagraph, Excel, LaTeX, Matlab, R, ODV, etc. problem, you have all saved my Master's Thesis at one time or another, thank you! Thank you to DOSA for making my time in this department amazing: through Coffee, Snack, Seadogs and Friday Beer, you were always there when needed! Finally, thank you to all of my friends, both in- and out-side of the department, and my family for your continuing support.

CHAPTER 1

INTRODUCTION

1.1 Motivation

The freshwater balance of the North Atlantic Ocean is changing due to increased sea-ice and ice-sheet melt; understanding the current composition of this water, and the freshwater input in particular, is essential in order to manage any subsequent changes to the earth's climate and hydrological system, as a result of this continuing shift in water composition (*Manabe and Stouffer*, 1995; *Curry et al.*, 2003). Any changes to the water mass composition of the North Atlantic Ocean will also affect coastal harbours and inlets supplied by this water. Halifax Harbour, located on the Atlantic coast of Nova Scotia, is the second largest natural harbour in the world and a major Canadian coastal estuary, supporting: the Canadian Coast Guard & Navy, offshore oil and gas supply, commercial fisheries, tourism, recreational facilities, and residential development (*Fader and Buckley*, 1995; *Gardner Pinfold Consulting Economists Ltd.*, 2004; *Fader and Miller*, 2008). As such, any variability in the freshwater inputs to this coastal estuary could have detrimental effects on the city of Halifax, both environmentally and economically.

To study changes in the water mass composition of Bedford Basin, a deep fjord at the northwestern end of Halifax Harbour, a water mass tracer can be used. The use of only salinity as a water mass tracer does not function in coastal inlets with multiple freshwater inputs as it cannot distinguish between independent freshwater sources. By measuring the isotopes of water (δ^{18}O and δ^{2}H) and pairing these values with salinity measurements, it is possible to distinguish between freshwater inputs in order to identify and quantify the composition of water sources in Bedford Basin.

The δ^{18}O-Salinity relationship has been used in a number of studies to differentiate

water masses and freshwater sources in the ocean. *Craig and Gordon* (1965) first classified these variations of δ^{18}O in the ocean and atmosphere, illustrating the use of δ^{18}O as an oceanographic tracer. A number of studies have used the δ^{18}O-S relationship to identify different water masses in the ocean and on land, however few studies have used the isotopic composition of water to provide a detailed assessment of the mixing between fresh and ocean water in estuaries (*Martin and Letolle*, 1979; *Karim and Veizer*, 2002; *Corlis et al.*, 2003; *MacLachlan et al.*, 2007; *Stalker et al.*, 2009). As such, the use of the δ^{18}O-S relationship allows us to characterize and distinguish freshwater inputs with distinct δ^{18}O-S signatures in an estuary, where multiple inputs of freshwater are present. By defining these inputs (δ^{18}O and salinity), it is possible to examine how changes to these source waters can affect the δ^{18}O-S signature of the estuary. By differentiating freshwater inputs, such as wastewater, run-off, precipitation or riverine water, it may be possible to identify the proportion of these source waters in an estuary, and as such any inputs they may carry (i.e. fertilizers, pesticides, road salt, etc.). Insight into the water composition of Bedford Basin and its approaches not only gives us the ability to identify the current composition (δ^{18}O and salinity) of Bedford Basin and its inputs, it also provides the first measurements of δ^{18}O in Halifax, essential for the future understanding and governance of this coastal estuary.

1.2 Water Mass Analysis

1.2.1 Introduction to Stable Isotopes

An isotope is a nuclide of an element with a unique atomic mass; for a given element the number of protons is set, however the number of neutrons can vary, resulting in different isotopes. The relative abundances of isotopes are typically expressed in delta (δ) notation, which can be written as the difference between the measured ratios of the sample and a reference material, over the measured reference material ratio (Equation 1.1).

$$\delta = \frac{R_{sample} - R_{standard}}{R_{standard}} \tag{1.1}$$

R is defined as the ratio between the rare (often heavy) and common (often light) isotopes of an element. For oxygen, the most abundant isotope, ^{16}O, represents 99.796% of all

oxygen on earth, while ^{18}O, the next most abundant isotope, represents 0.204% (*Clark and Fritz*, 1997). The ratio (R) of oxygen isotopes can be seen in Equation 1.2.

$$R = \frac{^{18}O}{^{16}O} \tag{1.2}$$

Since we are interested in differences in the stable isotope (i.e. ^{16}O or ^{18}O) ratios in a sample, rather than the actual abundance of these isotopes, a ratio is used (*Clark and Fritz*, 1997). This ratio differs depending on instrumental and operational variability, so a known reference standard is analyzed on the instrument at the same time to account for any operational differences (*Clark and Fritz*, 1997). This means that all measurements are made relative to a standard. When measuring the isotopes of water (δ^{18}O and δ^{2}H) the standard currently used is Vienna Standard Mean Ocean Water (VSMOW) (*Pilsen*, 1998), however different standards are required to calculate δ values for different elements (e.g. PeeDee belemnite (PDB) for δ^{13}C) (*Coplen*, 1996). As δ values for natural samples are typically very small, they are represented in parts per thousand (permil, ‰). To report the isotopic composition of oxygen (δ^{18}O) in a sample, the following formula is used (Equation 1.3):

$$\delta^{18}O = \frac{(^{18}O/^{16}O)_{sample} - (^{18}O/^{16}O)_{VSMOW}}{(^{18}O/^{16}O)_{VSMOW}} * 1000‰ \tag{1.3}$$

A positive δ^{18}O value signifies that the sample has more ^{18}O than the reference, meaning that it is isotopically enriched, or “heavier”. A negative δ^{18}O value, in contrast, means that the sample has less ^{18}O than the reference, making it isotopically depleted, or “lighter”.

1.2.2 Isotope Fractionation in Water

Isotopes fractionate naturally due to mass differences between species with identical chemical properties. The result of this fractionation is a disproportionate concentration of one isotope over the other, expressed by the fractionation factor (α) (*Clark and Fritz*, 1997),

$$\alpha = \frac{R_{reactant}}{R_{product}}$$

Isotopes are fractionated by physicochemical reactions under equilibrium or non-equilibrium (kinetic) conditions, or by molecular diffusion (also a kinetic fractionation) (*Urey*, 1947; *Clark and Fritz*, 1997). *Urey* (1947) first described isotopic fractionation as an exchange of isotopes (e.g. ^{16}O and ^{18}O) between any two molecular species or phases that are participating in a reaction. These reactions may be changes of state,

$$H_2O_{water} \leftrightarrow H_2O_{vapour}$$

or chemical transformations,

$$CO_2 + H_2O \leftrightarrow H_2CO_3$$

(*Clark and Fritz*, 1997). Physicochemical isotopic fractionation is driven by differences in the strength of bonds formed by heavy and light isotopes of an element (*Clark and Fritz*, 1997). This difference in bond strength allows for different reaction rates; heavy isotopes tend to have stronger bonds that require more energy to break (*Clark and Fritz*, 1997).

For equilibrium fractionation to occur, chemical equilibrium must exist (i.e. forward and backward reaction rates need to be the same). Under equilibrium conditions, bonds are continually breaking and reforming; stronger bonds will survive statistically for longer so it is usually the heavy isotope that is partitioned into the more condensed phase (i.e. solid phase in solid-liquid reactions and liquid phase in vapour-liquid reactions) (*Clark and Fritz*, 1997). Therefore, the heavier isotope will become concentrated in the chemical species that has the strongest (or most) bonds to its atom. This can be seen in the condensation and evaporation of water (at 100% humidity); at equilibrium, ^{16}O is enriched in the vapour phase, while ^{18}O is enriched in the liquid phase (*Clark and Fritz*, 1997). The rate of evaporation in water depends on hydrogen bond strength, while the rate of condensation depends on the concentration of water in the gas phase (*Clark and Fritz*, 1997). At 100% humidity, these two fluxes are equal and at equilibrium. Since an ^{18}O-H bond between molecules is stronger than a ^{16}O-H bond, ^{16}O accumulates preferentially in the vapour phase (*Clark and Fritz*, 1997). Changing temperatures also drive changes in equilibrium isotopic fractionation. In addition, any sudden changes in temperature that move a system past thermodynamic equilibrium can lead to kinetic isotopic fractionation (*Clark and Fritz*, 1997).

Non-equilibrium, or kinetic, fractionation occurs when reactions are irreversible and unidirectional and, unlike equilibrium fractionation, forward and backward reaction rates are not the same (*Clark and Fritz*, 1997). This includes fractionation by both non-equilibrium physicochemical reactions and molecular diffusion (*Clark and Fritz*, 1997). In a kinetic fractionation reaction, bonds between the lighter isotopes are broken more easily than the same bonds of heavier isotopes, resulting in an accumulation of the lighter isotopes in the products, while residual reactants are enriched in heavy isotopes (*Kendall and MacDonnell*, 1998). Kinetic fractionation can occur in response to sudden temperature changes, molecular diffusion, enzymatic reactions, or evaporation when humidity is less than 100% (*Clark and Fritz*, 1997).

The isotopic fractionation of water in the atmosphere is typically subjected to kinetic, rather than equilibrium, fractionation. This is because the atmosphere is a non-equilibrium system, and the transport of water molecules through the air is an important control on the fractionation of water vapour and precipitation (*Craig and Gordon*, 1965; *Merlivat and Jouzel*, 1979; *Cappa et al.*, 2003). Kinetic fractionation is affected by surface temperature, wind speed, salinity and humidity (*Clark and Fritz*, 1997). At humidities of less than 100%, water vapour exchange decreases and evaporation becomes increasingly non-equilibrium.

Rainout, or condensation in clouds, is governed by equilibrium fractionation (humidity=100%), and to produce rain, cooling of a vapour mass must first occur. This cooling causes equilibrium fractionation between the vapour and the condensing phases, which preferentially partitions ^{18}O and ^{2}H into rain (or snow) (*Clark and Fritz*, 1997). This results in the formation of isotopically enriched rain (+δ^{18}O and +δ^{2}H), while the residual vapour becomes isotopically depleted (*Clark and Fritz*, 1997). Resultant rainouts are now depleted, with respect to earlier rainfall events, according to a Rayleigh-type distillation (-δ^{18}O and -δ^{2}H) (*Clark and Fritz*, 1997). Snowfall, or any other type of solid precipitation, is also formed in this way. However, the isotopic composition of solid elements is frozen in, while raindrops undergo continuous molecular exchange as they fall towards the ground, and as such can be adjusted to equilibrium through ambient moisture (*Gat*, 2010). The predictable fractionation of ^{18}O and ^{2}H associated with meteorological processes allows us to trace the origin of water through the hydrological cycle.

1.2.3 Tracing ^{18}O through the Hydrological Cycle

1.2.3.1 δ^{18}O of Ocean Water

Stable isotopes of water (^{18}O and ^{2}H) naturally fractionate by meteorological processes, providing distinct "fingerprints", or isotopic signatures, that can be used to identify the origin of water. Although $\delta^{18}O_{VSMOW}$ = 0‰, representing standard mean ocean water, is used as a reference for δ^{18}O and δ^{2}H, the mean isotopic composition of modern seawater is estimated to be 0.5‰ VSMOW (*Clark and Fritz*, 1997). Variations in δ^{18}O of near surface waters correlate with salinity and these variations can be attributed to changes in sea surface evaporation or the introduction of meteoric waters and, to some extent, sea-ice formation or melting (*Clark and Fritz*, 1997).

1.2.3.2 δ^{18}O of Meteoric Water

In comparison to ocean waters, meteoric waters (i.e. atmospheric moisture, precipitation and its derivatives: ground and surface waters, glacial and surface ice) are mostly depleted in the heavy isotopes (^{18}O and ^{2}H) of water (*Mook*, 1982). Meteoric waters are depleted relative to $\delta^{18}O_{VSMOW}$ = 0‰, resulting in negative δ values (-δ^{18}O and -δ^{2}H).

Craig (1961) found that δ^{18}O and δ^{2}H of meteoric water correlate on a global scale. By averaging many local and regional meteoric lines, *Craig* (1961) established the global meteoric water line (GMWL) (Equation 1.4), representing the global relationship between δ^{18}O and δ^{2}H in precipitation (*Clark and Fritz*, 1997) (Figure 1.1):

$$\delta^2 H = 8\,\delta^{18}O + 10‰\ SMOW \tag{1.4}$$

The GMWL, while representing global relationships, is not always a good indicator of regional and local meteoric water lines. As such, studies have established local meteoric water lines (LMWL). The Canadian meteoric water line (*Clark and Fritz*, 1997) was found to be:

$$\delta^2 H = 7.75\,\delta^{18}O + 9.83‰\ SMOW$$

While the LMWL of Truro, NS, the closest International Atomic Energy Agency (IAEA) site to Halifax ($\sim$100 km North), was found to be (*Clark and Fritz*, 1997):

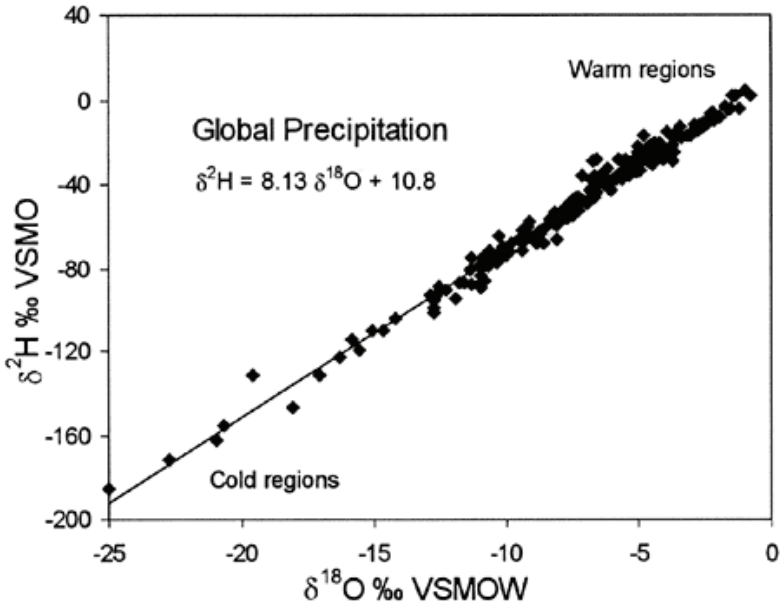

Figure 1.1: The relationship between δ^{18}O and δ^{2}H in precipitation. This Global Mean Water Line was determined by *Craig* (1961) and compiled in *Rozanski et al.* (1993). Figure from *Clark and Fritz* (1997).

$$\delta^2 H = 7.43\, \delta^{18} O + 5.57‰\ SMOW,$$

which can also be seen in Table 1.1.

There is a strong correlation between temperature and δ^{18}O in the hydrological cycle as isotopic fractionation is strongly dependent on temperature under equilibrium conditions (e.g. condensation). As decreasing temperatures drive condensation and isotopic fractionation, precipitation becomes more depleted in ^{18}O and ^{2}H leading to more negative

Table 1.1: Local meteoric water line for Truro, NS (Aug 1975 - July 1982), from *Fritz et al.* (1987).

		δ^{18}O vs. δ^{2}H		
Station	Season	Slope	Intercept	r^2
Truro	Year	7.43	5.57	0.948
	Summer	7.82	8.34	0.813
	Winter	7.39	5.16	0.935

δ^{18}O and δ^{2}H values (*Clark and Fritz*, 1997). Additional factors, such as re-evaporation and atmospheric mixing, can complicate this relationship, however overall precipitation becomes more isotopically depleted with decreasing temperature, causing a "temperature effect". *Dansgaard* (1964) defined five major "isotope effects" that have characteristic and predictable effects on the isotopic composition of precipitation: latitude, altitude, continental, amount, and seasonal.

All of these "isotope effects" are influenced by a number of physical processes that can contribute to these effects, including: temperature, progressive rainout, and fraction of solid precipitation (*Dansgaard*, 1964). Smaller scale, local isotope effects on land, such as coastal fog and secondary evaporation can also modify the isotopic composition (δ^{18}O and δ^{2}H) (*Dansgaard*, 1964; *Mook*, 1982; *Clark and Fritz*, 1997). As precipitation condenses from an air mass while it moves across a continent (e.g. ascending a mountain, changing topography, or moving towards more polar regions), ^{18}O and ^{2}H are progressively removed, causing progressive rainouts to be increasingly isotopically depleted (-δ^{18}O and -δ^{2}H) (Figure 1.2).

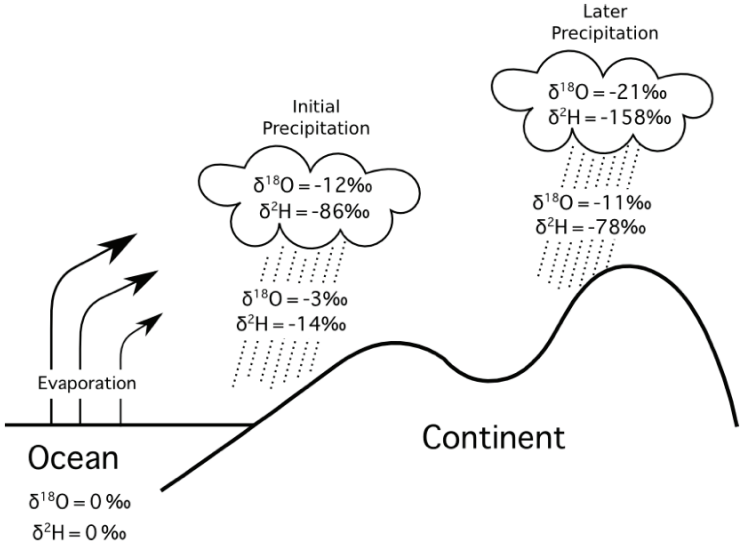

Figure 1.2: Schematic of the isotopic fractionation of δ^{18}O and δ^{2}H in the hydrological cycle, associated with precipitation, condensation and evaporation; image adapted from *Brand and Coplen* (2012) and *Hoefs* (1997).

1.2.4 δ^{18}O-Salinity Relationship

Using the proportion of isotopes in water (δ^{18}O) as a water mass tracer is advantageous, particularly when compared with salinity, the other commonly used conservative tracer

in ocean water (*Epstein and Mayeda*, 1953; *Craig and Gordon*, 1965; *Bigg and Rohling*, 2000). The salinity of water varies with the salt content of a water source, and not the water (i.e. ^{16}O or ^{18}O) itself, and as such cannot differentiate between freshwater inputs (*Craig and Gordon*, 1965). During the process of sea-ice melt, the salinity of sea-ice and brine will have differing salinity values, but an unchanged δ^{18}O measurement due to the invariance of δ^{18}O with freezing, leading to a flat δ^{18}O-S relationship (*Tan and Strain*, 1980; *Bigg and Rohling*, 2000). In addition, all freshwater inputs to the ocean have the same salinity ($\sim$0 psu), but can have different δ^{18}O values depending on the source: precipitation (*Dansgaard*, 1964), river inflow (*Mook*, 1982), glacier calving (*Craig and Gordon*, 1965), or sea-ice melt (*Bigg and Rohling*, 2000). *Epstein and Mayeda* (1953) found differing δ^{18}O values in regions of considerable sea-ice melt water influx when the salinity measurements were constant (0 psu), meaning that different water sources must be present (*Craig and Gordon*, 1965).

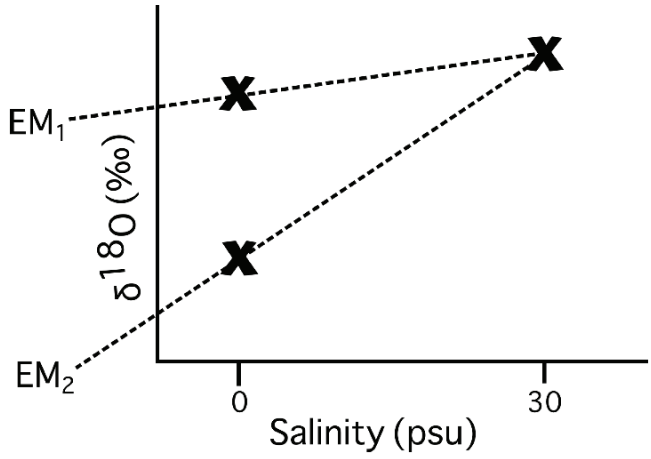

Figure 1.3: Schematic of the δ^{18}O-Salinity relationship with potential end members (EM), represented by an "x", and EM mixing lines (EM_1 and EM_2) identified.

It is evident that δ^{18}O and δ^{2}H measurements provide us with additional information with respect to the origin of source waters, particularly when salinities are the same. When paired with salinity, δ^{18}O can be used as a tracer for the intermixing of ocean waters with run-off, sea-ice melt, and brine release (*Bigg and Rohling*, 2000). Figure 1.3 presents three distinct water masses with different properties (δ^{18}O and salinity), the potential end member mixing lines associated with these three distinct water masses, and the need to use the δ^{18}O-S relationship to accurately distinguish between water sources. Different water

masses have distinct salinity and δ^{18}O values that characterize and differentiate source waters, and as such these defined end members can be used to identify and quantify the proportion of source waters in a body of water.

1.3 Oceanographic Setting of Halifax Harbour and its Approaches

1.3.1 Halifax Harbour

Halifax Harbour has been the focus of a large number of oceanographic studies, primarily due to its proximity to both Dalhousie University and the Bedford Institute of Oceanography (BIO); this estuary also has a strong environmental and economic impact on the Halifax Regional Municipality (HRM), which makes understanding this region of critical importance (*Gardner Pinfold Consulting Economists Ltd.*, 2004; *Halifax Regional Municipality*, 2004). Halifax Harbour is a world-class seaport that has seen tremendous economic growth in recent years (*Halifax Regional Municipality*, 2004) with increased tourism and port-related industries, such as the awarding of a $25-billion contract in 2011 to build combat ships for the Canadian Navy (*Jupia Consultants Ltd.*, 2011; *Visser*, 2011).

The pollution of Halifax Harbour has been the main focus of a number of studies in the area, beginning with *Huntsman*'s 1924 study on the circulation and distribution of polluted waters in and around Halifax. Prior to the construction of Wastewater Treatment Facilities (WWTFs) in 2008, raw sewage and wastewater were dumped into Halifax Harbour for more than 200 years (*Buckley and Winters*, 1992; *Fournier*, 1990; *AMEC Earth and Environmental*, 2011). In 1995, the harbour was receiving up to 170 million litres of raw, untreated sewage a day from 40 outfalls around Halifax and Dartmouth (in addition to run-off, landfills, industrial activity, and dredging) (*Fader and Buckley*, 1995; *Nicholls*, 1989). *Buckley* (2001) found that industrial discharge, sewage waste, and leaching from land resulted in high levels of metal contaminants (Zn, Pb, Cu, and Hg) in surficial sediments of Halifax Harbour due to sediment trapping and the lack of flushing within the harbour (*Gearing et al.*, 1991; *Buckley and Winters*, 1992; *Buckley et al.*, 1995; *Fader and Buckley*, 1995).

Following the completion of the WWTFs, water quality has improved in the harbour; this has included a decrease in fecal coliform levels and total suspended solids (*Fournier*, 1990). However as of 2011, some of the guidelines for metal concentrations in the harbour,

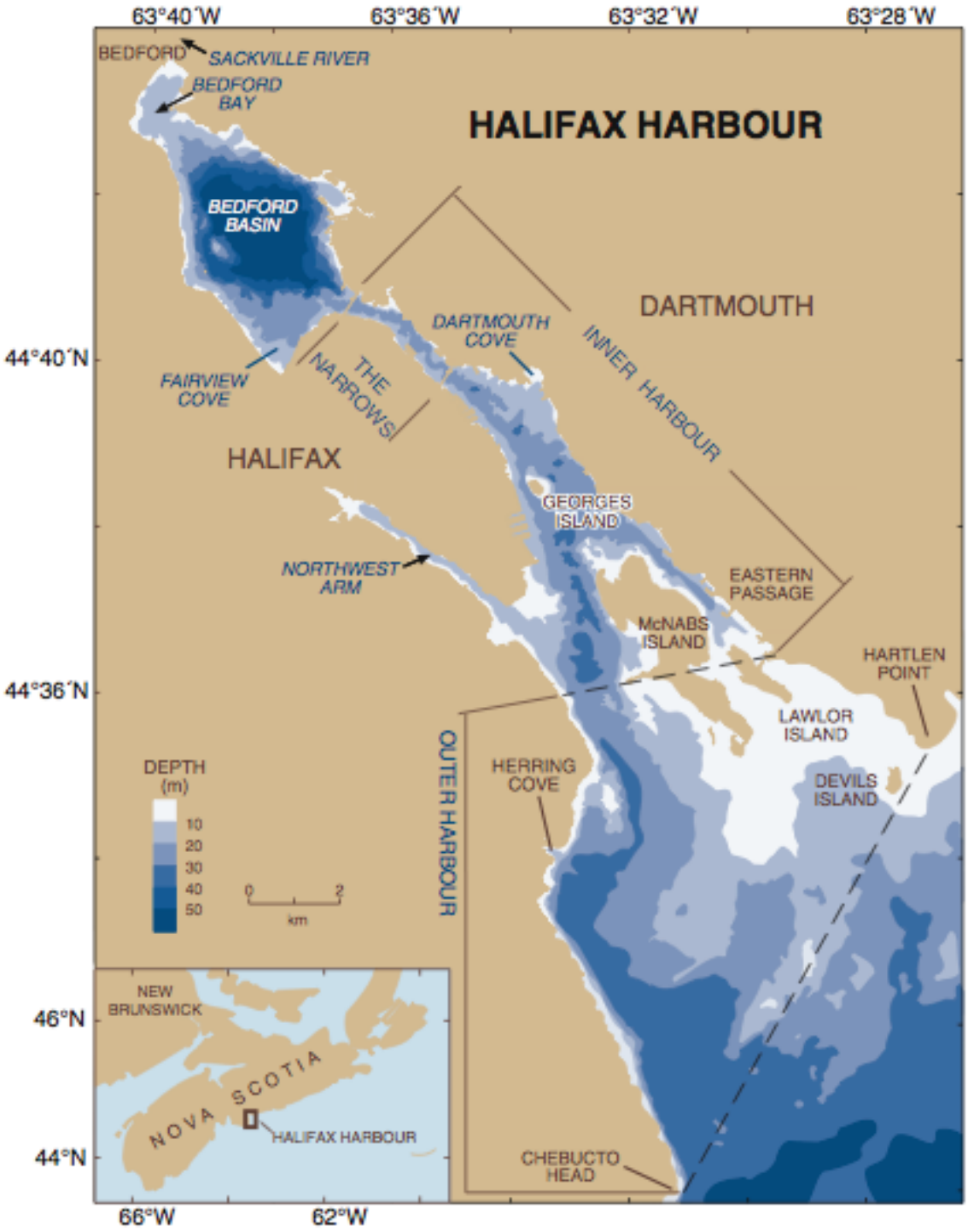

Figure 1.4: Geographic divisions of Halifax Harbour and the HRM including major communities and bathymetry. Figure from *Fader and Miller* (2008).

developed by the Halifax Harbour Task Force (HHTF) in 1989 (*Fournier*, 1990; *AMEC Earth and Environmental*, 2011), were still not being met, with occasional exceedances of copper and mercury in particular (*AMEC Earth and Environmental*, 2011). Intense precipitation events associated with storms can exceed the processing capacity of the WWTFs. This may result in flooding of the WWTFs, causing increased bacteria levels to be introduced into the harbour through raw untreated sewage and storm water (*AMEC Earth and Environmental*, 2011; *Shan and Sheng*, 2012). In addition, the water quality of Halifax Harbour is also influenced by water circulation and flushing rates. An increased understanding of water quality and circulation will provide insight into this environmentally critical body of water and mitigate pollutant levels.

1.3.1.1 Geography

Halifax Harbour is commonly divided into five geographic divisions: the Outer Harbour, Inner Harbour, Northwest Arm, Narrows and Bedford Basin (Figure 1.4). Bedford Basin is a deep fjord, in an otherwise shallow harbour, with a maximum depth of $\sim$71 m near its centre. The Narrows connects Bedford Basin to the Inner Harbour via a shallow ($\sim$20 m) sill that constrains the flow of water in the bottom layers of Bedford Basin, isolating large amounts of dense bottom-water. This can be partially-renewed by periodic upwelling of dense bottom water over this sill, seen in both temperature and salinity data (*AMEC Earth and Environmental*, 2011; *Burt et al.*, 2013). Deep water ventilation events, leading to mixing of the deep and surface layers, can result from wind-induced deep vertical mixing (*Punshon and Moore*, 2004), or lateral mixing, as a result of strong along-shore winds and large tides (*Burt et al.*, 2013). Sackville River contributes the largest single input of fresh water into Halifax Harbour and enters through Bedford Bay, at the northern end of Bedford Basin.

1.3.1.2 Freshwater Inputs

In 1993, *Gregory et al.* found that the tidal to freshwater inflow volume ratio of Halifax Harbour was $\sim$373.01 (i.e. Tidal Inflow/Freshwater Inflow). The average annual discharge of fresh water into Halifax Harbour is approximately 15.7 m^3/s, with 16% of this water originating from the HRM sewage system (*Fader and Buckley*, 1995). This breakdown of fluvial and sewage discharges into Halifax Harbour is given in Table 1.2, adapted from *Buckley and Winters* (1992) to include distributed discharges with the known

Table 1.2: Fluvial and effluent discharges in Halifax Harbour, adapted from *Buckley and Winters* (1992). Distributed discharges were added to the total average discharge locations in the corresponding subregions. An error of 0.1 m^3/s is associated with these additions.

Location	**Average Discharge** (m^3/s)
Head of Bedford Basin	
Sackville River	5.41
Eastern Bedford Basin	
Wrights Brook	0.98 ± 0.1
Western Bedford Basin	
Paper Mill Lake flume	1.38 ± 0.1
Fairview Cove storm drain	0.27 ± 0.1
Bedford - Sackville sewage treatment plant	0.37 ± 0.1
Fairview Cove storm and sewer	0.19 ± 0.1
Eastern Middle Harbour	
Banook Lake flume	1.85 ± 0.1
Tufts Cove Sewer	0.25 ± 0.1
Dartmouth Cove Sewer	0.31 ± 0.1
Western Middle Harbour	
Duffus Street Sewer	1.02 ± 0.1
Duke Street Sewer	0.69 ± 0.1
Northwest Arm	
Chocolate Lake flume	0.24 ± 0.1
Frog Lake brook	0.20 ± 0.1
Williams Lake brook	0.20 ± 0.1
Point Pleasant sewer	0.15 ± 0.1
Eastern Lower Middle Harbour	
Eastern Passage sewage treatment plant	0.46 ± 0.1
Western Lower Middle Harbour	
Purcells Lake brook	0.21 ± 0.1
Eastern Outer Harbour	
Distributed	0.29 ± 0.1
Western Outer Harbour	
Powers Pond flume	1.15 ± 0.1
Herring Cove sewer	0.15 ± 0.1

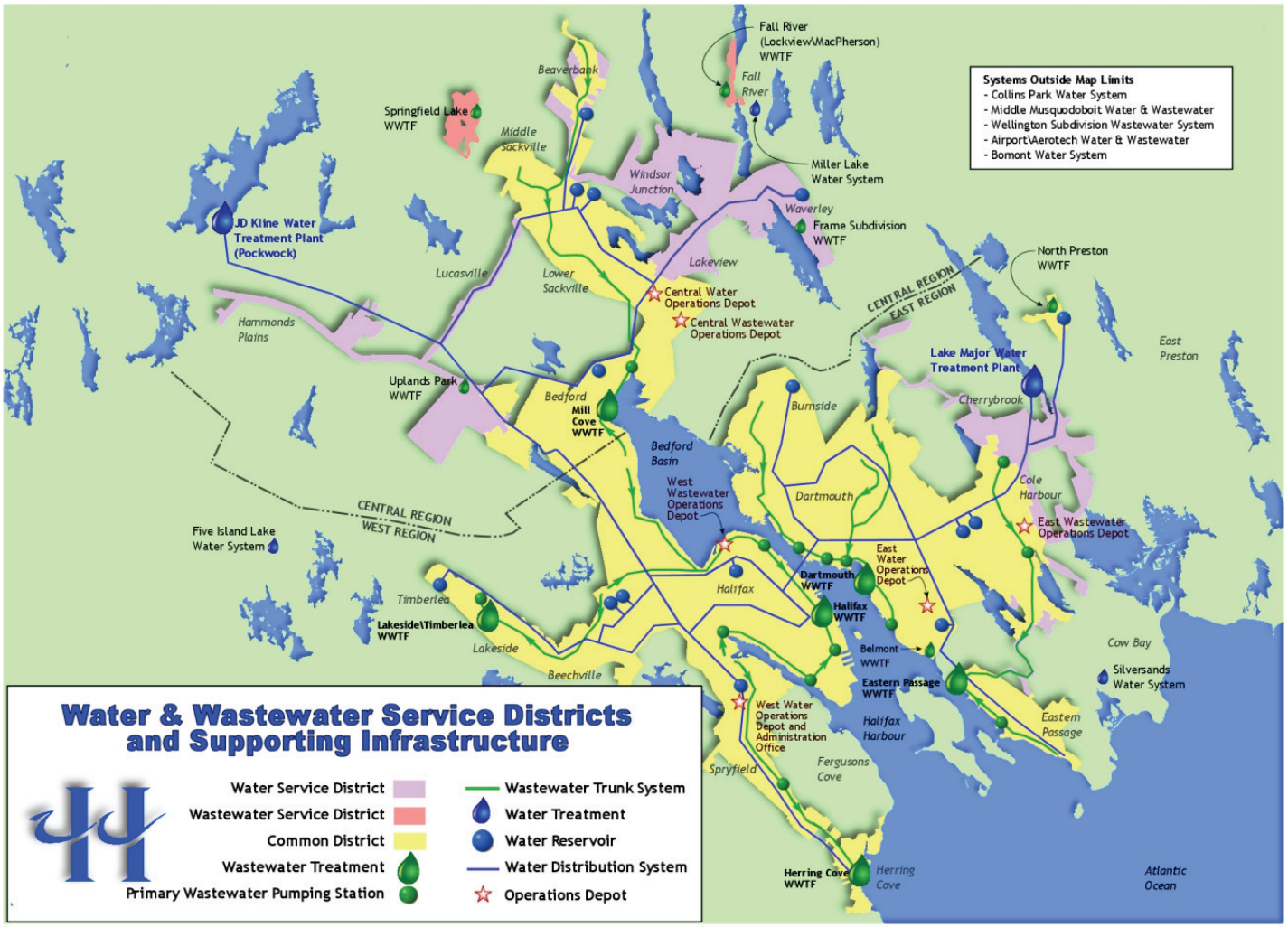

Figure 1.5: Water and wastewater service districts around the HRM. Figure from *Halifax Water* (2012).

discharges from each region. In 2012, *Shan and Sheng* modeled a tracer experiment to determine which areas of Halifax Harbour were the most likely to accumulate sewage pollutants. Tracer concentrations were set to 1 at sewage outfall sites, and 0 in the rest of the harbour, beginning on January 1, 2006 (*Shan and Sheng*, 2012). After 365 days, higher concentrations of pollutants were seen in the Northwest Arm, Bedford Basin, and locations close to sewage outfall sites, with tracer concentrations of 0.45, >0.5, 0.2, and <0.15 in Bedford Basin, the Northwest Arm, the Narrows & Inner Harbour, and the Outer Harbour respectively (*Shan and Sheng*, 2012). During flood & ebb tides, and storm events, the tracer concentrations in the Narrows, Inner Harbour, and Outer Harbour were found to vary (*Shan and Sheng*, 2012). The rate of wastewater discharge varies with daily use and precipitation; the locations of wastewater discharge sites around Halifax Harbour are presented in Figure 1.5.

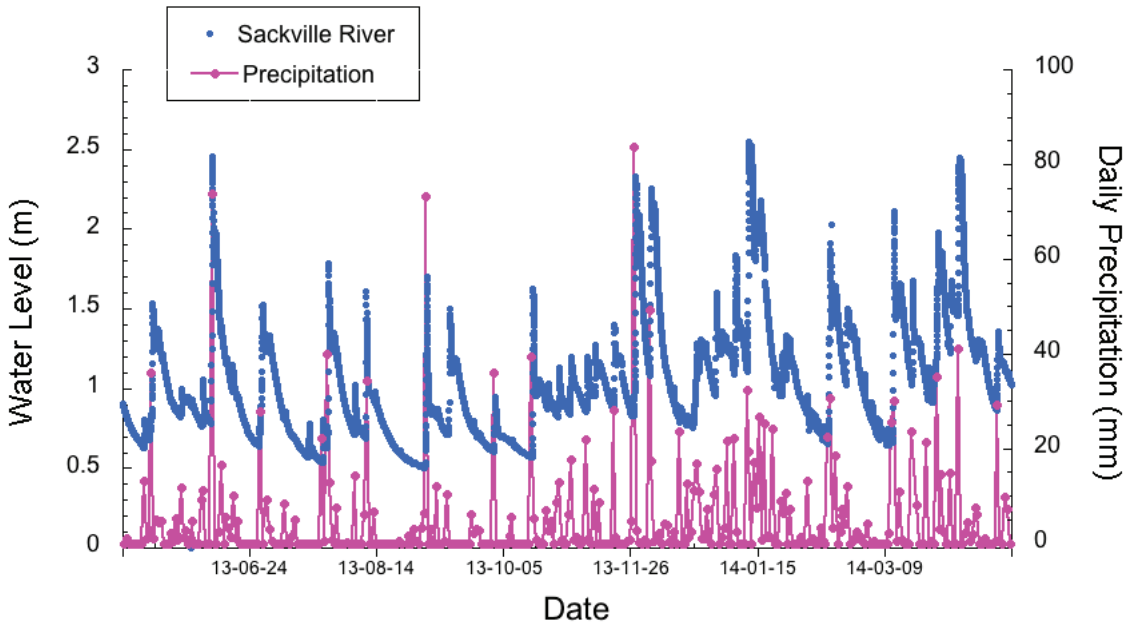

Figure 1.6: Change in water level (m) of Sackville River (*Environment Canada*, 2013) and daily precipitation (mm) recorded at the Halifax International Airport (*Government of Canada - Climate*, 2014) from May 1^{st} 2013 to April 30^{th} 2014. Sackville River data were collected using a continuous gauge recorder operated by Environment Canada.

Previous studies have found that Sackville River, which delivers the largest individual input of fresh water into Halifax Harbour, has an average discharge of 5.41 m^3/s (*Buckley and Winters*, 1992), ranging from 2 m^3/s to 9 m^3/s in the summer (July - September) and

spring respectively (*Fournier*, 1990). Although Sackville River is the largest individual source of fresh water to this region, its mean discharge is relatively small and makes up only one third of the total fresh water entering the harbour; additional fresh water is added by a number of streams and sewers (*Buckley and Winters*, 1992). *Shan* (2010) illustrates, through his model, that despite its relatively small drainage area and discharge speed, Sackville River plays an important role in maintaining a salinity front within Bedford Basin. Sackville River water level has been monitored, using water gauges operated by Environment Canada, from 1970 to present. The variability in Sackville River water level from May 1^{st} 2013 - April 30^{th} 2014 is presented in Figure 1.6 alongside historical precipitation (mm) data collected from the Halifax International Airport (*Government of Canada - Climate*, 2014).

Precipitation, both rain and snow, contributes fresh water to Halifax Harbour both directly and indirectly (through run-off and riverine inputs); the average amount of yearly precipitation recorded at the Halifax Citadel climate station (44°39'00"N, 63°35'00"W) between 1981 and 2010 was found to be $\sim$1468.1 mm (*Government of Canada - Climate*, 2014). The amount of precipitation in Halifax varies throughout the year, with the most, on average, occurring in November (151.4 mm) and the least in August (96.4 mm) (*Government of Canada - Climate*, 2014). Using these historical precipitation data (*Government of Canada - Climate*, 2014) and the known area of Bedford Basin (*Gregory et al.*, 1993), the average yearly rate of precipitation directly entering Bedford Basin was found to be 0.79 m^3/s, with a rate of 0.99 m^3/s in November (maximum input) and 0.61 m^3/s in August (minimum input). The direct volumetric input of precipitation over time is smaller than the average discharge of Sackville River (5.41 m^3/s) into Bedford Basin or other minor fluvial and effluent inputs presented in Table 1.2. Strong storms throughout the year can also introduce additional precipitation into Halifax Harbour, including hurricanes, tropical storms, and major snow falls, leading to greater volumetric flow rates.

1.3.1.3 Circulation

Huntsman (1924) conducted the first study on the circulation of water in Halifax Harbour to understand the distribution of polluted water in the area with respect to the horizontal circulation. There is an overall flow of salt water into the harbour that mixes with fresh water entering from land. To examine the general circulation pattern of this estuary, *Huntsman* (1924) collected a number of samples to determine both salinity and temperature

at various depths (1 & ∼10 m) and stations throughout the harbour. By looking at the change in salinity through the harbour, *Huntsman* (1924) identified an inflow of salt water that tends to stay towards the right in both the Northwest Arm and Outer Harbour (Figure 1.7(a)). When this incoming saline water reaches Bedford Basin, it mixes with fresh water, introduced from Sackville River and any other meteoric inputs present, and then flows outwards along the opposite side of the harbour (Figure 1.7(a)).

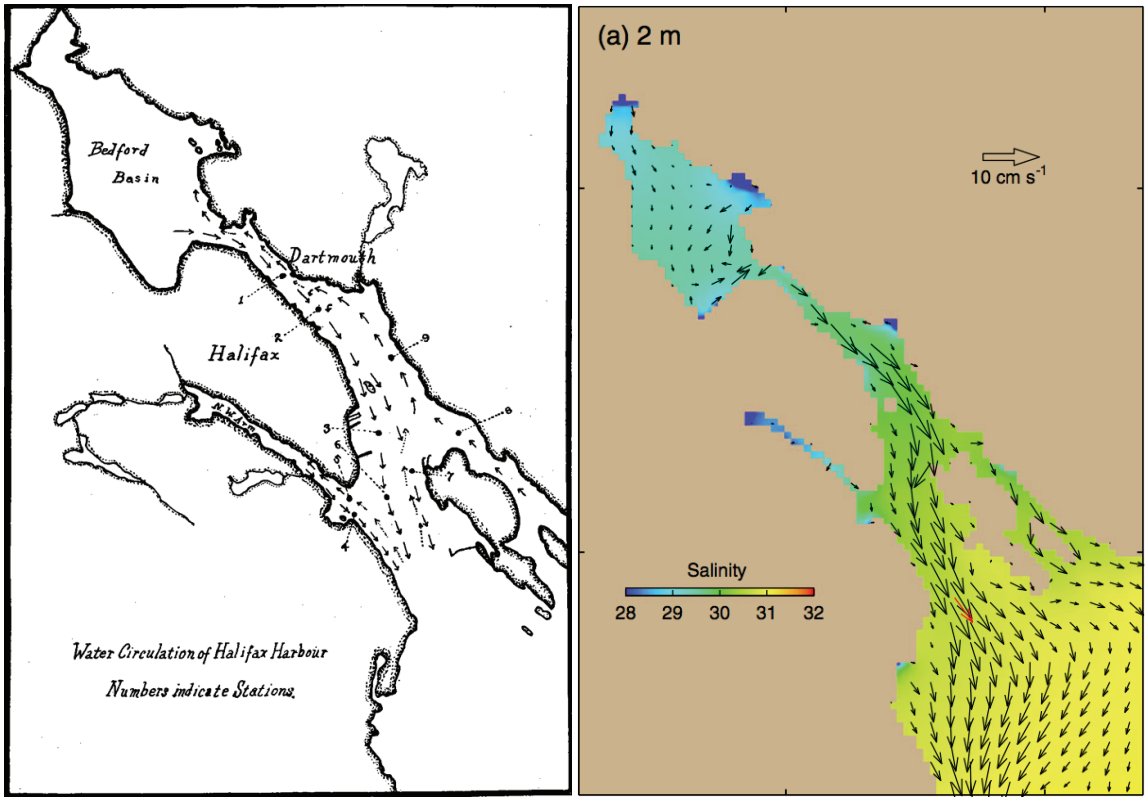

(a) (b)

Figure 1.7: Horizontal circulation of water in Halifax Harbour at the surface from (a) *Huntsman* (1924) (solid arrows) and (b) *Shan et al.* (2011), using calculated annual mean currents and velocities.

In comparison, in 2011, *Shan et al.* developed a nested ocean circulation model of Halifax Harbour including tides, wind, barometric pressure, air-sea fluxes of heat, and buoyancy fluxes associated with both river and sewage discharge. To determine the predictive skill of this model, it was compared to independent observations of sea level, currents and monthly climatology, created using all available temperature and salinity observations in Halifax Harbour over the last century (*Shan et al.*, 2011). These authors modeled the horizontal circulation of Halifax Harbour; at 2 m depth the model predicts

seaward flow throughout the harbour, while landward flow is presented at 10 m and below, characterizing the overall circulation of the harbour as a "two-layer estuarine circulation", consistent with previous studies (e.g. *Fournier* (1990)). *Shan et al.* (2011)'s model suggests weak near-surface circulation in Bedford Basin, with relatively stronger flows in the Narrows, Inner and Outer Harbour (Figure 1.7(b)).

The vertical circulation of water in Halifax Harbour is characterized by a two-layered flow (Figure 1.8); incoming saline water is dense and moves along the bottom of the harbour, while outflowing fresh water is found at, or near, the surface (*Fournier*, 1990; *Shan et al.*, 2011). This two-layered flow is also influenced by thermal stratification and winds that help to support this pattern of deep-water inflow and surface-water outflow (*Fader and Miller* (2008)). The vertical circulation of water in Bedford Basin also shows this same two-layered flow, characteristic of a silled estuary (Figure 1.8).

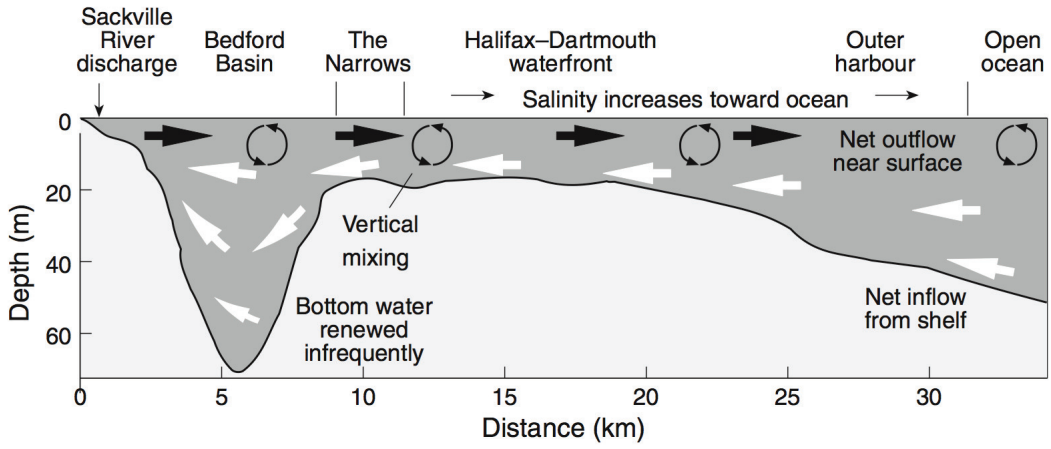

Figure 1.8: Schematic of water circulation in Halifax Harbour. Figure from *Fader and Miller* (2008).

Using the numerical model developed and presented in *Shan et al.* (2011), *Shan and Sheng* (2012) examined the flushing time and dispersion of water in Halifax Harbour using passive tracers. To quantify the flushing time in Halifax Harbour, passive tracers were utilized in (1) the entire Bedford Basin (Tracer 1), and (2) the upper 20 m of Bedford Basin (Tracer 2) *Shan and Sheng* (2012). Based on these model results, the flushing time of water in Bedford Basin was estimated to be approximately 90.6 days for the entire basin and 39.2 days for the top 20 m (*Shan and Sheng* (2012)).

1.3.2 Scotian Shelf

The Scotian Shelf is a 700 km-long region on the continental shelf off of Nova Scotia that varies in width from 120 to 240 km, covering 120,000 km^2, with an average depth of 90 m. This region is bounded by the Laurentian Channel to the northeast and by the Northeast Channel and Gulf of Maine to the southwest (*Shadwick and Thomas*, 2011).

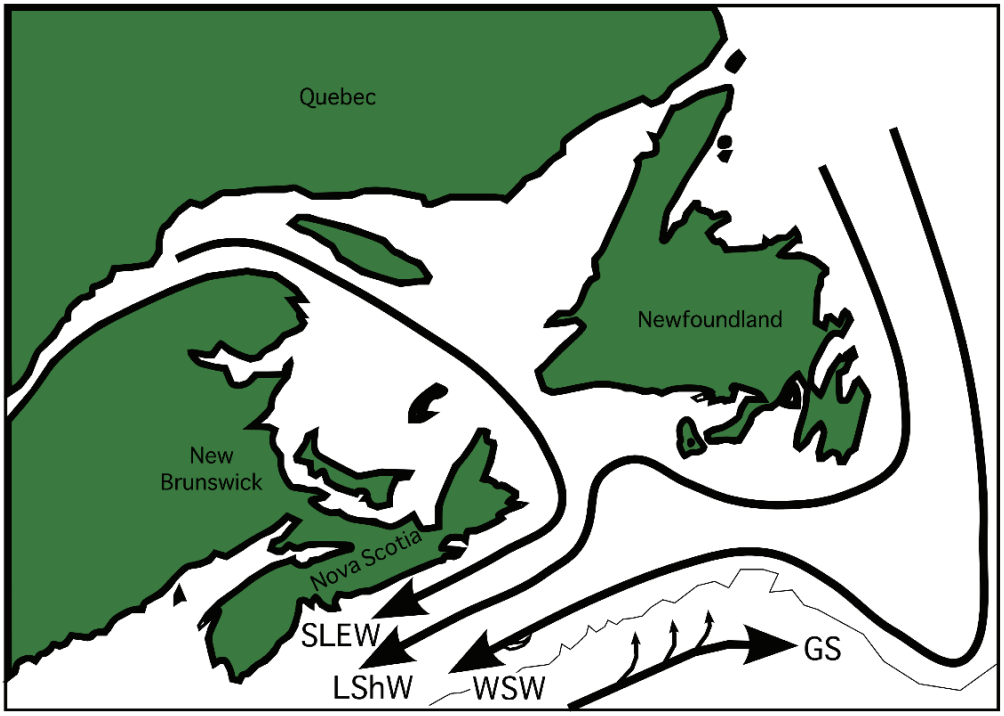

Figure 1.9: General movement of water masses along the Scotian Shelf, based on water mass analysis by *Shadwick and Thomas* (2011) and *Khatiwala et al.* (1999). SLEW: St. Lawrence Estuary Water, LShW: Labrador Shelf Water, WSW: Warm Slope Water, GS: Gulf Stream.

1.3.2.1 Water Composition

Studies identifying the origin of water on the Scotian Shelf date back to *Huntsman* (1924), who found - through temperature and salinity measurements - that this seawater originates from the ocean to the east of the Grand Banks and is a mixture of Labrador Current water, Gulf Stream water and coastal water from the Gulf of St. Lawrence. This water is then carried inward from the Scotian Shelf to Halifax Harbour, before reaching Bedford Basin. Through oxygen isotope measurements, *Khatiwala et al.* (1999) found that the primary upstream water sources to the Scotian Shelf are Labrador Slope Water (LSW), Labrador Shelf Water (LShW) and St. Lawrence River Water (SLRW).

Table 1.3: Scotian Shelf End Members proposed by *Khatiwala et al.* (1999).

Water Mass	**Abbreviation**	**Salinity**	δ^{18}**O (‰)**
Labrador Shelf Water†	LShW	32.78	-1.53
Labrador Slope Water	LSW	34.804	0.22
Warm Slope Water†	WSW	35.16	0.36
St. Lawrence Estuary Water†	SLEW	29.5	-2.4
St. Lawrence River Water	SLRW	0	-10.3

† LShW, WSW and SLEW will be used as the Scotian Shelf End Members

Using the δ^{18}O-Salinity relationship on the Scotian Shelf, *Shadwick and Thomas* (2011) were able to identify three source waters: (1) Warm Slope Water (WSW), which is modified LSW mixed with the warm salty waters of the Gulf Stream (GS), (2) LShW, which enters the Gulf of St. Lawrence via the inner branch of the Labrador Current, and (3) St. Lawrence Estuary Water (SLEW), which is strongly influenced by fresh water flowing out of the St. Lawrence River. These source waters line up with the analysis of *Khatiwala et al.* (1999), however *Shadwick and Thomas* (2011) take into account the mixing of water masses and the modifications that take place as this water travels southward. Table 1.3 presents all of the Scotian Shelf end members identified by *Khatiwala et al.* (1999); this includes SLRW and LSW which will be disregarded in this analysis, as SLEW and WSW were found to better represent the source waters found along the Scotian Shelf (*Shadwick and Thomas*, 2011). Figure 1.9 illustrates the general movement of these water masses along the Scotian Shelf based on previous water mass analyses (*Shadwick and Thomas*, 2011; *Khatiwala et al.*, 1999).

1.3.2.2 Freshwater Origin

Oxygen isotope analysis of waters in and around the Scotian Shelf and Scotian Slope suggest that dominant freshwater inputs must originate at high-latitudes, rather than locally (*Khatiwala et al.*, 1999; *Fairbanks*, 1982). The two main sources of freshwater to the Scotian Shelf originate from high-latitude (Arctic) run-off and SLRW, with SLRW contributing $\sim$35% of this freshwater input to the central Scotian Shelf (*Khatiwala et al.*, 1999). Water in the western-Scotian Shelf and Gulf of Maine show higher proportions of SLRW (40 - 50%), likely due to seasonal changes and phase lags in SLRW run-off and LShW flow (*Khatiwala et al.*, 1999). Meteoric outflow from the Arctic with a δ^{18}O of $\sim$

-21‰, rather than local precipitation, dominates the freshwater component of the North Atlantic (*Khatiwala et al.*, 1999; *Frew et al.*, 2000) (Figure 1.10). This is reflected in Figure 1.10, which presents the δ^{18}O-S relationship for water collected in the Labrador Sea and Scotian Slope, identifying the freshwater end member associated with this water (-21.67‰). The freshwater component is identified by the zero-salinity intercept of the slope in Figure 1.10, which is the δ^{18}O value associated with a salinity of 0, or the meteoric (freshwater) input. Although the North Atlantic is associated with a freshwater end member of -21‰, *Fairbanks* (1982) determined a freshwater end member of -15.55‰ for the Scotian Shelf, comparable to water found north of the Gulf of St. Lawrence (*Tan and Strain*, 1980; *Bedard et al.*, 1981).

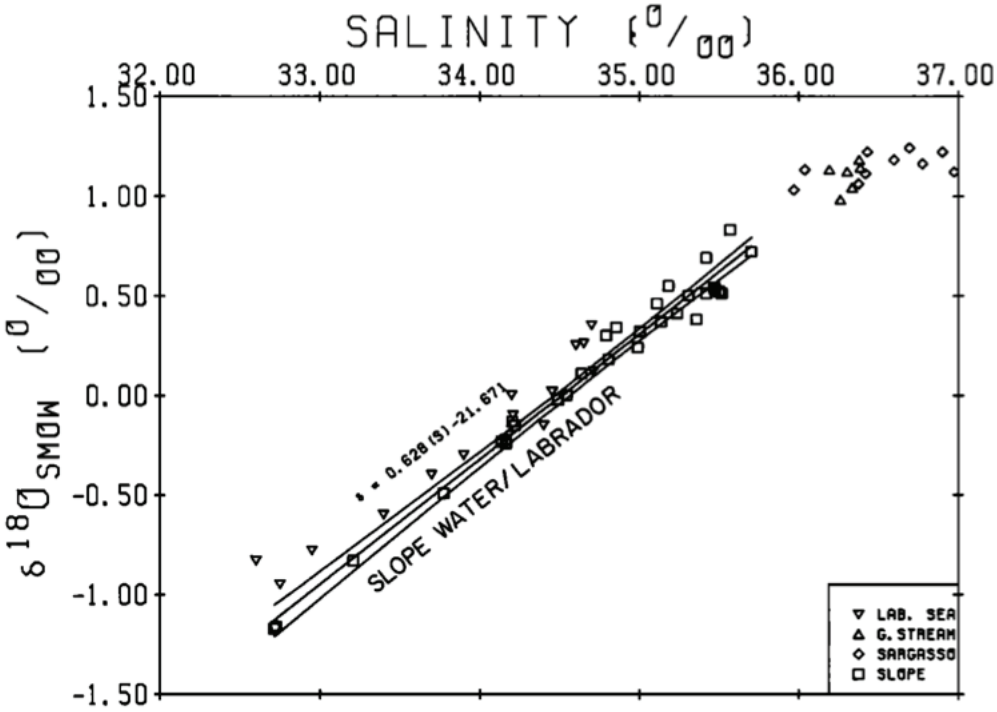

Figure 1.10: δ^{18}O-Salinity relationship for Scotian Slope and Labrador Sea water (*Fairbanks*, 1982). The linear regression line (δ^{18}O = 0.628(S) - 21.671) and 95% confidence interval are presented. Figure from *Fairbanks* (1982).

1.4 Objectives

The main goal of this study is to define the variability of δ^{18}O and salinity in Bedford Basin and its approaches, never before studied in Halifax. Once all inputs to Bedford

Basin have been identified, sampled, and analyzed, an annual cycle can be defined and the variability in these inputs (both fresh and saline) throughout the year can be identified. This study was also performed to:

- Augment the current weekly data collection in Bedford Basin [Bedford Basin Monitoring Program (BBMP)] by measuring an additional variable (δ^{18}O/δ^{2}H), never before measured in this estuary. This should augment the current understanding of Bedford Basin water mass composition, while allowing us to compare these measurements to a long-standing time series (BBMP: 1992 - present).
- Identify the main inputs of freshwater to Bedford Basin (i.e. riverine, precipitation, and/or wastewater) and define the δ^{18}O of these sources through daily, weekly, and yearly sampling. By defining the annual cycle of these inputs, it is possible to determine if these inputs are isotopically distinct from one another and thus defined as separate inputs to Bedford Basin.
- Identify the composition of offshore Scotian Shelf water to define an offshore end member (δ^{18}O and salinity) representative of water on the Scotian Shelf entering Halifax Harbour.
- Perform mass balance calculations on samples collected in Bedford Basin using the end members established in this study. This will identify and quantify the inputs to Bedford Basin and its change in water mass composition (δ^{18}O and salinity) over different seasons and depths.
- Determine if additional inputs to Bedford Basin may be present.
- Establish the freshwater inputs to Bedford Basin surface and deep waters throughout the year.
- Identify vertical intrusion events in Bedford Basin surface and deep waters using δ^{18}O measurements.

Overall, this study aims to define the composition (δ^{18}O and salinity) of Bedford Basin and its inputs. These defined inputs can be used in future studies in and around Halifax Harbour to investigate changes in water mass composition.

CHAPTER 2

METHODS

2.1 Field Sites

2.1.1 Halifax Harbour

To examine the variability in δ^{18}O and salinity in Halifax Harbour, water samples were collected between May 2012 and October 2013. Sample sites are presented in Figure 2.1, which identifies each site by its abbreviation (Table 2.1). Table 2.1 lists the site coordinates, depths sampled and number of samples collected in Halifax Harbour over this sampling period.

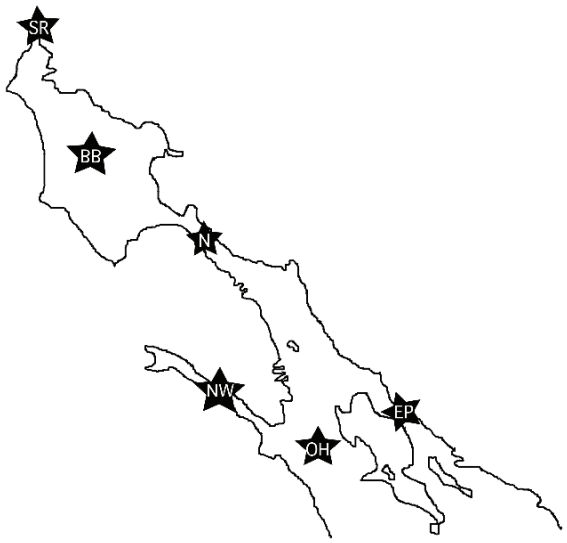

Figure 2.1: Halifax Harbour sampling locations: Sackville River (SR), Bedford Basin (BB), Narrows (N), Northwest Arm (NW), Outer Harbour (OH), and Eastern Passage (EP).

Table 2.1: Latitude and longitude (decimal degrees) of sample stations (with abbreviations) in Halifax Harbour. Depths (m) and number of samples (#) taken at each station and depth over this study (May 2012 - October 2013) are also presented.

Station	Abbrev.	Latitude	Longitude	Depth (m)	Samples (#)
Bedford Basin	BB	44.694	-63.640	1	54
				5	54
				10	54
				60	54
Eastern Passage	EP	44.622	-63.520	1	5
				10	2
				20	5
Narrows	N	44.673	-63.596	1	5
				10	2
				20	5
Northwest Arm	NW	44.633	-63.600	10	25
Outer Harbour	OH	44.6120	-63.543	1	5
				10	2
				20	5
Sackville River	SR	44.739	-63.655	1	17

2.1.2 Scotian Shelf

Samples from Atlantic Zone Monitoring Program (AZMP) cruises, collected in October 2008 and April 2009 by Helmuth Thomas' group at Dalhousie University (Helmuth Thomas, *personal communications*), were used in this analysis to represent offshore water entering Halifax Harbour. The position of these sites on the Scotian Shelf are presented in Figure 2.2, with the Halifax Line (HL) identified. When the coordinates were plotted, one station (HL-3) was found to the west of the sampling line, off this transect. Since the coordinates of HL-3 were identical in both sample years (October 2008 and April 2009), it was assumed that this offset was not due to sampling difficulties or a diversion off course. Instead, this offset is likely due to an error in recording coordinates, rather than the actual position of the ship. When compared with the Halifax Line coordinates from other AZMP cruises, HL-3 is found along the Halifax Line transect, so to correct for this error in recording, HL-3 coordinates from another AZMP cruise were substituted in this analysis (Table 2.2).

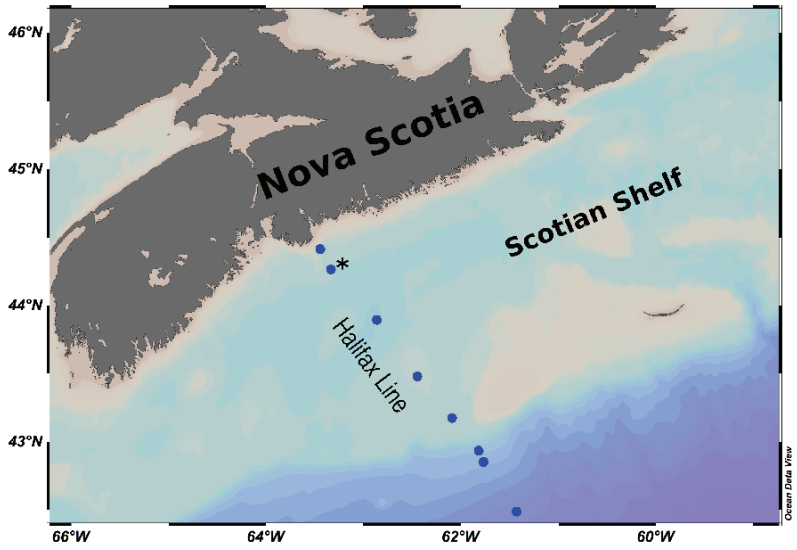

Figure 2.2: Halifax Line AZMP sample sites in October 2008 and April 2009, with HL-1 located closest to shore. HL-2 is identified with a "*".

Table 2.2: Recorded and replaced longitude and latitudes (decimal degrees) for Station HL-3 on the Halifax Line, from AZMP cruises in October 2008 and April 2009.

	Recorded Coordinate	**Replaced Coordinate**
Latitude	43.880	43.894
Longitude	-63.881	-62.864

2.2 Halifax Harbour Water Sampling

2.2.1 Bedford Basin

Bedford Basin water samples (44.694 N, 63.640 W) were collected weekly, from the Canadian Coast Guard Ship (CCGS) *Sigma T*[1], at the deepest part of Bedford Basin ($\sim$ 71 m) in conjunction with the Bedford Basin Monitoring Program (BBMP)[2]. Any variability in station position was due to drifting of the ship over time. When movement away from the station was evident, sampling was paused, and the ship was returned to the station. As Bedford Basin is sheltered, minimal ship movement occurred while sampling was taking place, so repositioning of the ship only took place a few times over the entire collection period (May 2012 - October 2013).

A Niskin bottle was used to collect water at 1, 5, 10, and 60 m; water collected at each depth was transferred to a 4 L Nalgene bottle, before being brought back to Dalhousie University. These large Nalgene bottles were placed in a cooler during transport, and upon arrival, transferred into glass bottles. Samples for δ^{18}O/δ^{2}H and salinity analysis were collected in 60 ml and 250 ml amber glass (Boston Round) bottles, respectively. These bottles were sealed using a phenolic cap with a polyethylene (PE) cone liner, and wrapped with electrical tape to prevent evaporation during storage. Samples for δ^{18}O/δ^{2}H analysis were placed in a fridge (4°C), while salinity samples were stored in the laboratory until analysis could take place. Storage ranged from a few days to one month for δ^{18}O/δ^{2}H, and up to 3 months for salinity. Following analysis, samples were re-capped, taped, and stored in a walk-in fridge (4°C) ensuring minimal evaporation, in case these samples needed to be analyzed additionally. Depth profiles of temperature and salinity in Bedford Basin were also measured with a CTD system as part of the BBMP.

[1]CCGS *Sigma T* Vessel Information: http://www.ccg-gcc.gc.ca/Fleet/Vessel?vessel_id=96
[2]BBMP: http://www.bio.gc.ca/science/monitoring-monitorage/bbmp-pobb/bbmp-pobb-eng.php

2.2.2 Sackville River

Samples were collected by lowering a bucket into Sackville River from a pedestrian bridge located 1.2 km from the mouth of the river. The bucket was rinsed with water three times before a surface sample was collected and directly transferred into 60 ml and 250 ml glass sample bottles. Historical water level data were collected using a continuous gauge recorder operated by Environment Canada and accessible from the "Real-time Hydrometric Database" (*Environment Canada*, 2013). The continuous gauge recorder is connected to an orifice line buried on shore and anchored to a concrete block on the river bed (Guy Leger, *personal communications*). Water levels are collected throughout the year, but in winter discharges are adjusted due to the backwater effect caused by ice (Guy Leger, *personal communications*).

2.2.3 Halifax Harbour

Additional samples were collected from sites around Halifax Harbour - Narrows (N), Outer Harbour (OH), and Eastern Passage (EP) - to augment the Bedford Basin samples collected once a week, and to further illustrate the movement of water through this estuary (Figure 2.1). These samples were collected five times over this study period (May 2012 - October 2013) using a Niskin bottle deployed from the Department of Oceanography's zodiac. Water was collected at 1, 10 and 20 m at all three sites, and directly transferred from the Niskin bottle into δ^{18}O/δ^{2}H and salinity glass sample bottles to reduce any evaporation during transport.

2.2.4 Northwest Arm

Samples were collected from the Northwest Arm seawater intake line, which supplies the Department of Oceanography Aquatron at Dalhousie University. This water is collected at $\sim$10 m depth in the Northwest Arm, filtered and stored in a large tank, where it is supplied throughout the Life Sciences Centre (LSC) building. Since a time lag may occur between the time this water is collected and the time a sample from the intake line is taken, the isotopic composition (δ^{18}O/δ^{2}H) of a sample from the intake line was compared to a Northwest Arm grab sample. A surface grab sample ($\sim$1 m) was taken as a deeper sample could not be collected at the time. A comparison between this surface sample and one collected from the intake line on the same day can be seen in Table 2.3. The offset between

Table 2.3: "Intake Line" compared with "Grab" samples for the Northwest Arm (June 21, 2012).

Description	**Depth (m)**	δ^{18}**O (‰)**	δ^{2}**H (‰)**
Grab Sample	1	-1.79	-12.82
Intake Line	10	-1.77	-12.61

the two samples, 0.02‰ for δ^{18}O and 0.21‰ for δ^{2}H, is within the precision of the Picarro L2130-i isotopic water analyzer used in this study (0.05‰ for δ^{18}O and 0.3‰ for δ^{2}H). We therefore assume that intake line samples are representative of water in the Northwest Arm at the time of sampling, so all subsequent Northwest Arm samples in this analysis were collected through the intake line.

2.2.5 Wastewater

Wastewater samples were collected at the five major wastewater treatment facilities (WWTFs) in Halifax: Herring Cove, Halifax, Mill Cove, Dartmouth, and Eastern Passage (Figure 1.5). Samples were collected from outflowing, treated water, which should best-represent wastewater entering Halifax Harbour. Due to differences in the operation of the WWTFs, samples were placed in either Nalgene or glass bottles before being transferred to Dalhousie University, where all samples were stored in 60 ml glass bottles.

2.2.6 Sampling Uncertainty

A number of experiments were performed to quantify the uncertainty in δ^{18}O and δ^{2}H associated with sampling. First, the variability in Bedford Basin δ^{18}O and δ^{2}H within the 4 L sample bottles brought back to Dalhousie University was examined. Three 60 ml (1, 2, 3) glass sample bottles were filled with water from each 4 L Nalgene bottle (1 and 60 m). Before analysis took place, three 2 ml (.1, .2, .3) vials were then filled with water from each of the three 60 ml glass sample bottles (Table 2.4). The nine resulting water samples for each depth (1 and 60 m) were analyzed on the Picarro L2301-i isotopic liquid isotope analyzer to determine the range in δ^{18}O and δ^{2}H associated with a 4 L sample of Bedford Basin water. By determining this range, it is possible to factor in this sampling uncertainty with the precision of the instrument (0.05‰ for δ^{18}O and 0.3‰ for δ^{2}H). This experiment was performed on water collected at both 1 and 60 m, as water at 1 m may be more isotopically variable due to strong inputs of freshwater from land (Table 2.4).

Table 2.4: Variability in δ^{18}O and δ^{2}H of two 4 L (1 & 60 m) Bedford Basin water samples collected on July 11, 2013. Three 60 ml sample replicates (1, 2, 3) were filled with water from each 4 L water sample, and three 2 ml replicates (.1, .2, .3) were then filled from each 60 ml sample. Averages and standard deviations are included.

Depth	**Vial**	δ^{18}**O (‰)**	**Average**	**St. Dev.**	δ^{2}**H (‰)**	**Average**	**St. Dev.**
1 m	1.1	-2.17			-15.33		
	1.2	-2.11			-14.94		
	1.3	-2.10	-2.13	0.036	-14.99	-15.09	0.210
	2.1	-2.12			-14.78		
	2.2	-2.14			-14.93		
	2.3	-2.11	-2.13	0.012	-14.89	-14.87	0.075
	3.1	-2.17			-14.99		
	3.2	-2.17			-14.91		
	3.3	-2.16	-2.16	0.007	-15.06	-14.99	0.074
Total			-2.14	0.027		-14.98	0.152
60 m	1.1	-1.75			-12.74		
	1.2	-1.65			-12.25		
	1.3	-1.69	-1.70	0.050	-12.24	-12.41	0.286
	2.1	-1.64			-11.98		
	2.2	-1.65			-11.97		
	2.3	-1.71	-1.67	0.036	-12.03	-11.99	0.029
	3.1	-1.65			-11.87		
	3.2	-1.69			-11.96		
	3.3	-1.67	-1.67	0.020	-11.87	-11.90	0.053
Total			-1.68	0.035		-12.10	0.278

All of the measurements of these replicates are within the stated instrumental precision (0.05‰ for δ^{18}O and 0.3‰ for δ^{2}H), given by Picarro Inc., the manufacturer of this instrument. No significant difference in δ^{18}O or δ^{2}H was found between different samples taken from the same 60 ml bottle (.1, .2, .3), or from the same 4 L bottle (1, 2, 3) (Table 2.4). As a result, the measurement uncertainty associated with sub-samples of δ^{18}O and δ^{2}H from the same seawater sample (e.g. a 4 L bottle of Bedford Basin water) is not a source of error in this study.

Halifax Harbour samples (BB, N, OH, and EP), collected with Niskin bottles, were transferred into Nalgene bottles (1 to 4 L) before a 60 ml glass sample bottle was filled. This adds an additional step that increases the risk for evaporation in these samples, which may alter δ^{18}O and δ^{2}H. To determine the effect of transferring on the isotopic composition of water samples, 60 ml sub-samples were transferred immediately from a Niskin bottle ("Niskin") and from a 1 L Nalgene bottle (filled from the Niskin bottle) 2 - 4 hours after the original Niskin bottle sampling ("Bottle") (Table 2.5).

Table 2.5: "Niskin" samples were sub-sampled from the Niskin bottle, while "Bottle" samples were first transferred into a 1 L Nalgene bottle before a sample was collected (2 - 4 hours later).

Site	**Depth (m)**	**Niskin δ^{18}O (‰)**	**Bottle δ^{18}O (‰)**
Narrows	1	-1.62	-1.63
	20[†]	-1.55	-1.61
Outer Harbour	1	-1.55	-1.53
	20	-1.54	-1.52
Eastern Passage	1	-1.62	-1.59
	20	-1.59	-1.57

[†] Difference greater than stated instrumental precision (0.05‰)

All differences in δ^{18}O (Table 2.5) are within the stated instrument precision (0.05‰ for δ^{18}O), with the exception of water collected at 20 m depth in the Narrows (0.06‰). This greater difference may be a result of slight evaporation, or a difference in the δ^{18}O of these two samples. Despite this, it was decided that these two collection/transfer methods did not affect δ^{18}O systematically and therefore the method of collection ("Niskin" vs. "Nalgene") will not impact this analysis. Further, if evaporation was affecting the isotopic composition of water through this transfer step, all "Niskin" samples should be isotopically depleted (-δ), and all "Bottle" samples should be isotopically enriched (+δ), however this

is not the case.

2.3 Offshore Water Sampling

2.3.1 Glider and Station 2

Glider and Station 2 water samples were collected during instrument deployment or recovery. "Glider" samples were collected at the entrance to Halifax Harbour when the Teledyne Webb Research Slocum electric gliders, operated by the Ocean Tracking Network (OTN), were deployed or recovered, however the exact location varied with each trip. Station 2 samples were collected at the AZMP sample site "HL-2" on the Halifax Line, identified by a "*" in Figure 2.2. These samples were collected at various depths using a Niskin bottle and transferred into large Nalgene bottles (between 1 and 4 L), before being brought back to Dalhousie University.

2.3.2 Atlantic Zone Monitoring Program (AZMP) Stations

Measurements of Halifax Line δ^{18}O, temperature and salinity were made on the CCGS *Hudson* as part of the AZMP[3] cruises in October 2008 and April 2009, with 73 and 63 samples collected respectively. Seawater samples were collected from 20 L Niskin bottles, mounted on a General Oceanic 24-bottle rosette, and fitted with a conductivity, temperature and depth sensor (CTD, SeaBird). Water samples were collected at each site and sample depth for isotopic analysis (δ^{18}O and δ^{2}H); these samples were processed at the University of Ottawa using an isotope ratio mass spectrometer (IRMS). These AZMP samples were provided by Dr. Helmuth Thomas at Dalhousie University (Helmuth Thomas, *personal communications*).

2.4 Precipitation Sampling

Precipitation samples were collected from June 2012 to October 2013 in order to examine the variability in δ^{18}O and δ^{2}H of precipitation in Halifax, Nova Scotia.

2.4.1 Rainfall Sampling

A 500 ml pyrex bottle with a large funnel ($\sim$135 mm in diameter) was used to collect rainwater samples over the course of this study (Figure 2.3). The collection bottle was

[3]For details of the AZMP: http://www.meds-sdmm.dfo-mpo.gc.ca/isdm-gdsi/azmp-pmza/index-eng.html

Figure 2.3: 500 ml sample bottle used to collect rainwater over the course of this study. Funnel diameter is ∼135 mm.

placed on the roof of the Oceanography building at Dalhousie University, away from any potential sources of contamination (other buildings, trees, etc.). Samples were typically collected in the morning (8:00 - 10:00), from Monday to Friday. On occasion a sample would be collected later in the day, following the cessation of a rainfall event. This was done to collect samples representative of a single rainfall event, rather than splitting an event into multiple samples. However, if a significant amount of rain fell over a longer time period, samples were collected throughout the rainfall event to limit any potential for evaporation or overflow. Samples were left on the roof from ∼ 17:00 on Friday to ∼ 9:00 the following Monday. This collection method was developed based on *Peng et al.* (2004), with daily collection during the week and no collection between Friday evening and Monday morning.

Following the collection of rainfall from a precipitation event, a 60 ml amber glass bottle was filled, capped, taped and placed in the fridge. The volume of the remaining sample was measured and then transferred into a large (1 L) glass bottle, containing all of the precipitation samples from that month. The δ^{18}O, δ^{2}H, and volume of each precipitation event were recorded to calculate amount-weighted averages, discussed in Section 2.4.3.

2.4.1.1 Evaporation Test

A test was performed in the laboratory to determine the effect of evaporation on precipitation samples. *Craig et al.* (1963) found that evaporation rates in laboratory experiments

were comparable to rates from open-air experiments, and as such, these test results should be indicative of any evaporation in the precipitation samples. In addition, by performing this evaporation test in the lab, it prevents any addition of precipitation (that would alter the water's isotopic composition), and ensures stable air temperature. This evaporation test can be used to establish a potential rate of evaporation (mg/cm^2·hr) and fractionation of δ^{18}O and δ^2H associated with the precipitation samples collected in this study.

For the purpose of this study, it is assumed that external conditions in Halifax were similar to laboratory conditions. Although *Gat* (1996) found that differences in air temperature and relative humidity will affect the evaporation of water, changes in these factors were not considered. Higher air temperatures lead to increased evaporation; to incorporate the fact that changes in temperature could not be considered within this test, if substantial evaporation was believed to have occurred before precipitation samples were collected, they were not included in the final analysis (i.e. samples were not collected on a hot (30°C) day).

Five 60 ml and five 250 ml bottles were filled with tap water and left uncovered in the laboratory over the course of this experiment. Sample bottles were used in lieu of the precipitation collection bottle as there was only one collection bottle, and the results using sample bottles will be comparable. Understanding the effect of evaporation on different volumes of water is essential, as the volume of precipitation collected during each rainfall event over this study ranged from 60 to 1100 ml. To get an accurate measurement of the volume of water present in each sample before and after collection, samples were weighed using a laboratory scale, significant to 0.01 g. All of the sample bottles were left uncovered in the laboratory for 0, 1, 2, 5 or 8 days, and then weighed again. The difference (Δ) in weight represents the water that has evaporated over this time period (Table 2.6).

Following *Craig et al.*'s 1963 study, the evaporation rate (E) was calculated by taking the change in sample weight (mg) over the area available for evaporation (cm^2) and the time in which evaporation has taken place (hr) (Equation 2.1). The water samples were filled to the neck of the sample bottles; as a result, the total area in which this evaporation can take place was calculated by taking the surface area of the bottleneck (πr^2). Surface areas of 3.14 cm^2 and 4.15 cm^2 were calculated for the 60 and 250 ml bottles respectively.

$$E = \frac{\Delta \text{Weight}}{A \cdot \Delta T} \tag{2.1}$$

Table 2.6: Evaporation (E) test results for 60 and 250 ml samples. F (%) is the fraction of water left in the bottle after evaporation has taken place, calculated by measuring the change (Δ) in sample weight. To calculate E, bottleneck diameter is used as area (cm^2).

Volume	**ΔT**	**ΔWeight (g)**	**F (%)**	**δ-$\delta^{\circ}[\delta^{2}H]$**	**δ-$\delta^{\circ}[\delta^{18}O]$**	**E (mg/cm^2·hr)**
60 ml	0	-	100	-	-	-
	24	0.14	99.89	-0.057	0.020	1.86
	48	0.25	99.80	0.094	0.101	1.66
	120	0.59	99.52	0.670	0.317	1.57
	192	1.01	99.17	1.373	0.550	1.67
250 ml	0	-	100	-	-	-
	24	0.30	99.94	0.107	0.005	3.01
	48	0.63	99.86	0.266	0.018	3.16
	120	1.43	99.69	0.515	0.087	2.87
	192	2.39	99.48	1.062	0.269	3.00

As time progresses, more evaporation takes place and the total surface area available for evaporation increases. At the start of the experiment the bottle was filled just up to the neck. To examine the effect of different surface areas on the evaporation rate (mg/cm^2·hr), evaporation rates for the 60 ml samples on "Day 8" were calculated using the minimum and maximum potential surface areas, the bottleneck (Equation 2.2), and width of the bottle (Equation 2.3).

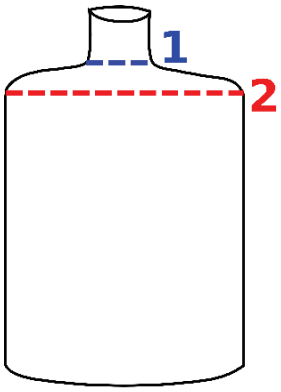

$$E_1 = \frac{1010\text{mg}}{3.14\text{cm}^2 \cdot 192\text{hr}}$$
$$E_1 = 1.67\text{mg/cm}^2 \cdot \text{hr} \qquad (2.2)$$

$$E_2 = \frac{1010\text{mg}}{13.20\text{cm}^2 \cdot 192\text{hr}}$$
$$E_2 = 0.398\text{mg/cm}^2 \cdot \text{hr} \qquad (2.3)$$

Depending on the surface area (A), the rate of evaporation (E) changes (Equations 2.2 and 2.3). Under the same laboratory conditions, water in a 250 ml glass bottle had a greater evaporation rate when compared with water in a 60 ml glass bottle (Table 2.6). This

increase in the rate of evaporation is directly related to the area available for evaporation to take place, meaning that under stable conditions, area drives the evaporation rate (E). In the laboratory, where conditions (e.g. temperature or humidity) are stable, the evaporation rate of a sample should not vary greatly, as seen in this experiment (Table 2.6).

The exact change in surface area over time was not measured throughout the experiment due to difficulties in accurately measuring bottle diameter. As a result, the minimum surface area (bottleneck diameter) was always used to calculate the evaporation rate, while noting the error associated with this selection. The evaporation rate presents the continuous evaporation of water, however it is the fraction of water left in the bottle (%), driven by evaporation, that affects δ^{18}O and δ^{2}H.

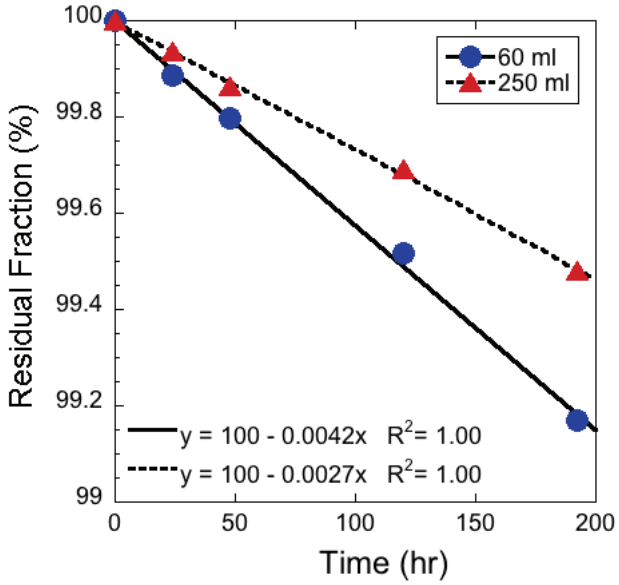

Figure 2.4: Change in residual fraction of water (%) with time, as a result of evaporation.

The fraction of water (%) remaining in these water samples over time, as a result of evaporation, is calculated using Δ weight (Figure 2.4). Evaporation changes the isotopic composition of water, as residual water is progressively enriched in the heavier isotope (^{18}O or ^{2}H). Figure 2.5 illustrates the variability in δ^{18}O (Figure 2.5(a)) and δ^{2}H (Figure 2.5(b)) in the 60 and 250 ml samples with the change in the residual fraction (%) of water. Assuming that any evaporation in our precipitation samples would take place under similar conditions to this laboratory test, we can calculate the enrichment in δ^{18}O and δ^{2}H over time, as a result of evaporation. This assumption of stable conditions leads to an additional source of error in this evaporation test. It is also assumed that evaporation would only

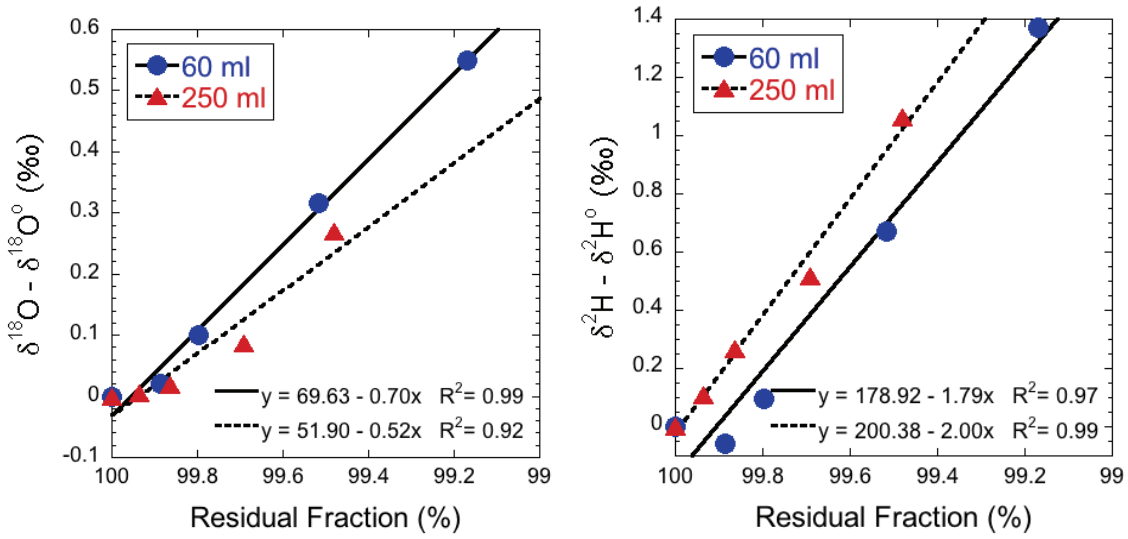

(a) δ^{18}O (b) δ^{2}H

Figure 2.5: Change in (a) δ^{18}O and (b) δ^{2}H with evaporation for 60 ml and 250 ml samples.

affect the isotopic composition of water following the cessation of a precipitation event, up until the time of collection.

Although a greater rate of evaporation (E) was calculated for the 250 ml evaporation tests (Table 2.6) as a result of increased area, the variability in δ^{18}O and δ^{2}H (δ - δ°) associated with the residual fraction of water is smaller in the 250 ml samples (Figure 2.5). The greater volume of water (250 ml) results in the loss of a smaller fraction of water (%) with evaporation, resulting in a more gradual enrichment in δ^{18}O and δ^{2}H over time.

2.4.1.2 Rainfall Sampling Uncertainty

Based on the evaporation tests and sampling techniques presented above, it is possible to estimate an error associated with rainfall sampling. There is an enrichment in δ^{18}O and δ^{2}H with evaporation over time (Table 2.6). As the majority of samples were collected less than a day after the cessation of a precipitation event, the sampling error is less than the instrumental precision guaranteed by Picarro (0.05‰ for δ^{18}O and 0.3‰ for δ^{2}H).

It should be noted that a depletion in δ^{2}H (δ-δ°[δ^{2}H]) can be seen after 24 hours in the 60 ml sample, rather than the expected enrichment due to evaporation (Figure 2.5(b)). This depletion is likely a result of the analytical uncertainty associated with δ^{2}H measurements in this thesis, as the depletion in δ^{2}H (0.057‰) is less than the measurement precision associated with the Picarro WS-CRDS isotopic water analyzer (0.3‰) (Table 2.6). This

Table 2.7: Calculated δ^{18}O and δ^{2}H enrichment in samples after 72 hours.

Enrichment (‰)	**60 ml**	**250 ml**
δ^{18}O	0.18	0.07
δ^{2}H	0.38	0.37

error, associated with sampling uncertainty, emphasizes the small effect of evaporation on the isotopic composition of water over a few (1-2) days.

However, after 8 days, an enrichment in δ^{18}O of 0.55‰ in 60 ml and 0.27‰ in 250 ml, and an enrichment in δ^{2}H of 1.37‰ in 60 ml and 1.06‰ in 250 ml bottles can be seen (Table 2.6). Although this emphasizes a significant (greater than the instrumental precision) increase in δ^{18}O and δ^{2}H due to evaporation, the longest time a sample was left on the roof following the completion of a precipitation event was 3 days. Therefore, the results of these evaporation tests can be used to determine the maximum possible change in δ^{18}O and δ^{2}H as a result of evaporation in this study.

The residual fraction (%) of water in a sample (60 or 250 ml) after 72 hours can be calculated using the linear regression equation determined in Figure 2.4. Once this has been calculated, the enrichment in δ^{18}O and δ^{2}H can be determined using the linear regression equations in Figures 2.5(a) and 2.5(b) respectively. These calculated enrichment values (Table 2.7) are greater than the guaranteed precision of the instrument (0.05‰ for δ^{18}O, 0.3‰ for δ^{2}H), so they will be factored into the final analysis.

Delayed precipitation collection (>1 day) occurred once a month (or less) during this study. To determine the impact of "evaporation-correction" on monthly and yearly amount-weighted averages of δ^{18}O, the average δ^{18}O for July 2013 was calculated "before" and "after" factoring in the potential enrichment in δ^{18}O due to evaporation. Between June 28^{th} and July 2^{nd} of 2013, the precipitation sample bottle was left on the roof to collect rainfall. To look at the maximum potential effect of evaporation on δ^{18}O of this sample, it was assumed that evaporation was possible over four days, and an enrichment of 0.102‰ (δ^{18}O) was calculated. To remove the effect of evaporation on this sample (July 2^{nd}), 0.102‰ was subtracted from the measured δ^{18}O value, -3.46‰.

First, the average amount-weighted δ^{18}O value for July 2013 was calculated with this "evaporation-corrected" δ^{18}O value for July 2^{nd}. When this value is included in the monthly average amount-weighted δ^{18}O calculation for July 2013, a value of -4.95‰ is calculated,

compared with -4.91‰ when evaporation is not considered. The difference in these amount-weighted monthly averages is less than the guaranteed instrumental precision (0.05‰ for δ^{18}O). In addition, when this "evaporation-corrected" value is used to calculate the annual amount-weighted yearly average of δ^{18}O (August 1^{st} to July 31^{st}), and compared to the annual average calculated when evaporation is not considered, the same value (-7.01‰) is found. As such, it is assumed that factoring in the effect of evaporation on the precipitation samples will not impact the final analysis and thus samples were not corrected for the effect of evaporation on δ^{18}O and δ^{2}H.

2.4.2 Snow Sampling

The rainfall sampling technique presented above could not be adapted for snow collection, as snow became trapped in the funnel. Based on sampling techniques outlined by the *University of Colorado: Institute of Arctic and Alpine Research* (2005), a bucket weighed down with rocks and lined with plastic was placed on the roof of the Department of Oceanography building to collect snowfall from January to April 2013. Falling snow can be strongly influenced by the wind, leading to inconsistent snowfall accumulation amounts in the collection bucket (*Motoyama et al.*, 2005). The inconsistency in the amount of snowfall collected during a single event meant that some of these samples could not be amount-weighted. This occurred on three occasions in February 2013, when large snow drifts were present on the roof and the collection of snow in the bucket was not representative of the amount of snow that fell.

Once the snow was collected, and before it could melt, the samples were brought into the laboratory and transferred to 1 L Nalgene bottles. These bottles were capped, taped and then placed in the fridge to allow the snow to melt gradually. This was done to reduce any sublimation and fractionation associated with the melting process. Once the snow was melted, the volume of water was recorded and a sample of the melt water was transferred into a 60 ml glass bottle for δ^{18}O and δ^{2}H analysis. Any remaining melt water was added to the total monthly precipitation sample bottle (with the exception of the three snowfalls that could not be amount-weighted).

To examine the isotopic variability within a single snowfall event ("Test 1"; Table 2.8), two separate samples (1 & 2) were collected during a single snow storm. "Sample 1" was collected from the bottom of the collection bucket and represents the earlier snowfall during this event, while "Sample 2" represents the later snowfall and was collected from

Table 2.8: Tests illustrating how δ^{18}O and δ^{2}H during a snowfall event can vary. "Test 1" presents the difference between two samples collected at different times during the same snowfall event, while "Test 2" outlines the effect of melting on snow.

Test 1			**Test 2**		
Description	δ^{18}**O (‰)**	δ^{2}**H (‰)**	**Description**	δ^{18}**O (‰)**	δ^{2}**H (‰)**
Sample 1	-10.31	-66.03	Pre-melt	-13.25	-87.07
Sample 2	-12.11	-80.49	Post-melt	-11.16	-68.50

the top of the bucket (Table 2.8). The second sample of snow is more isotopically depleted than the first, which aligns with *Dansgaard* (1964)'s "amount effect". During a large storm event, precipitation becomes progressively depleted as more isotopically enriched precipitation is rained out first (Section 3.1.1.1). This isotopic variability illustrates the need to collect precipitation from the entire collection bucket to determine representative δ^{18}O and δ^{2}H values.

δ^{18}O and δ^{2}H of snow is modified by the melting process as it undergoes kinetic fractionation, similar to evaporation, indicating mass exchange between vapour and snow (*Clark and Fritz*, 1997). Both *Cooper* (1998) and *Taylor et al.* (2001) have illustrated the effects of isotopic fractionation in melt water. *Blasch and Bryson* (2007) allowed frozen samples to thaw completely at room temperature before any samples were collected to eliminate the effects of fractionation between phases (i.e. re-freezing and melting). To examine the effect of melting and temperature on δ^{18}O and δ^{2}H of snow ("Test 2"), samples were collected "pre-melt" and "post-melt" during a snowfall event on February 4, 2013 (Table 2.8). For the "pre-melt" sample, snow was immediately collected and placed in a 1 L Nalgene bottle, capped, taped and left in the fridge to thaw. The rest of the snow was left in the collection bucket (indoors) and allowed to melt at room temperature; once this snow had melted, a 60 ml sample of melt water was collected. The snow left to melt at room temperature in the bucket (collected "post-melt") was found to be more isotopically enriched than the samples of snow collected immediately, "pre-melt" (Table 2.8). This may illustrate the isotopic enrichment of melt water, due to kinetic fractionation, and supports the need to sample snow before thawing begins, in order to more gradually melt this snow in the fridge, minimizing the effects of fractionation between phases.

In addition, the variability between the "pre-" and "post-melt" samples also outlines how thawing and re-freezing before collection may result in an isotopic composition that is different from the snow that fell, adding a source of error to snowfall samples (*Clark and Fritz*, 1997; *Zhou et al.*, 2008). Although the variability in a single snowfall event can lead to isotopic variability, illustrated through "Test 1", the isotopic enrichment of the melted ("post-melt") sample suggests that kinetic fractionation has occurred within the sample as a result of melting, and not the "amount effect". Based on the results of "Test 2", snowfall samples were collected immediately following a storm, before any melting could occur.

Due to the relatively few snowfall events (9) over this sampling period, any potential error associated with sampling snow should not affect the average amount-weighted δ^{18}O and δ^{2}H values determined for Halifax.

2.4.3 Amount Weighting of Precipitation

Amount-weighted averages were calculated for monthly and yearly precipitation as both the number of precipitation events and the amount of precipitation that falls in a single event are variable. Since the amount of precipitation in these events was extremely variable ($\sim$50 to 1200 ml), averaging the δ^{18}O and δ^{2}H of individual samples without amount-weighting the data would bias any averages. These calculations were performed using the R functions: wt.mean(x, wt) and wt.sd(x, wt) from the package SDMTools. To perform this amount-weighting, the total amount of precipitation measured from each event was defined as "wt" and δ^{18}O or δ^{2}H measurements were defined as "x". The following equation was used to perform the amount-weighted averages ($\bar{x}$) of δ^{18}O and δ^{2}H for years, months and seasons.

$$\bar{x} = \frac{\sum_{i=1}^{N}(wt_i \cdot x_i)}{\sum_{i=1}^{N}(wt_i)}$$

The standard deviations for these amount-weighted monthly averages were calculated using the function wt.sd(x,wt).

2.4.3.1 Justification of the Amount-Weighting Technique

To test this approach to amount-weight monthly samples, all of the samples from each precipitation event in a month were collected and placed into a 1 L bottle(s) and then

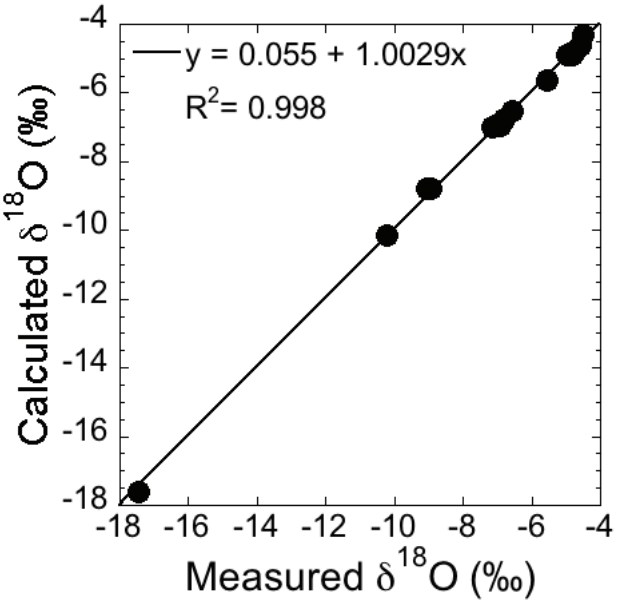

Figure 2.6: "Calculated" vs. "measured" average amount-weighted monthly δ^{18}O of precipitation in Halifax (June 2012 - Oct 2013).

mixed to create one representative 60 ml precipitation sample for a single month. This 60 ml monthly sample ("measured") was then analyzed using the Picarro L2301-i isotopic water analyzer and the monthly δ^{18}O and δ^{2}H averages were compared to the "calculated" amount-weighted averages for each month. The "measured" and "calculated" averages of monthly δ^{18}O for the 16 months in this study were not significantly different, with an r^2 value of 0.998 (Figure 2.6). Since there is no significant difference between the "measured" and "calculated" values, the calculated amount-weighted averages will be used in this analysis.

2.5 δ^{18}O and δ^{2}H Measurements

The δ^{18}O and δ^{2}H of each sample (60 ml) collected in this study was measured using the CERC.OCEAN Picarro L2301-i isotopic water analyzer. This WS-CRDS (wavelength-scanned cavity ring down spectroscopy) isotope analyzer vapourizes liquid water samples and, using light from a tunable laser, measures its isotopic composition. The measurement precision associated with this instrument is 0.05‰ for δ^{18}O and 0.3‰ for δ^{2}H, guaranteed

by Picarro[4].

Figure 2.7: Picarro L2301-i WS-CRDS isotopic water analyzer used in this study.

2.5.1 Cavity Ring-Down Spectroscopy

The Picarro L2301-i isotopic water and vapour analyzer (Figure 2.7) utilizes wavelength-scanned cavity ring down spectroscopy (WS-CRDS) to measure the optical absorption spectrum of gases to determine stable isotope composition. This high precision isotopic water (δ^{18}O and δ^{2}H) analyzer utilizes an A0211 high precision vapourizer and an HTC-xt Leap Pal Technologies autosampler. The autosampler injects liquid water samples (both fresh and saline) into a vapourizer (140°C), which converts samples into water vapour, and then a gas-phased instrument measures the concentration and isotopic content of water in vapour form (*Gupta et al.*, 2009). During this process, salts can build-up in the vapourizer, increasing the memory effect and decreasing precision. The impact of this "memory effect" on measurements, and how it is improved with vapourizer cleaning, will be further discussed in Section 2.5.5.

Until recently, stable isotope analysis has been an expensive gas-based technique, using gas-source isotope ratio mass spectrometry (IRMS) (*Munksgaard et al.*, 2011). Because

[4] https://picarro.app.box.com/s/egtr6oileur5qt74ly7v

of this, fewer isotopic measurements have been performed, as they relied on IRMS in a laboratory setting, eliminating the possibility of real-time field use (*Gupta et al.*, 2009). Over recent years, laser spectroscopy water isotope analyzers have become more advanced, portable and practical for use in the field and lab (*Gupta et al.*, 2009), and commercially available, bench-top CRDS systems have allowed for an increase in isotopic measurements.

CRDS instruments use absorption spectroscopy, with an infrared laser, to quantify different isotopologues of water (δ^{18}O and δ^{2}H) (*OKeefe and Deacon*, 1988; *Munksgaard et al.*, 2012). This works under the principle that every small gas-phased molecule (i.e. H_2O) has a unique, near-infrared, absorption spectrum that can be measured using this laser-based technology.

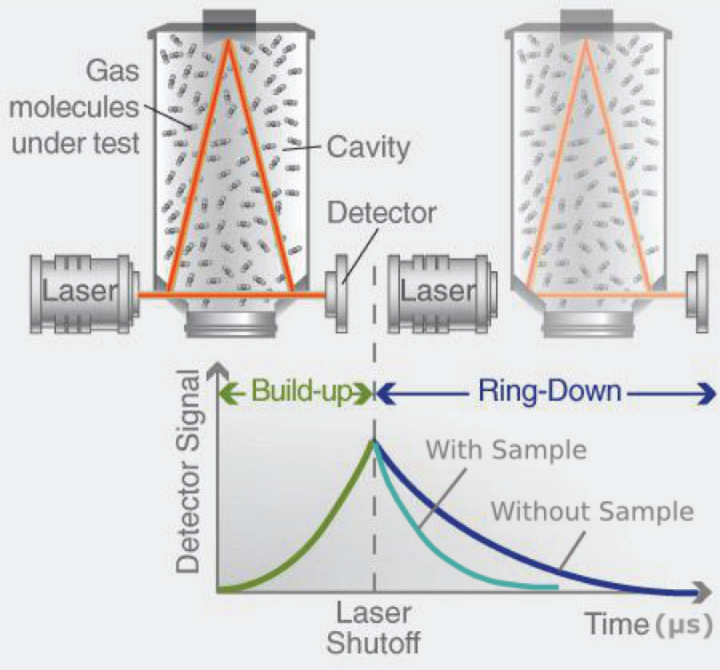

Figure 2.8: Schematic of cavity ring-down spectroscopy in the Picarro L2301-i isotopic water analyzer. The change in ring-down time with a sample (i.e. H_2O) (light blue) and without (dark blue) is depicted. This image was modified from *Picarro* (2014).

The concentration of a species can be determined by measuring the strength of absorption, or the specific absorption-peak height (*Picarro*, 2014). A beam from a single-frequency laser diode enters a cavity defined by three highly-reflective mirrors, which supports a continuous traveling light wave that circulates throughout the cavity (*Picarro*, 2014). In the Picarro L2301-i isotopic water analyzer, three mirrors create a path length of

over 20 km (from a cavity of only 25 cm), allowing gases to be measured in seconds or less (Figure 2.8).

When the photo-detector reaches a threshold, the laser is turned off; the light inside the chamber continues to bounce off the mirrors while the light intensity decays to 0 in an exponential fashion (*Picarro*, 2014). This decay, or "ring-down", of light is measured in real time, and the amount of time it takes for the cavity to empty is determined using the reflectivity of the mirrors (*Picarro*, 2014). If there is a gas species inside the chamber that absorbs this light (i.e. H_2O vapour) then there is a second loss mechanism that accelerates the ring-down time (*Picarro*, 2014). This instrument can then directly compare the ring-down time of the cavity with and without the absorption of H_2O gas. So, the final concentration determined using this instrument is derived from the distance between ring-down times, meaning that it is independent of the laser intensity or power (*Picarro*, 2014). This technique is described in Figure 2.8, with the change in ring-down time with a sample (i.e. H_2O vapour), and without.

The δ^{18}O of seawater has been historically measured using IRMS, a complex procedure with numerous laboratory-based steps, however with the advent of laser spectroscopic (i.e. CRDS) bench-top isotope analyzers, such as the Picarro L2130-i, high spatial-resolution stable isotope measurements can now be performed (*OKeefe and Deacon*, 1988). However, with a number of groups (including this thesis work) presently using CRDS systems to measure δ^{18}O in the ocean (*Munksgaard et al.*, 2011, 2012; *Bass et al.*, 2014), the stability, precision, and accuracy of δ^{18}O measurements and inter-comparability between IRMS systems must be determined. *Walker et al.* (in prep.) performed the first inter-laboratory calibration of IRMS and CRDS systems over a range of salinities, as high salt content is problematic for CRDS systems. Studies on the inter-comparison of freshwater samples have been performed, and have shown that IRMS and CRDS δ^{18}O results were directly comparable (*Bass et al.*, 2014; *Walker et al.*, in prep.).

In addition to the potential influence of salt on the precision and accuracy of δ^{18}O measurements of differing salinities, it is possible that variations in δ^{18}O measurements occur between different Picarro CRDS instruments, due to manufacturing, maintenance, or data quality differences (*Walker et al.*, in prep.). As such, to qualify CRDS-made isotope measurements, *Walker et al.* (in prep.) preformed a cross-comparison of CRDS and IRMS δ^{18}O results through an inter-laboratory study (Figure 2.9).

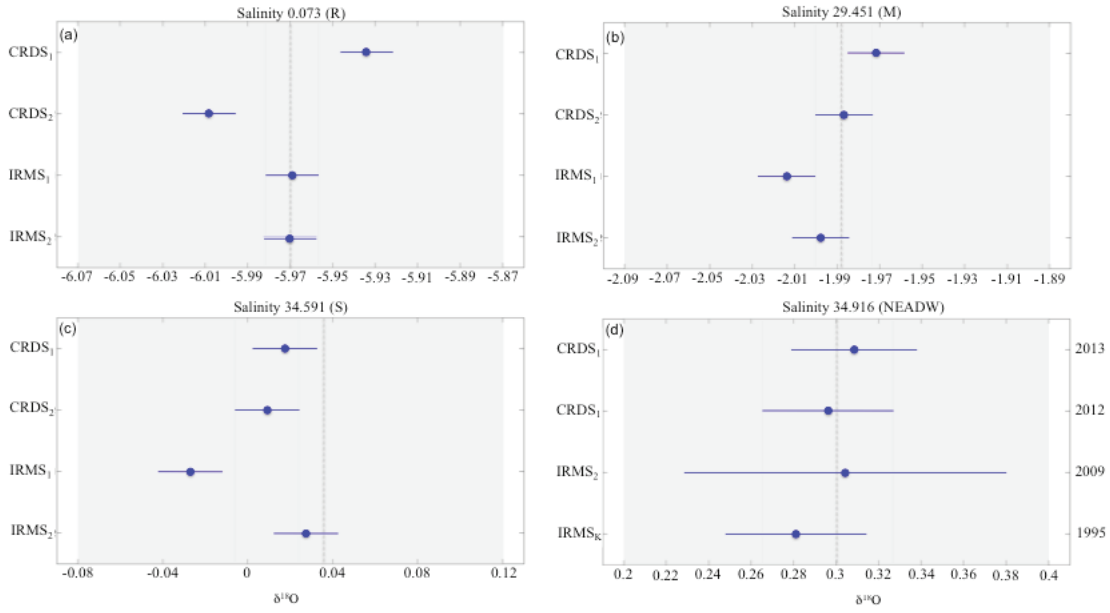

Figure 2.9: Differences in average δ^{18}O calculated in different labs (CRDS$_1$, CRDS$_2$, IRMS$_1$, and IRMS$_2$) for samples collected in (a) Sackville River (R), (b) Bedford Basin (M), (c) Scotian Shelf (S), and (d) North East Atlantic Deep Water (NEADW). Gray dashed lines indicate the combined δ^{18}O averages for the four labs and the gray shaded area represents an analytical uncertainty of 0.10 ‰. NEADW samples were analyzed in different years (2^{nd} y-axis) and at different labs (1^{st} y-axis). Figure from *Walker et al.* (in prep.).

These samples were analyzed by four independent and anonymous labs, with two labs measuring δ^{18}O with a CRDS analyzer (CRDS$_1$ and CRDS$_2$), and two with an IRMS analyzer (IRMS$_1$ and IRMS$_2$). To look at the influence of salt on this analysis, three samples with varying salt contents were analyzed (Sackville River, 0.07; Bedford Basin, 29.45; Scotian Shelf, 34.59) (*Walker et al.*, in prep.). *Walker et al.* (in prep.) found no significant difference ($<$0.10‰, or 1 standard deviation) between the average δ^{18}O values measured at these four labs using CRDS and IRMS techniques (Figure 2.9). In addition, δ^{18}O measurements of North East Atlantic Deep Water (NEADW) (a water mass with little freshwater inputs and thus a stable δ^{18}O and salinity over time) collected over different years (1995, 2009, 2012 & 2013) were not found to be significantly different (below 1 standard deviation) when measured with both CRDS and IRMS systems (Figure 2.9) (*Walker et al.*, in prep.). This illustrates the ability to directly compare IRMS and CRDS δ^{18}O measurements, and the ability to compare current CRDS δ^{18}O measurements to historical IRMS results from the Labrador Sea (*Walker et al.*, in prep.).

As such, the use of the CRDS (i.e.Picarro L2130-i) analyzer allows for more cost effective and mobile measurements of δ^{18}O that can be directly compared with IRMS δ^{18}O results. δ^{18}O measurements from both CRDS and IRMS systems will be directly compared in this thesis, as there is no significant difference between δ^{18}O results measured using these two systems.

2.5.2 Analyzing Water Samples

To analyze the water samples collected during this study, samples were agitated, filtered, and transferred into 2 ml sample vials. These vials were capped tightly, to prevent evaporation during analysis, and then placed into the HTC-xt Leap Pal Technologies autosampler. A 5 or 10 μl syringe was used to inject the samples into the vapourizer for analysis, through an injection port sealed with a septum. The syringe was replaced, or sonicated and rinsed with N-Methylpyrrolidone (NMP), between each run of the analyzer. Following every second run of the analyzer, the septum and steel wool in the instrument were replaced to limit the build-up of salt in the vapourizer. It should be noted that sample runs did not exceed 24 hours, as evaporation is negligible up until this point. Each sample takes approximately one hour to analyze, so up to 24 samples were analyzed during a single run.

For each sample analyzed by the Picarro L2301-i isotopic water analyzer, six replicate

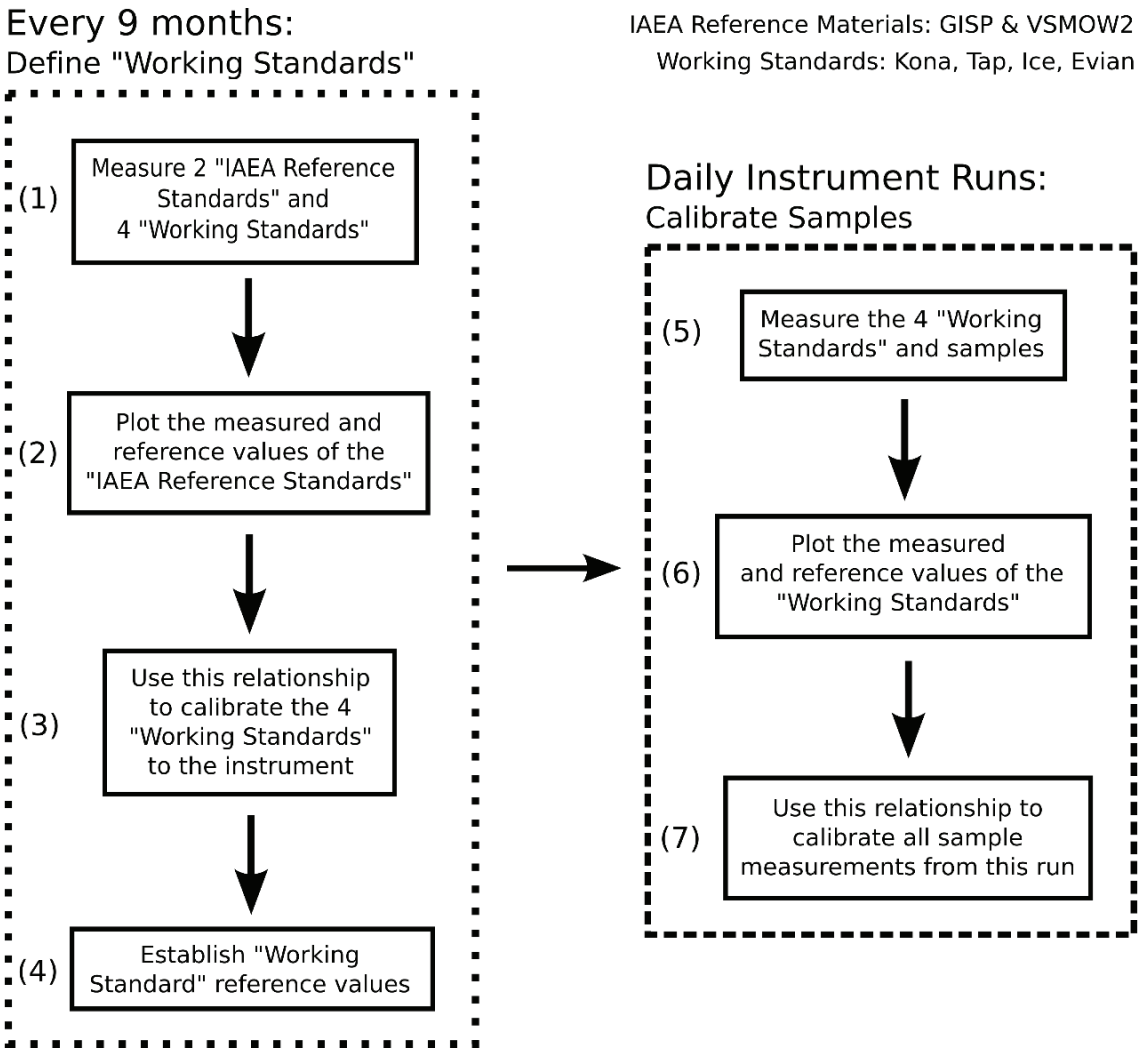

Figure 2.10: Flow chart outlining the steps associated with (1) calibrating "Working Standards" to the Picarro L2301-i isotopic water analyzer using IAEA Reference Materials, and (2) calibrating daily sample measurements with the established "Working Standards".

Table 2.9: IAEA Reference Materials; all measurements are in ‰.

	δ^{18}**O**	δ^{18}**O Uncertainty**	δ^{2}**H**	δ^{2}**H Uncertainty**
VSMOW2	0	0.02	0	0.3
GISP	-24.76	0.09	-189.5	1.2

measurements were taken. Once the sample run had finished, the average and standard deviation of these six measurements was taken. The first three of six measurements were rejected, to get a standard deviation between 0.01 and 0.05‰ for δ^{18}O, and up to 0.1‰ for δ^{2}H (*Walker et al.*, in prep.). If this standard deviation was not met, the sample was analyzed again. The first three replicates were rejected as there is a memory effect associated with this instrument, meaning that remnants of the last sample still present in the vapourizer will affect initial measurements of the following sample (Section 2.5.5). If there is an outlier in the replicates, greater than two standard deviations away from the average of the six replicates, this measurement was rejected.

2.5.3 Defining Working Standards

To account for day-to-day variability in the Picarro L2301-i isotopic water analyzer, standards with known reference values must be analyzed at the start of each run to calibrate sample measurements. “Working Standards”, developed within the laboratory, are used for daily sample runs in lieu of International Atomic Energy Agency (IAEA) Reference Materials, due to their high cost. However, these Working Standards must first be calibrated using Reference Materials. This calibration procedure is depicted stepwise with a flow chart (Figure 2.10), outlining first the process of defining Working Standards and then the use of these standards to calibrate daily sample measurements. Throughout this section, the flow chart will be referred to in order to succinctly describe the calibration of samples analyzed with the Picarro L2301-i isotopic water analyzer in the CERC.OCEAN laboratory.

Two IAEA Reference Materials, GISP (Greenland Ice Sheet Precipitation) and VSMOW2 (Vienna Standard Mean Ocean Water), with known reference δ^{18}O and δ^{2}H values (Table 2.9), were used to calibrate the four Working Standards used in this study (Kona, Icelandic, Evian and Tap water). These four Working Standards were selected to represent a range of δ^{18}O and δ^{2}H values (Step 1; Figure 2.10).

To calibrate the Working Standards to the instrument, four replicates (with six measurements per replicate) of VSMOW2, Kona, Tap, Ice, Evian and GISP were measured.

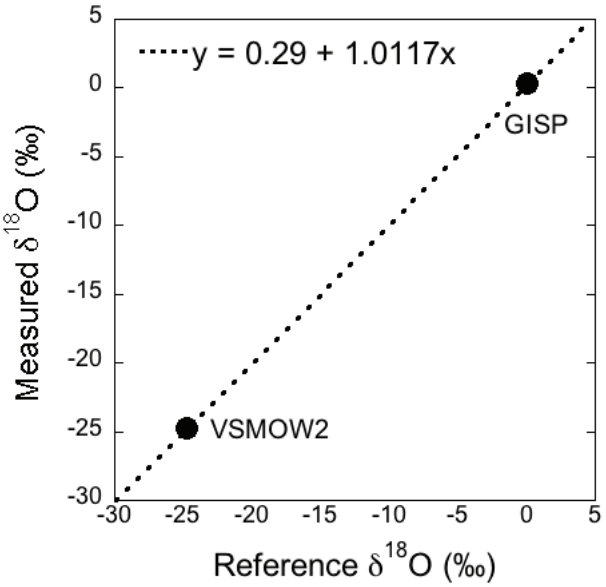

Figure 2.11: Calibration of IAEA Reference Materials GISP and VSMOW2 on the Picarro L2301-i isotopic water analyzer in September 2013.

The average of the last replicate (i.e. the six measurements for the fourth replicate) was calculated to define the δ^{18}O and δ^{2}H of each standard, as it was assumed that no memory effect would be present at this point (Section 2.5.5). The measured δ^{18}O and δ^{2}H values of GISP and VSMOW2 are plotted against the known δ^{18}O and δ^{2}H reference values (Table 2.9) to calibrate the IAEA Reference Materials to the instrument (Figure 2.11). The linear regression equation calculated for this relationship is used to calculate the Working Standard reference values (δ^{18}O and δ^{2}H) to be used in this study (Step 2 & 3; Figure 2.10).

Using the δ^{18}O and δ^{2}H measurements of the four Working Standards from this run, and the linear regression equation (Figure 2.11), the Working Standard reference values can be calculated. An example of this calculation is presented below for Kona water, measured during this run.

$$\begin{aligned} \delta^{18}O_{meas.\,Kona} &= 1.0117(\delta^{18}O_{ref.\,Kona}) + 0.29 \\ \delta^{18}O_{ref.Kona} &= \frac{0.65 - 0.29}{1.0117} \\ \delta^{18}O_{ref.Kona} &= 0.36\,‰ \end{aligned} \tag{2.4}$$

Table 2.10: δ^{18}O of Working Standards measured and calculated using IAEA Reference Materials GISP and VSMOW2 in September 2013.

Standard	Measured Reference (‰)	Calculated Reference (‰)
Kona	0.65	0.36
Tap	-6.39	-6.60
Ice	-7.42	-7.62
Evian	-10.02	-10.19

This calculation was performed on all four Working Standards to calculate the reference δ^{18}O values to use in daily instrument runs, calibrated to the instrument with the use of IAEA Reference Materials (GISP & VSMOW2). This technique was repeated to determine the reference δ^{2}H values for the Working Standards (Step 4; Figure 2.10). The Working Standard reference values calculated using the primary IAEA Reference Materials for δ^{18}O in September 2013, are presented in Table 2.10, with the original measurements (from the Picarro L2301-i isotopic water analyzer) and calculated reference values (using the IAEA Reference Materials).

The four Working Standards are stored in a laboratory fridge in 4 L amber glass bottles, capped tightly and taped to prevent evaporation. Over time, these standards can vary in isotopic composition, as a result of evaporation and day-to-day use; to ensure that evaporation does not affect this calibration, the Working Standards were re-calibrated with IAEA Reference Materials every 9 months (Table 2.11). Any differences in the isotopic composition of these Working Standards during calibrations are not related to changes in the instrument. For example, the variability in the isotopic composition of "Kona" between January 2013 and September 2013 (Table 2.11) is due to the addition of more water into the Working Standard bottles (4 L), resulting in a change to the isotopic composition of this Working Standard.

2.5.4 Calibrating Sample Run Measurements

To calibrate sample measurements, the established Working Standards, with known reference values (Table 2.11), are analyzed at the start of each run (Step 5; Figure 2.10). This calibration is performed during each sample run to account for any day-to-day variability in the instrument. In addition, this maintains a consistency in δ^{18}O and δ^{2}H measurements, despite potential instrumental variability, as all measurements are calibrated to IAEA Reference Materials (GISP and VSMOW2).

Table 2.11: Working Standard reference values used over the time of this study, calibrated to the instrument with IAEA Reference Materials: GISP and VSMOW2.

	δ^{18}**O (‰)**			δ^{2}**H (‰)**		
Standard	Apr 2012	Jan 2013	Sept 2013	Apr 2012	Jan 2013	Sept 2013
Kona	0.11	0.13	0.36	1.11	1.09	1.29
Tap	-6.89	-6.9	-6.60	-45.07	-45.4	-43.47
Ice	-7.57	-7.65	-7.62	-50.96	-51.36	-51.44
Evian	-10.12	-10.19	-10.19	-72.13	-72.53	-72.43

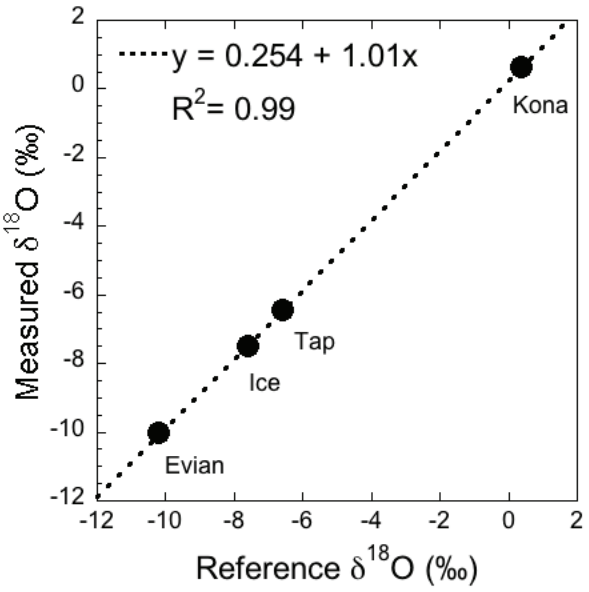

Figure 2.12: Measured δ^{18}O of Working Standards on October 7, 2013 using the Picarro L2301-i isotopic water analyzer, compared with established δ^{18}O reference values for Working Standards (calibrated September 2013).

The four Working Standards are analyzed at the start of each run, and these measured δ^{18}O and δ^{2}H values are plotted against the established Working Standard reference values (Table 2.11) to determine a linear regression equation (Figure 2.12). This linear regression equation is then used to calibrate the δ^{18}O and δ^{2}H measurements of all the samples in this run (Step 6; Figure 2.10).

Using the linear regression equation determined for the Working Standards analyzed on October 7, 2013 (Figure 2.12), all measurements of δ^{18}O during this run can be calibrated to the Working Standards. An example of this calculation, for a water sample (Bedford Basin 60 m depth on May 8, 2013) measured during this run, is presented below:

$$\delta^{18}O_{meas.\,sample} = 1.01(\delta^{18}O_{ref.\,sample}) + 0.254$$
$$\delta^{18}O_{ref.\,sample} = \frac{-1.35 - 0.254}{1.01}$$
$$\delta^{18}O_{ref.\,sample} = -1.59\,‰$$

This calibration was performed on all of the δ^{18}O measurements for samples during this run. The same technique was applied to the δ^{2}H measurements, using the measured and reference δ^{2}H values of the Working Standards to calibrate the δ^{2}H of the sample measurements to the Working Standards (Step 7; Figure 2.10).

Memory and drift tests were performed over the duration of this study; when these effects resulted in a standard deviation greater than the given instrumental precision (0.05‰ for δ^{18}O and 0.3‰ for δ^{2}H), the instrument was cleaned and re-calibrated. Any measurements that were affected by memory or drift and had a large standard deviation ($>2\ \sigma$) were run through the instrument again.

2.5.5 Memory Effect

The "Memory Effect" refers to the effect that trace amounts of the previous sample, still present in the vapourizer, may have on initial δ^{18}O and δ^{2}H measurements of the following sample. In the Picarro L2301-i isotopic water analyzer, this memory effect should be consistent, meaning that the same percentage of water is carried from the previous sample to the next during each injection. However, this memory effect is greater when the isotopic composition of two samples, run one after another, is significantly different (>2‰ for δ^{18}O).

To diminish this memory effect, samples are organized with respect to their (probable) isotopic composition before they are run through the isotope analyzer. The percentage of water carried over from the last sample should have a minimal effect on the measurement, as any remnants left over from the first sample will have a similar δ^{18}O and δ^{2}H to the next. If two samples are very different in their isotopic composition and the memory effect appears quite large, the first few injections (replicates) must be discarded until the results appear to be stable, with a standard deviation between 0.01 and 0.05‰ for δ^{18}O, and up to 0.1‰ for δ^{2}H. Since six injections are measured for each 2 ml vial, three injections can be removed to obtain a desirable standard deviation. If this is not possible, the sample is run through the analyzer again at a later date, no greater than three months following the initial collection.

2.5.5.1 Testing the Memory Effect

Using a pass/fail test (developed by Picarro) to test the memory effect, it is possible to determine whether the memory effect associated with our data is satisfactory (greater than 99% and 98% for δ^{18}O and δ^{2}H respectively)[5]. To test and quantify the memory effect, two Working Standards with significantly different (>20‰ for δ^{18}O), and well-defined, isotopic compositions are run through the instrument one after another (12 - 24 injections of each). The number of injections it takes for the sample to be unaffected by the previous sample, and the percentage of the past isotopic signature carried over to the next injection can be used to quantify the memory effect.

An example of a memory test, performed on August 24, 2012, is presented below for samples of Kona (δ^{18}O: -2.6‰) and Antarctic (δ^{18}O: -34.2‰) water. To calculate the memory effect, three vials (18 injections) of Antarctic water, four vials (24 injections) of Kona and then three additional vials (18 injections) of Antarctic water were analyzed with the Picarro L2301-i isotopic water analyzer. To determine the memory effect on these samples, the memory coefficient can be calculated:

$$\text{Memory Coefficient} = \frac{\text{Average } \delta^{18}\text{O of Antarctic - } \delta^{18}\text{O Value of n}^{th} \text{ Kona Injection}}{\text{Average } \delta^{18}\text{O of Antarctic - Average } \delta^{18}\text{O of Kona}}$$

[5]Guaranteed by Picarro:(https://picarro.app.box.com/s/egtr6oileur5qt74ly7v)

Table 2.12: Memory Test (Aug 24, 2012) on the Picarro L2301-i isotopic water analyzer, with the δ^{18}O of Kona (following 18 Antarctic water samples) and calculated memory coefficients. Only the first 6 (of 24) Kona samples are presented as the memory effect was 0.99 or 1 (i.e. no effect) for the samples following.

Injection Number	**Kona δ^{18}O (‰)**	**Memory Coefficient**
1	-7.54	0.84
2	-4.68	0.93
3	-3.84	0.96
4	-3.46	0.97
5	-3.22	0.98
6	-3.08	0.99

The "Average δ^{18}O" of Antarctic water is calculated by taking the average δ^{18}O of the last four injections of Antarctic water from the 18 injections that we ran (δ^{18}O: -34.2‰). The "Average δ^{18}O" of Kona water was also taken from the last four injections of 18, giving us a value of -2.6‰ for δ^{18}O. Only the last 4 injections were used to calculate "Average δ^{18}O" as it was assumed that the memory effect would have no effect on the samples at this point. The "nth" sample is the first δ^{18}O measurement of Kona water, directly following the 18 injections of Antarctic water. This calculation is repeated for all of the δ^{18}O values calculated for each Kona water injection. The memory effect should decrease with each successive injection.

According to Picarro[6], the memory coefficient of the first sample should be in the range of 0.94 to 0.97 and by the fourth injection, it should be approximately 0.99. Table 2.12 presents the memory coefficients for Kona samples analyzed immediately following 18 injections of Antarctic water samples.

Insoluble materials, such as salt, will accumulate in the vapourizer over time and increase the retention of the previous sample, thus strengthening the memory effect. The memory coefficient calculated for the first Kona sample (Table 2.12) is greater than the value Picarro ensures (for this analyzer), 0.84 instead of 0.94. This is due to a build-up of salt in the vapourizer, which will impact the memory effect until it is removed by cleaning (i.e. flushing with hot water). The memory effect is tested every 1-2 months, or when it is noted to be impacting δ^{18}O and δ^{2}H measurements (i.e. a standard deviation of 0.05‰ for

[6]Guaranteed by Picarro:(https://picarro.app.box.com/s/egtr6oileur5qt74ly7v)

Table 2.13: Memory coefficients for Kona calculated before and after vapourizer cleaning. These Kona samples were run immediately following 18 Antarctic water samples.

Injection Number	Before (Oct. 1, 2012)	After (Nov. 14, 2012)
1	0.83	0.92
2	0.92	0.97
3	0.95	0.98
4	0.97	0.99
5	0.97	0.99
6	0.98	0.99

δ^{18}O and 0.1‰ for δ^{2}H is not met for the last three injections of a sample). If the memory coefficient does not reach 0.99 by the fourth injection, the vapourizer is cleaned. Another memory test is performed on the isotope analyzer following vapourizer cleaning to ensure that the salt build-up has been removed and is no longer impacting the memory of the instrument. The vapourizer cleaning procedure is outlined by Picarro[7], and the effect of cleaning on the memory effect can be seen in Table 2.13.

Following vapourizer cleaning, the Working Standards must be re-calibrated to the instrument using IAEA Reference Materials. As cleaning the vapourizer is time consuming and costly, this is only performed when the memory effect is impacting the samples.

The memory effect will first impact samples with large differences in δ^{18}O and δ^{2}H ($>$2‰ for δ^{18}O). To avoid constant cleaning of the vapourizer, water samples that do not reach the desired standard deviation in six injections are sampled twice (i.e. 12 injections). This was done for laboratory standards ($\sim$0, -6.5, -7, -10‰ for δ^{18}O), as well as precipitation samples with variable δ^{18}O values ($\sim$ -2 to -20‰). Samples were duplicated instead of taking 12 injections from all of the samples in the run, as this would have drastically increased sample run time.

2.5.6 Drift Effect

Picarro also suggests that a precision and drift test should be performed once every 6 - 12 months to test the performance of the analyzer as it ages. 144 injections (24 samples) of the Working Standard “Tap” were analyzed with the Picarro L2301-i isotopic water analyzer

[7]Vapourizer Cleaning Procedure: (http://www.picarro.com/resources/knowledgebase/water_isotope_analyzers/vaporizer_cleaning)

Table 2.14: Precision and Drift test using the Working Standard "Tap" (Aug 23, 2012). The test is passed if the measured value is less than or equal to the guaranteed.

		Guaranteed	Measured	State
Precision	δ^2H	0.10	0.04	passed
	δ^{18}O	0.03	0.03	passed
Drift	δ^2H	0.80	0.20	passed
	δ^{18}O	0.20	0.17	passed

on August 23, 2012. 24 average δ^{18}O and δ^2H values were calculated by averaging the six replicates of each sample vial. Because the memory effect may be influencing the first few samples, the first 2 vials (12 injections) were not included in this analysis. The "precision" was calculated by taking the standard deviation of these 22 averaged δ^{18}O and δ^2H values, and the "drift" is calculated by subtracting the maximum δ^{18}O/δ^2H average by the minimum δ^{18}O/δ^2H average (i.e. highest and lowest values of these 22 averages). These measured values can then be compared to the values suggested by Picarro (Precision: 0.025/0.1% for δ^{18}O/δ^2H, Drift: 0.2/0.8% for δ^{18}O/δ^2H) to see if the tests were "passed". Since all of the tests were "passed" on August 23, 2012 (Table 2.14), there should be no significant variation between the measured δ^{18}O and δ^2H of samples, once the memory effect has been accounted for.

2.6 Salinity Measurements

Water samples for salinity measurement were collected alongside δ^{18}O/δ^2H samples. Samples were collected in a 250 ml Boston Round amber glass bottle, and capped using a phenolic cap with a polyethylene (PE) cone liner. This cone liner forms an exceptionally tight seal to limit the potential for evaporation. Following capping, the caps were wrapped with electrical tape to further limit evaporation. Since the salinometer used in this study requires that the samples are at room temperature for analysis ($\sim$21°C), to match the water bath temperature, these bottles were stored in the laboratory until analysis could take place at the Bedford Institute of Oceanography (BIO). Samples were run in September and December of 2012, as well as June and December of 2013.

These samples were analyzed using an Guildline Autosal 8400-B salinometer at BIO.

IAPSO Standard Seawater was analyzed with the instrument initially to calibrate the instrument. Samples were agitated before they were analyzed to ensure an accurate reading. The instrumental output is recorded in conductivity, so these measurements were converted to psu (practical salinity units) with the use of a DOS program (autosal.exe). The error associated with this instrument is 0.002 psu. It should be noted that the salinity used for the offshore AZMP samples was determined using a Seabird CTD (Helmuth Thomas, *personal communications*).

CHAPTER 3

SOURCES & VARIABILITY

In this chapter, the major sources of water to Halifax Harbour are identified and examined. The annual variability in these inputs will also be identified to examine the variability in Bedford Basin water composition throughout the year. Once these sources and their variability have been identified, end members can be selected for a mass balance analysis of Bedford Basin, presented in Chapter 4.

3.1 Freshwater Inputs

3.1.1 Precipitation

Precipitation samples were collected in Halifax, NS from July 2012 to October 2013 to examine the variability and range of δ^{18}O and δ^{2}H. In 1964, *Dansgaard* proposed that the relationship between δ^{18}O and δ^{2}H in precipitation varies depending on: latitude, altitude, amount of precipitation, distance from the coast, and air temperature (*Peng et al.*, 2004). In Halifax, the effect of air temperature and amount of precipitation on δ^{18}O and δ^{2}H are examined. In addition, the type of precipitation (snow or rain) and the annual variability will also be examined to determine what causes variability in δ^{18}O and δ^{2}H of precipitation.

3.1.1.1 Amount Effect

The amount effect, first proposed by *Dansgaard* (1964), can be used to investigate variability in δ^{18}O and δ^{2}H of precipitation in two ways. First, small rainstorms tend to have more positive δ values (+ δ^{18}O/δ^{2}H), as a result of evaporative enrichment, occurring as water droplets fall through dry air. Second, the amount effect can also be used to describe

the decrease in δ values (- δ^{18}O/δ^{2}H) during large, high magnitude, storm events, as more positive δ values are rained out first.

First, the effect of small rainstorms on δ^{18}O and δ^{2}H of precipitation in Halifax was investigated by plotting the amount of rain (ml) that falls for each precipitation event against δ^{18}O (Figure 3.1). Snow was not included in this analysis as the amount of snow collected was variable and dependent on wind and blizzard conditions. There appears to be no single relationship between δ^{18}O and the amount of rain (ml), with a weak r^2 of 0.0024 (Figure 3.1). This lack of significance is evident in small rainstorms, where there is no relationship between δ^{18}O and amount. Based on *Dansgaard*'s 1964 hypothesis, the relationship between δ^{18}O and amount should be the strongest when precipitation events are the smallest.

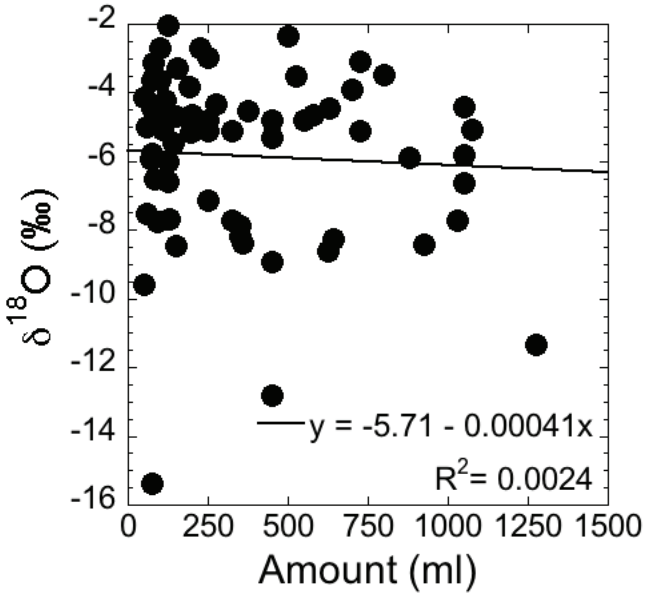

Figure 3.1: Variability in δ^{18}O with amount of rain (ml), collected from July 2012 to October 2013 in Halifax.

Dansgaard (1964) found that the "amount effect" occurred year-round at most tropical stations and in the summer time at mid-latitudes. A stronger influence of this "amount effect" can be seen in regions where precipitation during the low-rainfall months experiences evaporation in the air column before reaching the ground (*Clark and Fritz*, 1997). In Halifax, the factors required for this amount effect to occur are not present; there is significant rainfall during the summer months and the air column is humid.

Table 3.1: δ^{18}O of single rainfall events occuring over two days in Halifax, along with the amount (ml) collected.

Dates	**Day 1 (‰)**	**Amount (ml)**	**Day 2 (‰)**	**Amount (ml)**
Aug. 1 - 2, 2012	-2.97	310	-5.92	130
Sept. 20 - 21, 2012	-5.13	310	-4.46	690
Oct. 31 - Nov. 1, 2012	-2.70	60	-4.34	640
June 27 - 28, 2013	-4.80	160	-7.54	335
Sept. 16 - 17, 2013	-2.52	510	-4.65	60

Second, the "amount effect" can also refer to the total amount of precipitation that falls in a single storm event, leading to more negative δ values recorded during large storms. During a large storm, the δ^{18}O/δ^{2}H of precipitation should become progressively depleted as rain-out removes more enriched δ^{18}O/δ^{2}H values first. To investigate this effect, precipitation events that took place over multiple days were identified (Table 3.1). These rainfall events, lasting multiple days, were confirmed to be a part of a single rainfall event through weather radar, operated by the Government of Canada[1]. The δ^{18}O of precipitation collected on "Day 1" and "Day 2" were examined to see if these values decreased with increasing rain-out (Table 3.1).

With the exception of precipitation samples collected on September 20 and 21, 2012, there is a decrease in δ^{18}O on the second day of the rain storm (Table 3.1). This supports the hypothesis that increased rain-out results in lower δ^{18}O values. The increase in δ^{18}O occurring on September 20 and 21, 2012 may be a result of evaporation, or the presence of an additional air mass. Overall, the expected depletion in δ^{18}O/δ^{2}H with increased rainfall is evident (Table 3.1).

3.1.1.2 Temperature Effect

With decreasing temperature and rain-out, precipitation becomes increasingly depleted in δ^{18}O and δ^{2}H (*Clark and Fritz*, 1997). In-cloud temperatures control isotopic fractionation and condensation, however these temperatures are difficult to measure, so surface air temperature is measured instead (*Clark and Fritz*, 1997). To examine the relationship between δ^{18}O of precipitation and surface air temperature, these data were plotted in Figure 3.2(a). An r^2 of 0.28 was determined, showing that this relationship is not statistically

[1]Weather Radar - Halifax, NS: https://weather.gc.ca/radar/index_e.html?id=xgo

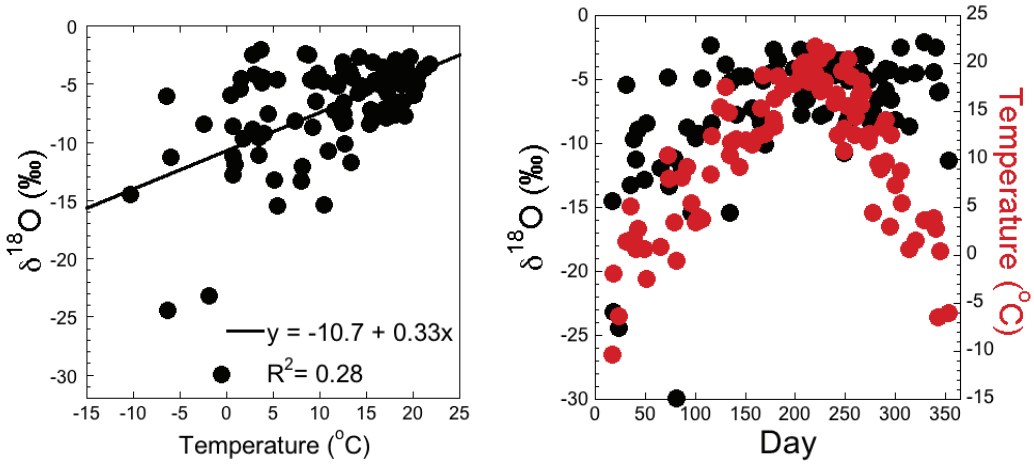

(a) (b)

Figure 3.2: Variability in δ^{18}O with (a) surface air temperature (°C), and (b) with time (July 2012 - Oct 2013) in Halifax. Day 0 represents Jan 1^{st}, while Day 365 is Dec 31^{st}.

significant; this may due to the fact that we are looking at surface air temperatures, rather than in-cloud temperatures.

In Figure 3.2(b), surface air temperature and δ^{18}O are plotted against time to examine the variability in these measurements over a year. Although it is evident that surface air temperature and δ^{18}O are significantly different (Figure 3.2(a): r^2= 0.28), trends may still be present. In Figure 3.2(b), we can see that more depleted δ^{18}O values are associated with colder, winter months, while more enriched δ^{18}O values are found in warmer, summer months. There is a correlation between δ^{18}O and temperature, however surface air temperature alone does not control the variability in δ^{18}O of precipitation in Halifax.

3.1.1.3 Type of Precipitation

In Halifax, there is a larger range in δ^{18}O associated with snow (-9 to -30‰), compared with rain (-2 to -15‰). A number of studies have examined the isotopic composition of a snow-pack over time (*Morgan*, 1982; *Masson-Delmotte et al.*, 2008)) or the mechanics associated with isotopic fractionation and snowfall (*Jouzel and Merlivat*, 1984) however few studies have examined the variability in the isotopic composition of falling snow over a year (*Motoyama et al.*, 2005; *Blasch and Bryson*, 2007). The large range associated with δ^{18}O of snow and the strongly isotopically depleted values measured in snow (max. -30‰) compared with rain (max. -15‰) are a result of equilibrium adjustment (*Gat*, 2010).

Raindrops undergo continuous molecular exchange as they fall towards the ground, and can be adjusted to equilibrium with ambient moisture (*Gat*, 2010). In comparison, the isotopic composition of solid precipitation is frozen in. As such, there is no re-equilibration at warmer temperatures in the lower atmosphere for this frozen precipitation, leading to a δ^{18}O value that does not change and better reflects in-cloud temperatures. In addition, different solid elements (snow flakes, graupel, hailstones, rimmed snow, etc.) differ in how they are formed in the cloud systems, leading to different isotopic signatures (*Gat*, 2010). Like rain, *Motoyama et al.* (2005) found that δ^{18}O samples of freshly fallen snow are correlated with air temperature.

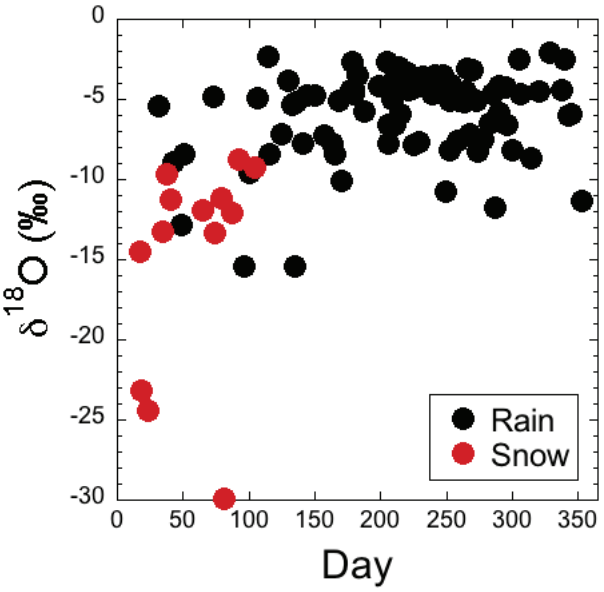

Figure 3.3: Yearly fluctuation in δ^{18}O of precipitation from July 2012 to October 2013, with rain (black) and snow (red) identified.

The type of precipitation (i.e. rain or snow) influences isotopic composition. Figure 3.3 illustrates the change in δ^{18}O in Halifax (July 2012 - October 2013), over both rain and snowfall events. This helps to emphasize the difference in δ^{18}O of rain and snow, with snowfall events typically more depleted in δ^{18}O than rainfall events. A Wilcoxon-Mann-Whitney rank sum test was performed on these data to see if the δ^{18}O of snow is significantly different from rain in Halifax. A p value of $<$0.0001 was found, showing that the isotopic composition of rain and snow is significantly different.

It is evident that the isotopic composition of snow and rain is statistically different over

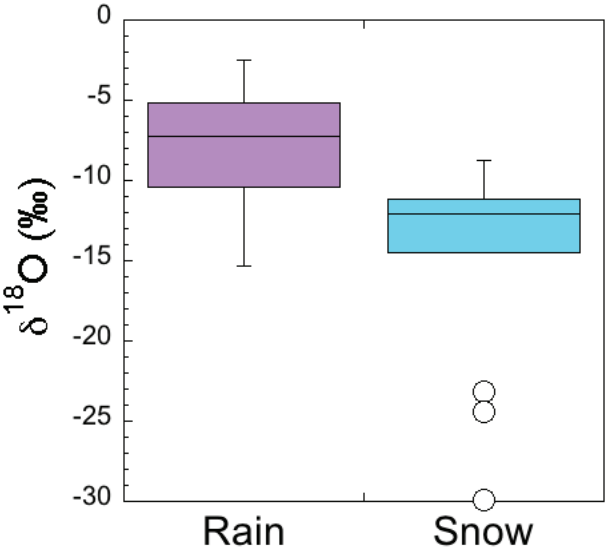

Figure 3.4: Variability in δ^{18}O with type of precipitation (snow or rain) collected between the first (January 17) and last (April 14) snowfall of winter/spring 2013. The median defines the center line and the box, representing interquartile distance, is closed by the upper and lower quartiles. The points identify the outliers, defined as LQ - 1.5*IQD and UQ + 1.5*IQD. N of rain is 12, N of snow is 13.

the entire collection period, however this may be due to seasonal differences, rather than the "type" of precipitation. As such, only precipitation data (both rain and snow) collected between the first (January 17) and last snowfall (April 14) of 2013 were included in this analysis, to see if seasonal effects or the difference in "type" are driving this significant difference (Figure 3.4). When a Wilcoxon-Mann-Whitney rank sum test was performed on these data, a p value of 0.003 was found, illustrating that the isotopic composition of rain and snow in Halifax, both seasonally and yearly, is statistically different (Figure 3.4).

3.1.1.4 Annual Variability

Precipitation samples were collected in Halifax from June 2012 to October 2013 (Figure 3.5). To examine the annual variability of δ^{18}O in precipitation, a year-long period must be defined, as the months of July, August, September, and October were sampled in both 2012 and 2013. Including all of the samples collected, from July 2012 - October 2013, in the amount-weighted yearly average would bias the summer months, making it seem as if an increased number of precipitation events occurred over these four duplicated months.

Since we have samples from July 2012 to October 2013, it is possible to determine

Table 3.2: P values determined with Tukey HSD post-hoc test, comparing different groupings of average yearly δ^{18}O of precipitation in Halifax. The month listed includes samples from the 1^{st} of that month in 2012 to the last day of the previous month in 2013.

	July	**August**	**September**	**October**	**November**
July	-				
August	0.9997	-			
September	1	0.9997	-		
October	0.9949	0.9777	0.9948	-	
November	0.977	0.938	0.9767	0.9997	-

*P <0.05 = statistically significant difference

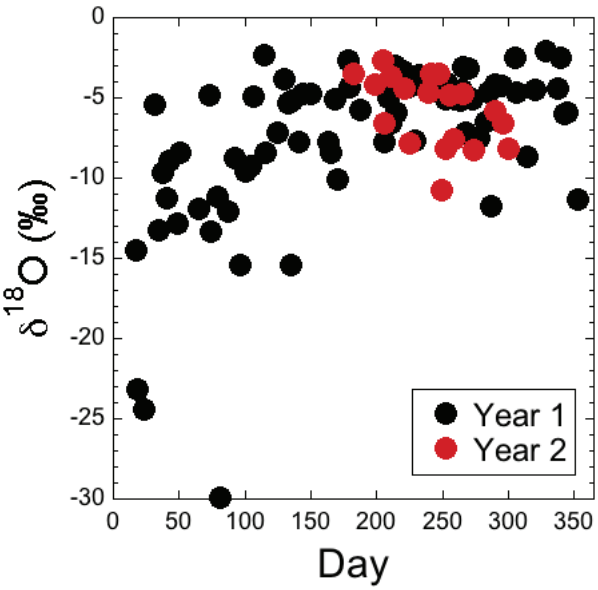

Figure 3.5: Yearly variability in δ^{18}O of precipitation (rain and snow) collected between July 2012 and Oct 2013. (Year 1: July 2012 - June 2013, Year 2: July - Oct 2013).

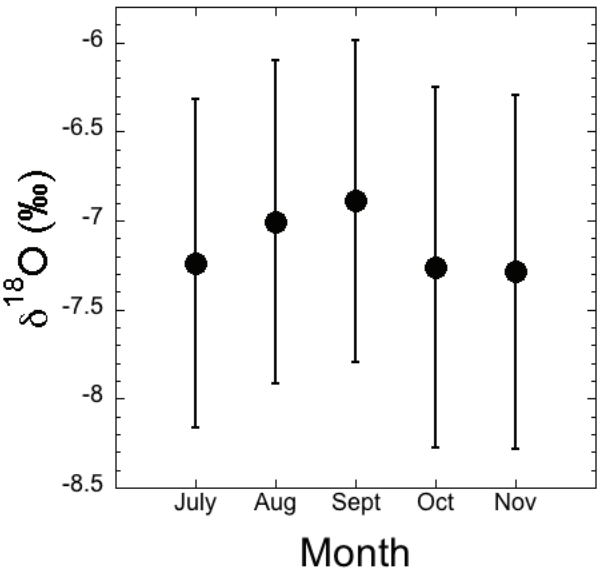

Figure 3.6: Yearly amount-weighted averages for δ^{18}O of precipitation with different yearly combinations. The month on the x-axis includes samples from the 1^{st} of that month in 2012 to the last day of the previous month in 2013. N values for July, Aug, Sept, Oct, and Nov are 60, 60, 58, 52, and 50 respectively. Error bars are 95% CIs.

a yearly amount-weighted average for the five potential "year" combinations over this sampling period: July 2012 - June 2013, August 2012 - July 2013, September 2012 - August 2013, October 2012 - September 2013, and November 2012 - October 2013. These five yearly averages were plotted (Figure 3.6) to illustrate the variability in these different groupings. Although there is some variability in the yearly average, depending on the monthly grouping, any differences are not significant (Figure 3.6). A one-way ANOVA test was also performed on these data to see if a statistically significant difference (p value $<$0.05) exists between these five yearly groupings. A p value of 0.937 was found, which shows that these five different yearly groupings are not statistically different. To examine individual differences between these yearly groupings, a Tukey HSD post-hoc test was also performed on these data; all of the yearly groupings are not significantly different, as a p value $>$0.05 was found for all combinations (Table 3.2). Since there is no difference between these yearly groupings, the yearly amount-weighted δ^{18}O average used in this study will be calculated from data collected over the first year, between July 1^{st} 2012 and June 30^{th} 2013. This yearly amount-weighted average for δ^{18}O of precipitation in Halifax, was found to be -7.24‰ with a 95% confidence interval (CI) of 0.92.

To determine the average monthly δ^{18}O of precipitation in Halifax, all of the samples collected within a month were amount-weighted (Table 3.3). The 95% CIs calculated for each monthly amount-weighted average of δ^{18}O ranged from 0.24 to 8.85 over this study period (Table 3.3). Differences in the 95% CIs of different monthly averages are a result of variations in the isotopic composition of precipitation events over these months, and not due to the number of samples collected or the effect of evaporation. When the highest 95% CIs were seen, in January (8.82) and March (8.85) of 2013, both rain and (more isotopically depleted) snow fell throughout the month. In January 2013, δ^{18}O of precipitation ranged from -5.44‰ for a small rainfall event, to -24.43‰, for a snowfall. Likewise, in March 2013, δ^{18}O of precipitation ranged from -4.81‰ (rain) to -29.92‰ (snow).

There is a difference between the average monthly δ^{18}O determined for July of 2012 (-6.96‰) compared with 2013 (-4.91‰) (Table 3.3). This is due to the range in δ^{18}O of precipitation over this month, which varies with the origin of air masses. More depleted δ^{18}O values can also be seen in June of 2013 (-6.75‰), particularly when compared to the month before (May 2013: -5.62‰) and after (July 2013: -4.91‰), which are more isotopically enriched (Table 3.3). Overall, δ^{18}O does vary throughout the year, however this is due to in-cloud temperatures and the origin of air masses, bringing more isotopically enriched or depleted precipitation, rather than any errors associated with collection (e.g. evaporation) or analysis.

As the months of July, August, September, and October were sampled both in 2012 and 2013, the year-to-year variability in these average monthly δ^{18}O values can be examined. When the average amount-weighted δ^{18}O of precipitation in a month was compared for two different sample years (2012 & 2013), it was found that these samples were not significantly different, as their confidence intervals overlapped (Figure 3.7). A Wilcoxon-Mann-Whitney rank sum test was also performed on each of these duplicated months (i.e. July 2012 vs. July 2013) to see if the average monthly δ^{18}O calculated in two different years is statistically different (p value $<$0.05). All of the duplicated months had p values greater than 0.05, showing that the δ^{18}O of precipitation in these duplicated months is not statistically different (Table 3.4).

To determine an average monthly δ^{18}O value for precipitation in these duplicated months, only one sample year can be chosen. Data from the same month in two different years

Table 3.3: Amount-weighted monthly average δ^{18}O of precipitation in Halifax (July 2012 to Oct 2013).

Month	**Year**	**N**	δ^{18}**O (‰)**	**St. Dev.**	**95% Conf. Int.**
July	2012	4	-6.96	1.22	0.24
August	2012	6	-4.32	1.96	1.62
September	2012	9	-4.60	1.03	0.64
October	2012	5	-5.14	1.36	1.30
November	2012	3	-4.30	1.07	1.81
December	2012	4	-8.79	3.66	4.30
January	2013	4	-17.62	7.49	8.82
February	2013	3	-9.62	2.32	3.92
March	2013	4	-8.82	7.52	8.85
April	2013	6	-7.56	3.55	2.91
May	2013	7	-5.62	2.75	2.02
June	2013	5	-6.75	2.27	2.17
July †	2013	4	-4.91	2.11	2.48
August †	2013	4	-4.79	1.79	2.11
September †	2013	3	-4.01	0.88	1.48
October †	2013	3	-6.99	1.55	2.62

† Duplicated sample months

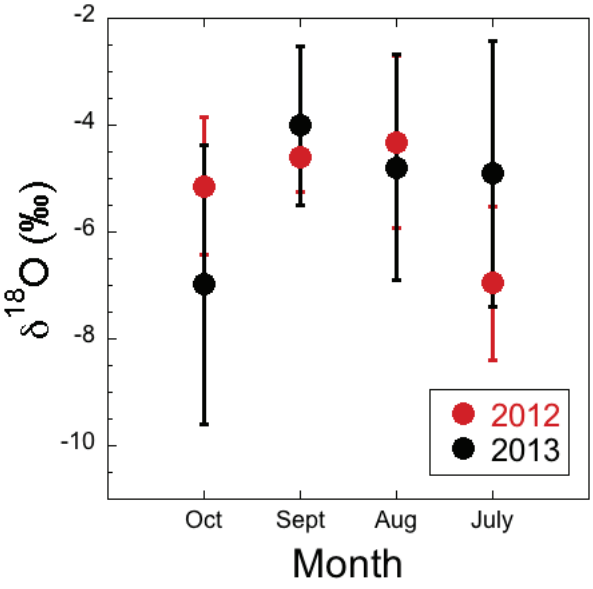

Figure 3.7: Year-to-year variability in monthly amount-weighted averages of δ^{18}O in July, August, September, and October of 2012 and 2013. N values are presented in Table 3.3.

Table 3.4: P values for the δ^{18}O of precipitation for each month sampled over two years (2012 & 2013), calculated using a Wilcoxon-Mann-Whitney Rank Sum Test.

Duplicated Sample Month (2012 & 2013)	**P Value**
July	0.111
August	0.412
September	0.220
October	0.230

*P $<$0.05 = statistically significant difference

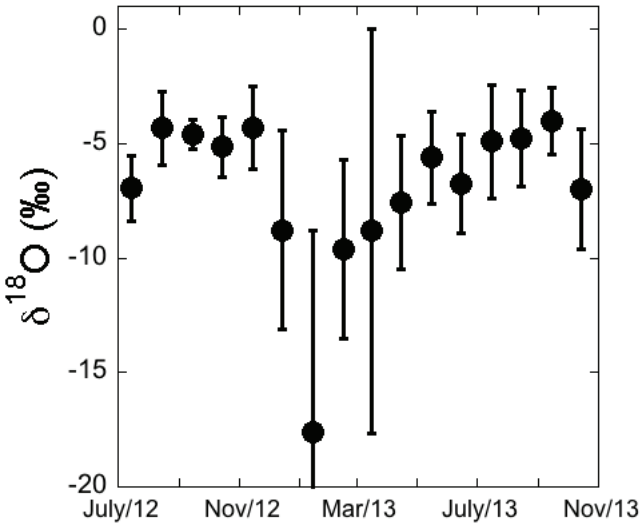

Figure 3.8: Amount-weighted monthly δ^{18}O of precipitation, collected in Halifax (July 2012 - October 2013), with 95% CIs (N values found in Table 3.3).

cannot be added together and averaged because these data must be amount-weighted. Since there is no significant difference in the average amount-weighted δ^{18}O of precipitation in these duplicated months (Figure 3.7), the first four sample months (sampled in 2012) will be used to determine the monthly averages of δ^{18}O in precipitation for the months of July, August, September, and October. These four months were selected to maintain a consistency with the yearly average, which was calculated by taking the amount-weighted average of δ^{18}O for the first twelve sample months. Despite the fact that only twelve months can be used to determine the yearly amount-weighted average, Figure 3.8 presents the monthly δ^{18}O averages for all of the months sampled in this study, illustrating the variability in δ^{18}O over this time period (July 2012 - October 2013).

3.1.2 Sackville River

Samples were collected at a depth of 1m from Sackville River between May 2012 and April 2014. The yearly fluctuation in δ^{18}O of Sackville River can be seen in Figure 3.9(a), with more isotopically depleted water measured in the spring months and an isotopic enrichment in the summer and fall. Between December 2012 and March 2013 there was a change in the isotopic composition of Sackville River from ∼-6‰ to ∼-9‰. Between these months, in January and February of 2013, the river was ice-covered and samples

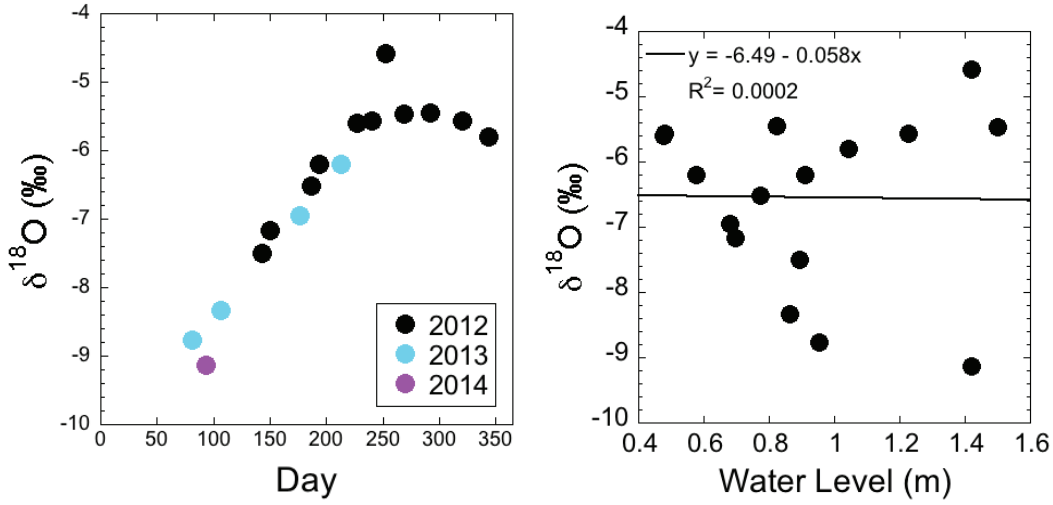

(a) (b)

Figure 3.9: Change in δ^{18}O of Sackville River surface water samples collected from May 2012 to April 2014 with (a) time (Day 0 - 365) and (b) water level (m) (*Environment Canada* (2013)). No samples were collected between Day 0 and 80 (January & February), as Sackville River was frozen over this time.

Table 3.5: Monthly variability in δ^{18}O of Sackville River surface samples (May 2012 - Apr 2014). 95% CI is associated with averages.

Month	**N**	δ^{18}**O (‰)**	**95% Conf. Int.**
January	0	NA	-
February	0	NA	-
March	1	-8.76	-
April	2	-8.75	0.785
May	2	-7.33	0.019
June	1	-6.95	-
July	2	-6.35	0.305
August	3	-5.80	0.392
September	2	-5.02	0.862
October	1	-5.45	-
November	1	-5.57	-
December	1	-5.81	-
Annual Average		-6.58	

could not be collected, making this change in δ^{18}O appear abrupt, as a more gradual change could not be sampled. Although the seasonal cycle of δ^{18}O in Sackville River was not constrained in January and February, it is evident that Sackville River becomes more isotopically depleted over these winter months. Despite the fact that Sackville River is often frozen in the winter, water levels are still collected over this time; discharges must be adjusted due to a backwater effect caused by the ice (Guy Leger, *personal communications*; *Environment Canada* (2013)). Although there is a shift in δ^{18}O of Sackville River over time, there is no relationship between δ^{18}O and changes in water level (m) (Figure 3.9(b)). The r^2 value (0.0002) calculated for this relationship illustrates the statistically significant difference between these two variables.

Although fluctuations in water level do not drive the isotopic composition of Sackville River, δ^{18}O varies throughout the year (Figure 3.9(a)). Table 3.5 presents δ^{18}O data collected between May 2012 and April 2014 in Sackville River. Despite the fact that samples were collected in different years, all data were used to calculate a yearly average as fewer samples were collected compared with precipitation, and amount-weighting of Sackville River data could not be performed. It should be noted that the amount-weighting of samples may result in a slightly different yearly average as a result of changes to river output throughout the year.

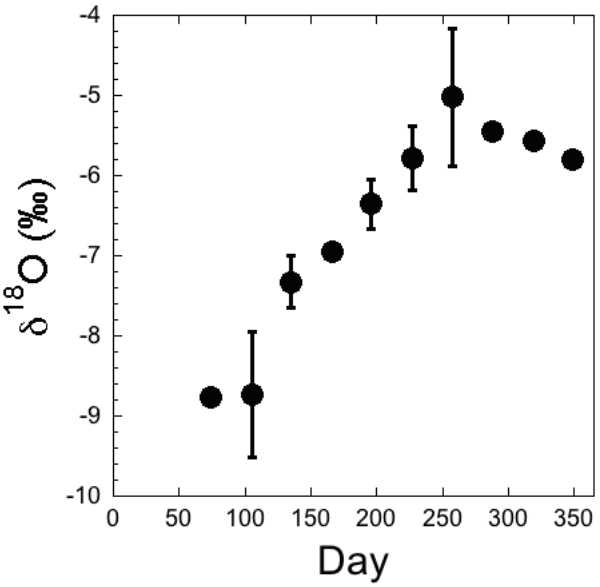

Figure 3.10: Monthly change in δ^{18}O of Sackville River over a year. Months with multiple samples are averaged and the error (95% CI) is presented. January and February are not included due to ice-cover. N values are presented in Table 3.5.

To calculate the annual average δ^{18}O of Sackville River, all of the data could not be averaged as this would bias the months sampled more than once. Instead, an average was calculated for each month, if possible, and the δ^{18}O values for the 10 months sampled were averaged (Table 3.5). Since samples could not be collected in January and February, the average yearly δ^{18}O value that is calculated may be more isotopically enriched than what is seen throughout the year, as these months with more isotopically depleted (-δ^{18}O) precipitation are not represented in the yearly Sackville River average. Due to variability in the timing of sample collection, a monthly δ^{18}O error cannot be defined. Monthly and yearly δ^{18}O averages are defined, however additional samples, collected more frequently and/or during times of ice cover, may provide us with a better understanding of the exact variability associated with δ^{18}O in Sackville River. The error associated with the samples collected in this study can be seen in Figure 3.10, which includes the 95% CI for any months with multiple samples (Table 3.5). All of these monthly δ^{18}O values can be averaged to determine a yearly Sackville River average δ^{18}O of -6.58‰.

Table 3.6: δ^{18}O of wastewater outfalls and Sackville River on April 3, 2014.

Sample Site	δ^{18}**O (‰)**
Herring Cove WWTF	-8.44
Halifax WWTF	-7.83
Mill Cove WWTF	-8.07
Dartmouth WWTF	-8.37
Eastern Passage WWTF	-8.16
Sackville River	-9.15

3.1.3 Wastewater

Table 3.6 presents δ^{18}O values of wastewater outfalls for the five different wastewater treatment facilities (WWTFs) entering Halifax Harbour, as well as the isotopic composition of Sackville River in April. Wastewater samples were collected to examine the connection between δ^{18}O of Sackville River and wastewater outfalls, where water is originating from two major lakes (Pockwock Lake and Lake Major) in Halifax (*Halifax Water*, 2012).

When these wastewater outfalls and Sackville River were sampled, it was found that the most isotopically depleted water (δ^{18}O) was found in Sackville River, -9.15‰, while the most isotopically enriched water was found at the Halifax WWTF, -7.83‰ (Table 3.6). The δ^{18}O of all five WWTFs ranged from -7.83 to -8.44‰, and the δ^{18}O of Sackville River measured approximately a year earlier, on April 16, 2013, is within this range (-8.33‰). All of the water in the WWTFs originates from watersheds around the Halifax Regional Municipality (HRM) (Figure 3.11), and is therefore not expected to show significant variability in δ^{18}O when compared with lakes and rivers around the area (i.e. Sackville River).

Figure 3.11 was adapted from *Halifax Water* (2012) to illustrate the transport of water and wastewater around Halifax. The blue represents the treatment of water, position of reservoirs, and its transport around the HRM. The green, in comparison, outlines the transport of wastewater, primary pumping stations, and major WWTFs. This image of a complex system illustrates the potential variability in the residence time of water in the wastewater treatment system, as it is unlikely that all of the water in the system would be present for the same amount of time.

The water sample collected at Sackville River should be the most representative of the δ^{18}O of lakes and rivers in the HRM on this collection day (April 3, 2014), while

wastewater outfall samples would have been present in the wastewater treatment system for variable amounts of time, accounting for observed differences in δ^{18}O values (Table 3.6). It should be noted that these wastewater samples (Table 3.6) were collected the day following a winter storm (April 2, 2014), which would have introduced isotopically depleted (- δ^{18}O) precipitation to the area. Because of this difference in residence times between the wastewater system and Sackville River, this isotopically depleted input of precipitation seems to result in a more depleted δ^{18}O value in Sackville River (-9.15‰) compared with the water in the wastewater outfalls (-7.83 to -8.44‰) (Table 3.5).

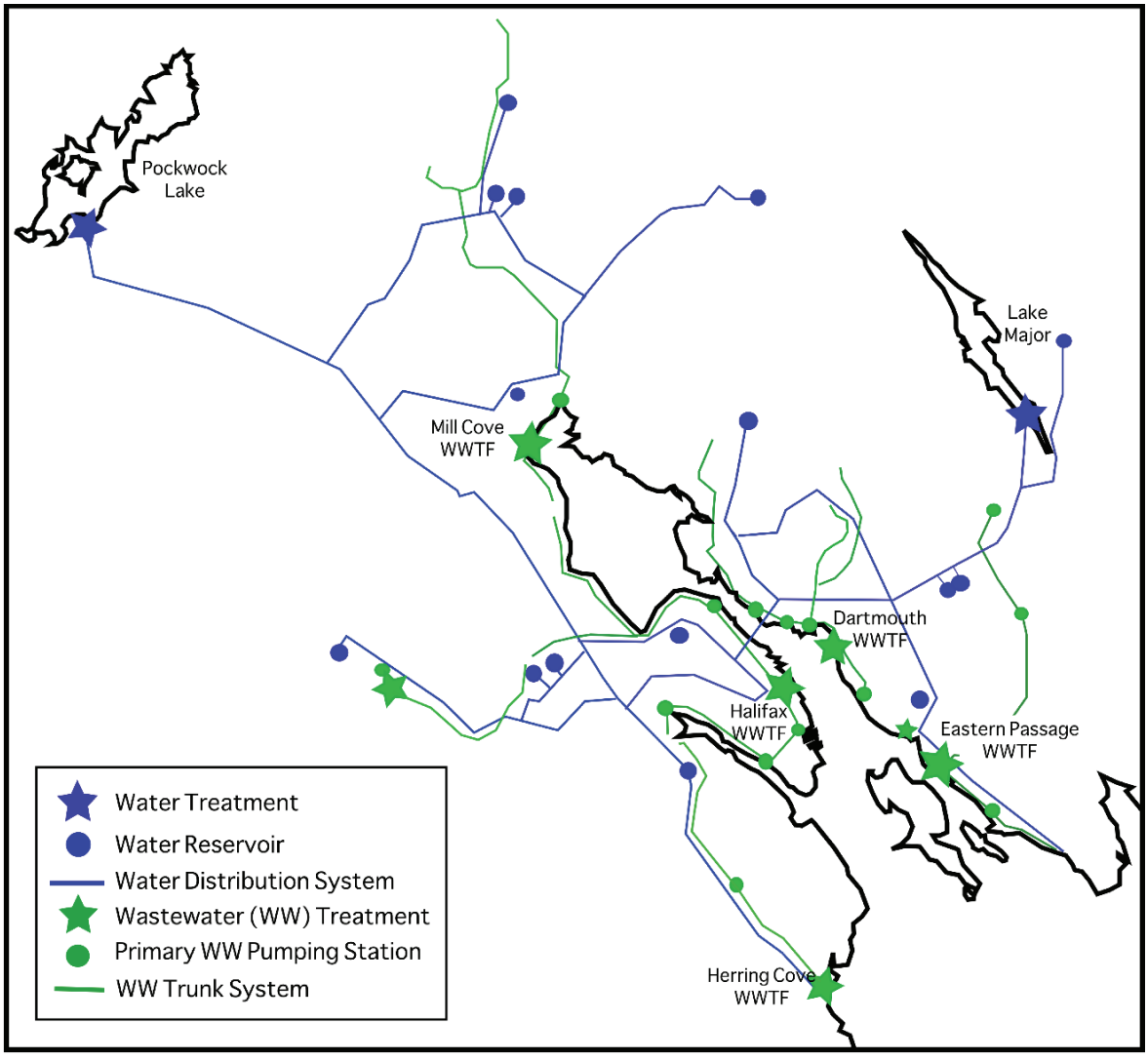

Figure 3.11: Water and wastewater service districts in the HRM, adapted from *Halifax Water* (2012), and outlining the major reservoirs and WWTFs.

If samples were collected following a period of little precipitation, it is likely that the δ^{18}O composition would be less variable in these wastewater outfalls as the isotopic composition of lakes and rivers around Halifax should be stable; any differences in residence time between Sackville River and the wastewater system should have a weaker effect on the isotopic composition of wastewater outfalls. Since any variability in δ^{18}O of wastewater (Table 3.6) is likely a result of variable WWTF residence times, wastewater samples can be considered to be representative of lacustrine and riverine water around Halifax that enters Bedford Basin.

3.1.4 Defining Freshwater End Members

To support a mass balance analysis in Bedford Basin (Chapter 4), freshwater inputs with isotopically distinct δ^{18}O values must be identified. The two main inputs of freshwater to Bedford Basin were found to be Sackville River (including wastewater) and precipitation. These inputs must first be defined as two separate and isotopically distinct inputs, or they cannot be defined as different end members in this analysis.

3.1.4.1 Sackville River & Precipitation

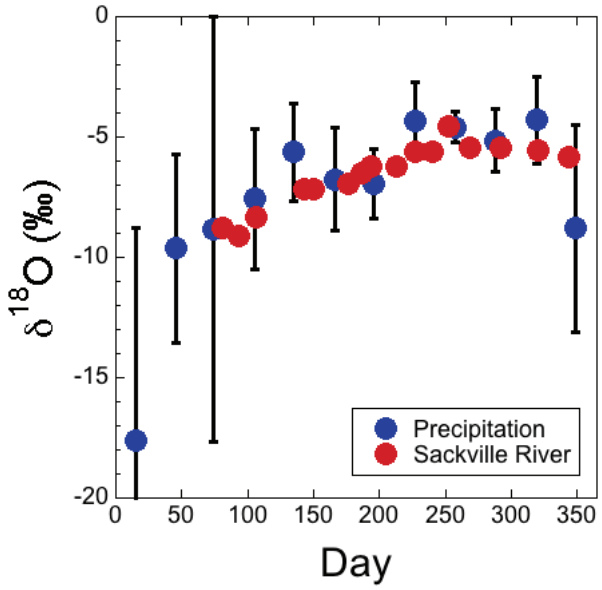

Figure 3.12: Yearly change in δ^{18}O of Sackville River surface water (May 2012 - Apr 2014) and precipitation (July 1^{st} 2012 - June 30^{th} 2013). Precipitation data are monthly amount-weighted averages with 95% CIs.

Figure 3.12 illustrates the relationship between δ^{18}O of precipitation and Sackville River surface samples collected over time; precipitation samples are amount-weighted monthly

averages (July 2012 - June 2013), while Sackville River samples are single measurements collected between May 2012 and April 2014. All Sackville River δ^{18}O samples fall within the error bars (95% CIs) of the amount-weighted monthly precipitation averages of δ^{18}O, and as such these two freshwater inputs to Bedford Basin cannot be distinguished from one another (Figure 3.12). To confirm this covariance, a Wilcoxon-Mann-Whitney rank sum test was performed on the δ^{18}O values for Sackville River and precipitation. A p value of 0.3895 was found, showing that these two inputs are not statistically different (p value $>$0.05).

Due to the fact that the δ^{18}O of Sackville River and precipitation co-vary throughout the year, they can be represented as a single freshwater, or meteoric, input to Bedford Basin. This single meteoric input to Halifax Harbour represents all local freshwater inputs, including Sackville River, precipitation, run-off, and wastewater outfalls.

3.1.4.2 Seasonally-Varying End Members

In Figure 3.12, a seasonal variation in the δ^{18}O of precipitation and Sackville River is evident. Samples are depleted in δ^{18}O in the winter months (December, January, and February), and comparatively enriched in the summer months (June, July, and August) (Figure 3.12). As this freshwater end member (representing all meteoric water entering Bedford Basin) varies seasonally, the difference in δ^{18}O over different times of the year must be considered when performing a mass balance analysis (Chapter 4). Therefore, isotopically distinct seasonal end members must be selected in order to determine the variability in freshwater inputs to Bedford Basin over this study (June 2012 - October 2013).

When determining seasonal freshwater end members for Bedford Basin (summer & winter), only data from precipitation samples were used. Sackville River samples are not included in the calculation of the summer and winter freshwater end members for a number of reasons. First, Sackville River samples are single measurements collected over multiple years (2012, 2013, & 2014), and these data cannot be merged with precipitation samples (which must be amount-weighted). Since precipitation samples were collected during every precipitation event, these data provide a well-defined survey of the annual variability in δ^{18}O of meteoric water. In addition, since the δ^{18}O of Sackville River co-varies with precipitation, these two inputs cannot be separated. As such, it is reasonable to assume that the amount-weighted average δ^{18}O of precipitation is also representative of Sackville

River (Figure 3.12). Like Sackville River, wastewater samples will also be grouped with the seasonal freshwater end members, as the δ^{18}O of these inputs also co-varies with precipitation. So, the seasonal end members, despite being based only on the amount-weighted averages of seasonal precipitation, are taken to be representative of all freshwater sources (wastewater, precipitation, and riverine) entering Bedford Basin.

3.1.4.3 Winter & Summer Freshwater End Members

To determine the winter end member, all of the precipitation samples collected in December 2012, January 2013 and February 2013 were amount-weighted and averaged. This provides us with a winter end member of -10.97‰ with a 95% CI of 2.96.

To determine the summer end member, an amount-weighted average δ^{18}O value was calculated using the summer months of June, July and August. However, since precipitation samples were collected in July, August, September, and October of 2012 and 2013, we have samples for June of 2012, July of 2012 and 2013, and August of 2012 and 2013. To determine which summer months to use for this end member, different groupings were amount-weighted and averaged. The first sampling year began in July of 2012 and ended in June of 2013. This means that if we use the first three sampled summer months then these months are not in succession (July & August of 2012, and June of 2013). The second option would be to use the first three summer months in succession: June, July, and August of 2013. Although this has entered into the second sampling year, all of the samples represent one summer.

The amount-weighted average δ^{18}O of the first three summer months (July and August of 2012 & June of 2013) was found to be -6.18‰, while the amount-weighted average of the three summer months in 2013 was -5.39‰ (Figure 3.13). There is some difference between the different summer groupings, however this difference is not statistically significant (p value $<$0.05), with a p value of 0.7338 found when a Wilcoxon-Mann-Whitney rank sum test was performed.

Based on the insignificant variability between years, the three summer months in 2013 were selected for the summer end member calculation as these three months were in succession. There is some yearly variability within precipitation, as discussed in Section 3.1.1, however by selecting three consecutive months, it should provide us with a better idea of the natural, seasonal, variability in δ^{18}O of precipitation over the summer. As such, we have a summer precipitation end member of -5.39‰ with a 95% CI of 0.96.

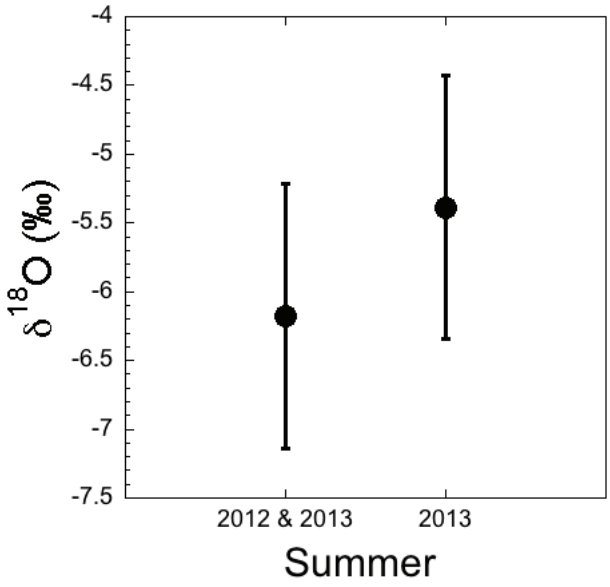

Figure 3.13: Average amount-weighted δ^{18}O of potential summer end member groupings, with 95% CIs. "2012 & 2013" includes July and August of 2012, and June 2013 (N = 15), while "2013" includes June, July, and August of 2013 (N = 13).

3.2 Offshore Inputs

To perform mass balance calculations in Bedford Basin (Chapter 4), an offshore end member must be determined. The offshore end member represents water from the Scotian Shelf that enters Halifax Harbour and mixes with the freshwater end members in Bedford Basin, defined in Section 3.1.4. To define an offshore end member, representative δ^{18}O and salinity values must be determined. By examining the composition of Scotian Shelf water, and the variability in its salinity and δ^{18}O composition over a year, it is possible to define an offshore end member to be used in this study.

3.2.1 Scotian Shelf

Using Halifax Line (HL) data collected during Atlantic Zone Monitoring Program (AZMP) cruises in October 2008 and April 2009, δ^{18}O and salinity measurements can be selected to characterize the composition of water on the Scotian Shelf (Figure 2.2). By defining its composition, it is possible to determine what water from the Scotian Shelf (depths and stations on this sampling line) enters Halifax Harbour. Once we know the origin of water in Bedford Basin, offshore salinity and δ^{18}O values can be selected as the offshore end member for our mass balance analysis (Chapter 4).

As discussed in Section 1.3.2, the Scotian Shelf is composed of three main source waters: St. Lawrence Estuary Water (SLEW: 29.5, -2.4‰), Labrador Shelf Water (LShW: 32.78, -1.53‰), and Warm Slope Water (WSW: 35.16, 0.36‰) (Table 1.3) (*Khatiwala et al.*, 1999; *Shadwick and Thomas*, 2011). The general movement of these water masses along the Scotian Shelf can be seen in Figure 1.9. Based on previous analyses of the source waters present on the Scotian Shelf (*Huntsman*, 1924; *Khatiwala et al.*, 1999; *Shadwick and Thomas*, 2011), it is likely that SLEW and LShW, which travel along the shelf, close to Nova Scotia, will have a greater influence on the water mass composition of Halifax Harbour (Figure 1.9), with the magnitude of SLEW input varying seasonally. WSW, which is composed of Labrador Slope Water (LSW) mixed with warmer and denser Gulf Stream (GS) water, is found deeper in the water column and further offshore (*Shadwick and Thomas*, 2011). The circulation of water on the Scotian Shelf is dominated by the Nova Scotia (NS) Current, an extension of the Labrador Current, which flows southwest, parallel to the coast (*Shadwick and Thomas*, 2011). Further offshore, the salinity of the Scotian Shelf increases due to the northward transport of warm and saline Gulf Stream waters (*Shadwick and Thomas*, 2011). Although the general position of these water masses on the Scotian Shelf is known, using these AZMP data we can illustrate the fluctuation in these water masses over a year (October 2008 & April 2009) to determine what water on the Scotian Shelf contributes water to Halifax Harbour.

Figure 3.14 presents transects for Halifax Line AZMP data (δ^{18}O, salinity, and temperature) collected in October 2008 and April 2009. In all of these transects, only data above 300 m depth are included. Stations HL 5.5, 6, and 7 included samples collected at depths greater than 300 m, however any samples deeper than 300 m showed no difference in δ^{18}O or salinity compared with the measurements taken at, or just above, 300 m at these stations. This allows us to focus on the different water masses present on the Scotian Shelf, rather than the Scotian Slope.

There is a distinction between the surface waters (1 - 100 m) and deep waters (100 - 300 m) in all of the transects (Figure 3.14), and when temperature is examined, distinct boundaries are evident. *Loder et al.* (1997) defined the Scotian Shelf as a two-layered system in the winter and three-layered in the summer. In the winter (April 2009), cold, relatively fresh shelf water overlies more saline slope-derived water, resulting in a two-layered system (Figure 3.14(f)). However, in the summer (October 2008) a warm shallow

surface layer overlays this two-layer system creating a three-layered system (Figure 3.14(e)). SLEW and LShW make up the cold, relatively fresh water, originating from the Gulf of St. Lawrence and the Labrador Shelf, while the warmer, more saline, underlying water is composed of WSW. Regardless of the season, fresher and colder, isotopically depleted waters are found closer to the coast and at the surface, while more saline and warmer, isotopically enriched slope waters are found at depth and further offshore (Figure 3.14).

The presence of WSW on the Scotian Shelf is evident in both October 2008 and April 2009 in δ^{18}O and salinity data (Figure 3.14). This dense, warm, and isotopically enriched

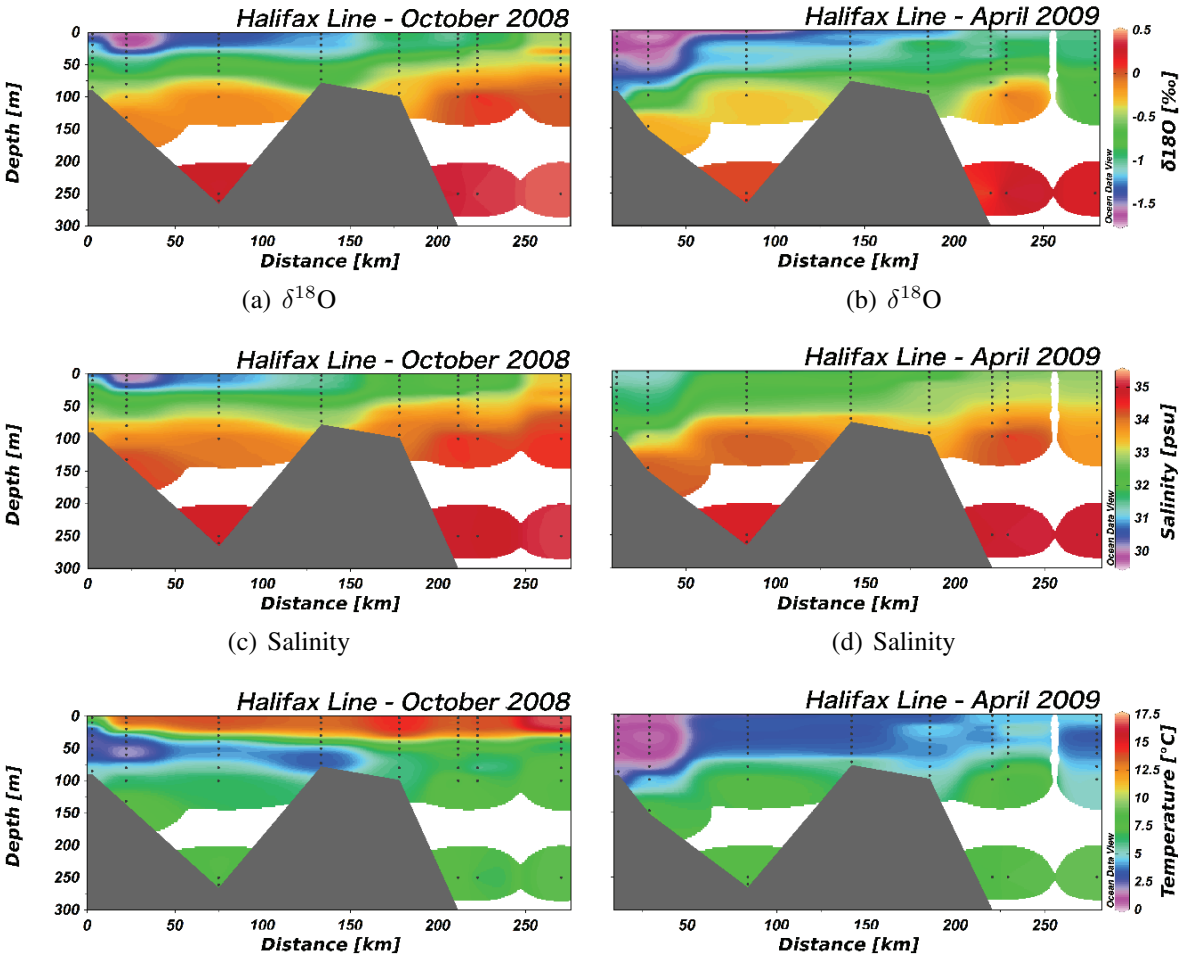

(a) δ^{18}O (b) δ^{18}O

(c) Salinity (d) Salinity

(e) Temperature (f) Temperature

Figure 3.14: Halifax Line AZMP δ^{18}O, salinity, and temperature measured in October 2008 (a, c, e) and April 2009 (b, d, f). Halifax Line station locations are presented in Figure 2.2. HL-1 is the first station, located to the far left of these transects.

water can be seen on the Scotian Shelf at depths greater than 60 m, and on the Scotian Slope. WSW gets closer to the surface, with increasing distance offshore, while LShW and SLEW dominate surface waters close to the coast (Figure 1.9).

SLEW flows along the coast of Nova Scotia, bringing fresh, and isotopically depleted water from the St. Lawrence Estuary; this input can be seen in Figure 3.14, with the most isotopically depleted and freshest water found near the coast. In October, the Scotian Shelf receives the maximum contribution from the Gulf of St. Lawrence, and as a result the contribution of SLEW is also at a maximum (*Shadwick and Thomas*, 2011). This can be seen in October of 2008, with a salinity of less than 30 (Figure 3.14(c)) and a δ^{18}O of less than -2‰ (Figure 3.14(a)) on the Scotian Shelf, illustrating the presence of SLEW (29.5, -2.4‰). In April, the contribution of SLEW is smaller due to the formation of sea ice in the Gulf of St. Lawrence in the winter; this leads to a stronger influence of LShW in April (winter) compared with October (summer) (*Shadwick and Thomas*, 2011). In April, more of the surface waters are dominated by LShW (32.78, -1.53‰) (Figures 3.14(d) & 3.14(b)). Based on these data, the distribution of water masses across the Scotian Shelf is evident, however the composition of water (δ^{18}O and salinity) that enters Halifax Harbour cannot be determined.

It should be noted that the use of colour-mapping and weighted average-gridding in the preparation of section plots (Figure 3.14) can provide some bias or subjectivity and may emphasize trends that are not actually present, or rather under- or over-emphasize trends. Nevertheless, it is evident that there is a strong distinction between the overlying, fresher surface waters (SLEW & LShW) and underlying, warmer, saltier waters (WSW).

In addition to the transects presented in Figure 3.14, temperature-salinity, or TS diagrams, can be used to examine the presence of different water masses on the Scotian Shelf (Figure 3.15). Greater variability is presented in October 2008, compared with April 2009, as a result of increased sea surface temperature and greater inputs of SLEW. Variability in the temperature and salinity of samples collected in October 2008 and April 2009 is evident, however below the seasonally-warmed surface layer (October 2008), the same trends can be seen (Figure 3.15).

Figure 3.15 illustrates the presence of these source waters on the Scotian Shelf and relates their presence to depth. With increasing depth on the Scotian Shelf, water becomes warmer and saltier, however for deep samples (>300 m) found on the Scotian Slope, a

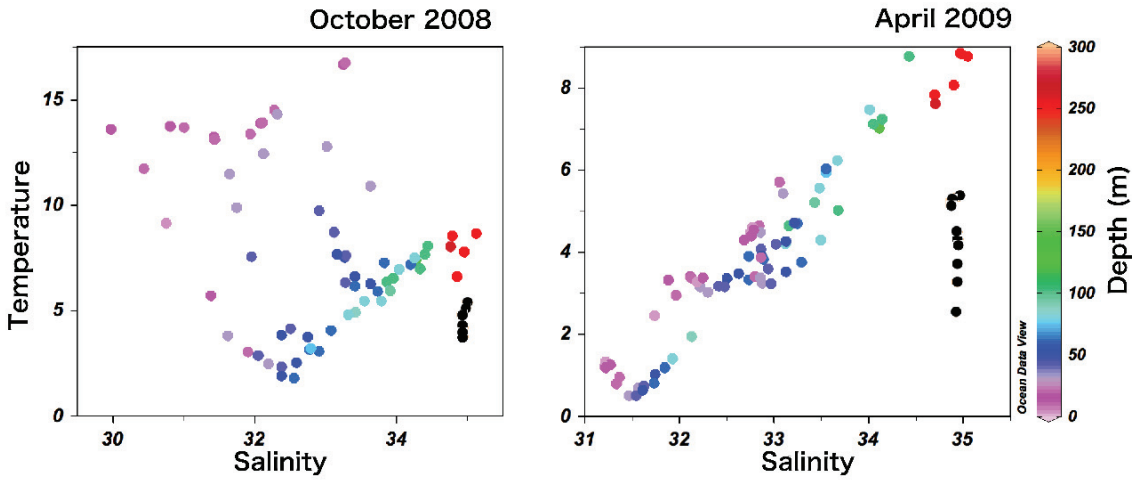

Figure 3.15: Temperature-Salinity plots for Halifax Line samples from October 2008 and April 2009 with depth plotted on the z-axis. Note the different scales on the x- and y-axes. Black points fall outside the depth range (i.e. >300 m).

decrease in temperature can be seen at a constant salinity ($\sim$ 35 psu). These samples are composed of the saltier WSW, however temperature decreases as these samples are found deeper in the water column (to a depth of 1500 m in October 2008 and 2500 m in April 2009). Figure 3.15 illustrates the influence of fresher SLEW and LShW close to the surface, with stronger inputs of WSW deeper in the water column, outlining the division of these source waters on the Scotian Shelf.

Finally, a δ^{18}O-S plot can be used to illustrate the relationship between the Halifax Line data and the end members present on the Scotian Shelf, as defined by *Khatiwala et al.* (1999). The δ^{18}O-S relationships for October 2008 and April 2009 Halifax Line samples are presented along with the Scotian Shelf end members (SLEW, LShW, and WSW) (Figure 3.16). In Figures 3.16(a) [October 2008] and 3.16(b) [April 2009], it is evident that there is no pure SLEW on the Scotian Shelf, as all of the water collected has a greater δ^{18}O and salinity than the SLEW end member (29.5, -2.4‰). LShW falls to the right of both mixing lines as a result of brine rejection during sea ice formation, increasing salinity without changing δ^{18}O (*Shadwick and Thomas*, 2011). No samples fall on the LShW end member, which may show that this water is a mixture of these water types, rather than pure LShW. Finally, there is a definite presence of salty WSW, with a number of samples around this end member.

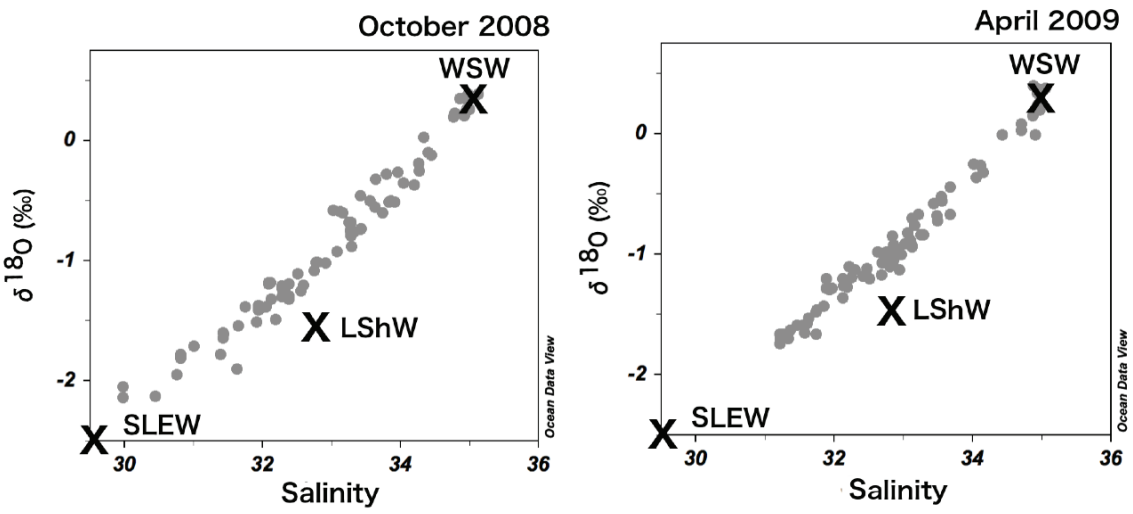

(a) October 2008 (b) April 2009

Figure 3.16: δ^{18}O-Salinity relationship for Halifax Line samples from (a) October 2008 and (b) April 2009 with Scotian Shelf end members included.

3.2.2 Defining an Offshore End Member

3.2.2.1 Scotian Shelf Water in Halifax Harbour

To date, no studies have specified the composition of water on the Scotian Shelf that enters Halifax Harbour. It is evident that water in Halifax Harbour is composed of Scotian Shelf water, however the exact input, and in particular the salinity and δ^{18}O composition, is unknown. The Nova Scotia (NS) current, which runs parallel to the coast, likely brings SLEW and LShW into the Harbour. However, infrequent, but strong, storm events may also bring water into Halifax Harbour, introducing deeper, saltier, WSW (Shiliang Shan, *personal communications*). To determine the water on the Scotian Shelf most likely to enter Halifax Harbour, water samples collected at stations in Halifax Harbour (October 2012 and April 2013) were added to the transects presented in Figure 3.14 (Figure 3.17). Samples from Bedford Basin, the Narrows, the Outer Harbour, and Station 2 (only April) were added to these transects (Figure 3.17). The coordinates for these locations can be found in Table 2.1.

As discussed, the input of SLEW is greater in October as a result of increased sea ice formation in the Gulf of St. Lawrence in April; this is reflected both on the Scotian Shelf, as well as inside Halifax Harbour (Figure 3.17). WSW, found in deeper parts of the Scotian Shelf and Scotian Slope, is not observed in Halifax Harbour in April or October. In both

the October 2008 and April 2009 data, a decrease in salinity and δ^{18}O can be seen as we move from further offshore into Halifax Harbour.

The δ^{18}O-S relationship can also be used to examine the influence of Scotian Shelf water on Halifax Harbour water composition. Figure 3.18 presents the δ^{18}O-S relationship for Halifax Line samples collected in April and September of 2008 from *Shadwick and Thomas* (2011). It is evident that there is a shift in the slope of this relationship with the input of SLEW, as fresher, more isotopically enriched samples are seen in September compared with April. LShW and WSW carry isotopically depleted Arctic river water (-21‰), while SLEW introduces more isotopically enriched St. Lawrence River water (-10.3‰) (*Khatiwala et al.*, 1999). As a result, the zero-salinity intercept of the δ^{18}O-S relationship for these samples will shift depending on the strength, or weakness, of the input of SLEW on the Scotian Shelf.

Figure 3.19 presents the δ^{18}O-S relationship for all of the Halifax Line AZMP samples collected in October 2008 and April 2009, and includes Halifax Harbour samples (BB, N, and OH) collected in October 2012 and April 2013. This increase in SLEW in the summer (October), and decrease in winter (April) can again be seen, with fresher and

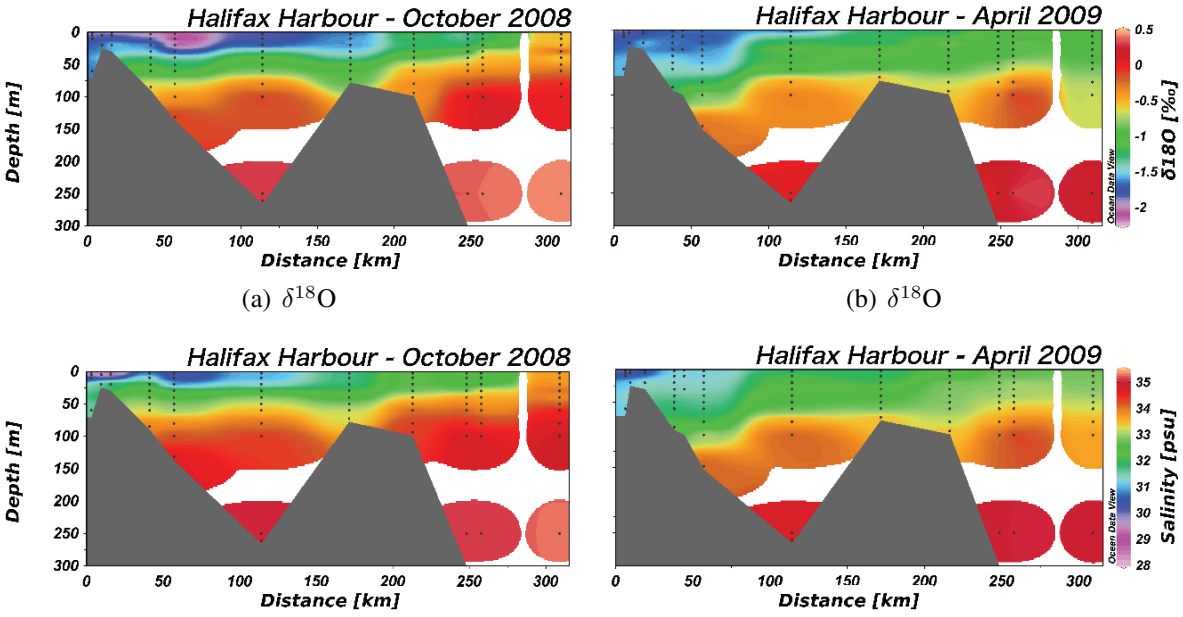

(a) δ^{18}O (b) δ^{18}O

(c) Salinity (d) Salinity

Figure 3.17: Halifax Line AZMP data for October 2008 (a, c) and April 2009 (b, d) with added Halifax Harbour samples collected in October 2012 and April 2013 respectively. Bedford Basin is located at the far left of these transects.

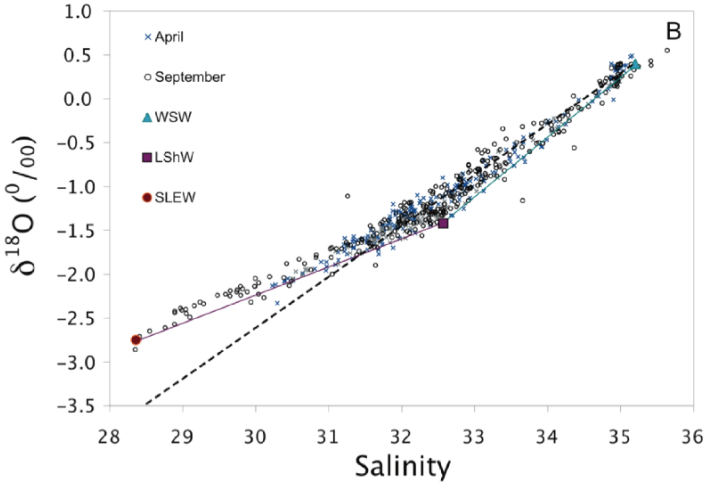

Figure 3.18: δ^{18}O-S relationship for Halifax Line AZMP samples collected in April and September of 2008. Figure from *Shadwick and Thomas* (2011).

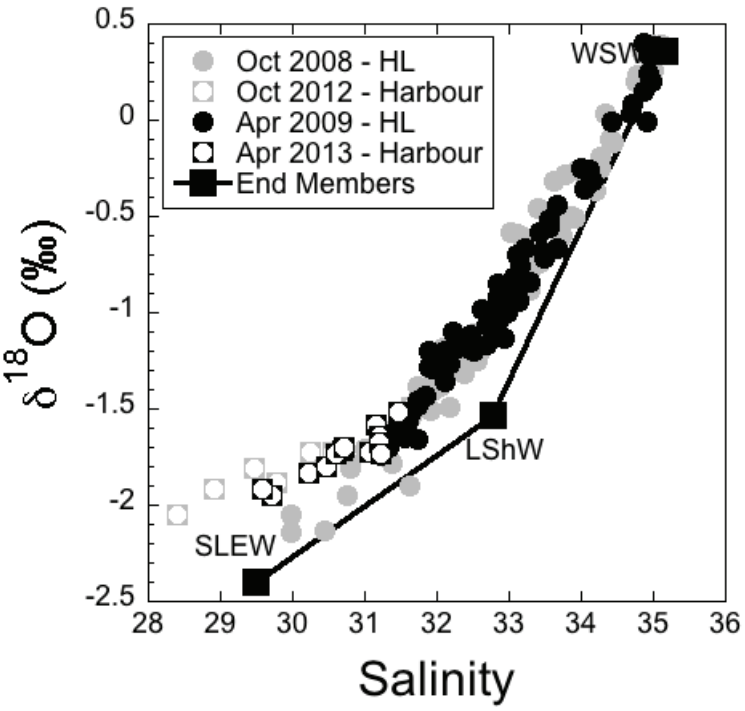

Figure 3.19: The δ^{18}O-salinity relationship for Halifax Line samples (Oct 2008 & Apr 2009) and Halifax Harbour samples (Oct 2012 & Apr 2013).

more isotopically depleted samples seen in October of 2008 (HL) and 2012 (HH). The relationship between Halifax Line AZMP samples and Halifax Harbour samples collected during this study will be further discussed in Section 4.1.2, where the intersect of these two lines (i.e. Figure 3.19) will be considered when selecting an offshore end member.

A number of Halifax Harbour samples are more isotopically enriched and fresher than SLEW (Figure 3.19). Halifax Harbour is not a closed system and there are additional freshwater inputs entering from land that could alter this relationship, adding freshwater more isotopically enriched than SLRW (-10.3‰) and Arctic river water (-21‰). This enrichment in Halifax Harbour samples suggests that there is an additional freshwater end member(s) present in this system, changing the slope and zero-salinity intercept of this relationship (Figure 3.19). The water entering Halifax Harbour from the Scotian Shelf is likely a combination of fresher and more isotopically depleted SLEW and LShW, with no direct influence of WSW.

3.2.2.2 Potential Offshore End Members

To perform a mass balance calculation in Bedford Basin, an offshore end member must be defined. To select the most representative value, and to determine the error associated with this selection, a number of potential end members were chosen. These potential end members were selected based on our knowledge of Scotian Shelf water composition, as discussed above.

First, the δ^{18}O and salinity of all Halifax Line samples collected in October 2008 and April 2009 were plotted (Figure 3.20) to determine the linear regression equation. The lowest (30.44) and highest (35.12) salinity points were selected from this plot. As the two lowest salinity points fall off (above) this regression line, they are likely influenced by a more isotopically depleted freshwater source (e.g. local freshwater or ice melt). As such, the third lowest salinity point was chosen for this analysis, as it is more representative of a low salinity value composed of Scotian Shelf water, falling on the δ^{18}O-S regression line. Although the low and high points selected are likely not representative of all water that enters Halifax Harbour via the Scotian Shelf, these points are representative of the extremes. By including these two extremes it is possible to look at how much the natural variability of water on the Scotian Shelf could alter this analysis, through the selection of a Scotian Shelf end member. A salinity in the middle of this plot (Figure 3.20) was also selected as a potential end member (32.63) to represent a salinity value between these two

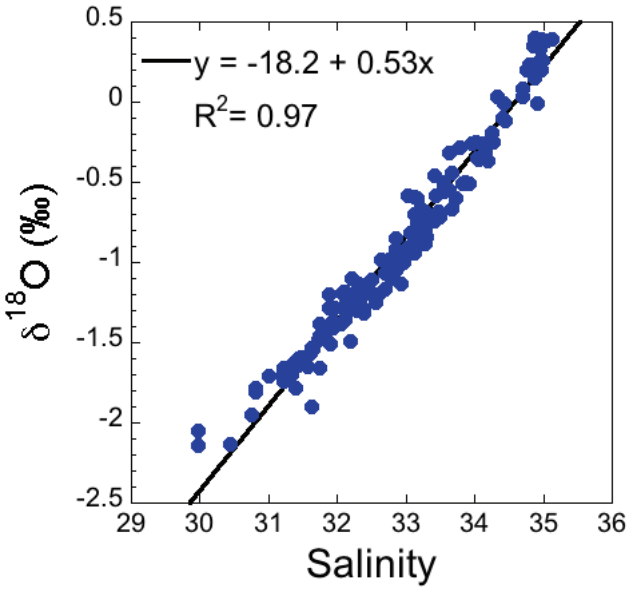

Figure 3.20: δ^{18}O-S relationship for Halifax Line AZMP samples (Oct 2008 & April 2009).

extremes.

Once these low, mid and high salinity points were selected, δ^{18}O was calculated using the linear regression equation of this relationship, presented below (Figure 3.20). This calculation, for the low salinity value, is shown below, and the δ^{18}O values, calculated for the low, mid and high salinity points on the Scotian Shelf, are presented in Table 3.7.

$$\begin{aligned} y &= 0.573x - 18.234 \\ y &= 0.573(30.44) - 18.234 \\ y &= -2.18‰ \end{aligned} \tag{3.1}$$

The average salinity and δ^{18}O of all Halifax Line samples (October 2008 & April 2009) were calculated. In addition, based on the analysis of Scotian Shelf water mass mixing, the salinity and δ^{18}O of the top 60 m of the first five HL stations (HL-1, HL-2, HL-3, HL-4, and HL-5) were also averaged.

When these five end members are added to a δ^{18}O-S plot, along with the previously defined freshwater end members (summer & winter) (Figure 3.21), it is possible to see how the selection of an offshore end member may alter the mass balance calculation.

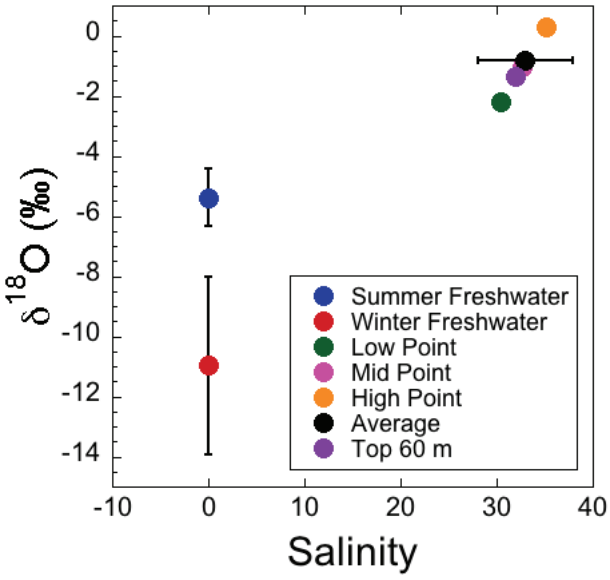

Figure 3.21: Bedford Basin end members (δ^{18}O and salinity). Winter and summer freshwater end members are included with the five potential offshore end members.

To examine the effect of different end members on mass balance calculations, each of the five potential offshore end members will be used in the Bedford Basin mass balance equations, presented in the following chapter. This will help to illustrate what effect the use of different offshore end members will have on this analysis and what errors may be associated with the selection of this point.

This chapter has defined the end members and uncertainty (Table 3.7) to be used in the following chapter on mass balance (Chapter 4). However, it is the definition (δ^{18}O and salinity) of these source waters (i.e. Sackville River, precipitation, and wastewater) and the variability in δ^{18}O throughout the year that are novel to this study, as they have never before been measured in Halifax. In summary, this chapter establishes the inputs of fresh and saline water to Halifax Harbour, while identifying the δ^{18}O and salinity of these inputs and their composition over time (daily, monthly, seasonally, and annually).

Table 3.7: Halifax Harbour freshwater and potential offshore end members. 95% CIs are presented for δ^{18}O and salinity (when possible).

End Member	**Potential Value**	**Salinity**	**95% CI**	δ^{18}**O (‰)**	**95% CI**
Summer		0	-	-5.39	0.96
Winter		0	-	-10.97	2.96
Offshore	Low Point	30.44	-	-2.18	-
	Mid Point	32.63	-	-1.03	-
	High Point	35.12	-	0.29	-
	Average	32.99	4.99	-0.84	0.10
	Top 60m	31.99	0.18	-1.37	0.08

CHAPTER 4

MASS BALANCE

Conservation equations for mass, salinity, and oxygen isotopes, derived by *Östlund and Hut* (1984) and *Khatiwala et al.* (1999), can be adapted to calculate the relative contribution of three water masses (defined in Chapter 3) in Bedford Basin (Equation 4.1). In Equation 4.1, F_W, F_S, and F_O refer to the fraction of winter precipitation, summer precipitation and offshore water respectively, and S_W, S_S, S_O, X_W, X_S, and X_O represent the corresponding salinity (S) and δ^{18}O (X) values.

$$\begin{aligned} F_W + F_S + F_O &= 1 \\ F_W S_W + F_S S_S + F_O S_O &= S_B \\ F_W X_W + F_S X_S + F_O X_O &= X_B \end{aligned} \tag{4.1}$$

To calculate the mass fraction of summer precipitation, winter precipitation, and offshore water in Bedford Basin, Equation 4.1 can be rearranged to solve for F_W, F_S, and F_O, presented in Equations 4.2, 4.3, and 4.4 respectively.

$$F_W = \frac{S_S(X_B - X_O) - S_O(X_B - X_S) + S_B(X_O - X_S)}{S_W(X_O - X_S) - S_S(X_O - X_W) + S_O(X_S - X_W)} \tag{4.2}$$

$$F_S = -\frac{S_W(X_B - X_O) - S_O(X_B - X_W) + S_B(X_O - X_W)}{S_W(X_O - X_S) - S_S(X_O - X_W) + S_O(X_S - X_W)} \tag{4.3}$$

$$F_O = \frac{S_W(X_B - X_S) - S_S(X_B - X_W) + S_B(X_S - X_W)}{S_W(X_O - X_S) - S_S(X_O - X_W) + S_O(X_S - X_W)} \tag{4.4}$$

As presented in Chapter 3, the offshore end member (δ^{18}O and salinity), representative of Scotian Shelf water entering Halifax Harbour, could not be defined. As a result, five "potential" offshore end members were selected based on historical literature of water mixing along the Scotian Shelf (Table 3.7) (*Khatiwala et al.*, 1999; *Shadwick and Thomas*, 2011). To determine the most representative offshore end member for this analysis, all five potential offshore end members (along with the two freshwater end members) were included in the mass balance calculations (Equation 4.1). By identifying the offshore end member that "performs best" in these mass balance calculations, explained in the following section (4.1), an offshore end member can be selected. In addition, by examining the differences in mass fraction results with the use of different offshore end members, it is possible to quantify the error associated with the selection of an offshore end member.

4.1 Mass Balance with Potential Offshore End Members

4.1.1 Error Associated with Offshore End Member Selection

In these mass balance calculations, only the salinity (S_O) and δ^{18}O (X_O) of offshore water will differ; the effect of altering these two variables on the mass fraction results (F_W, F_S, and F_O), and the associated error, will be discussed throughout this section. Figure 4.1 presents the five average potential mass fractions of water (F_W, F_S, and F_O) in Bedford Basin (1 & 60 m) from June 2012 to October 2013, calculated using Equation 4.1. The five potential offshore end members were substituted into this equation to determine the effect of using different offshore end members on mass fraction results. One-way ANOVA tests with Tukey's All Pairs Comparison were performed on these data to determine if differences between the mass fraction results calculated with different offshore end members were significant. Throughout this chapter, significant differences (p value $<$0.05) in these mass fraction figures are identified with a black "*" (e.g. Figure 4.1).

When included in the mass fraction calculations (Equation 4.1), both the "High Point" and "Low Point" offshore end members calculated significantly different (p value $<$0.05) average mass fractions for F_S, F_W, and F_O, when compared with the three other offshore end members (Figure 4.1(a) and 4.1(b)). For samples at 1 m depth, the use of the "Middle Point", "Top 60 m", and "Average" offshore end members did not calculate significantly different average mass fractions for summer precipitation (F_S) and offshore water (F_O), however significantly different (p value $<$0.05) winter precipitation (F_W) average mass

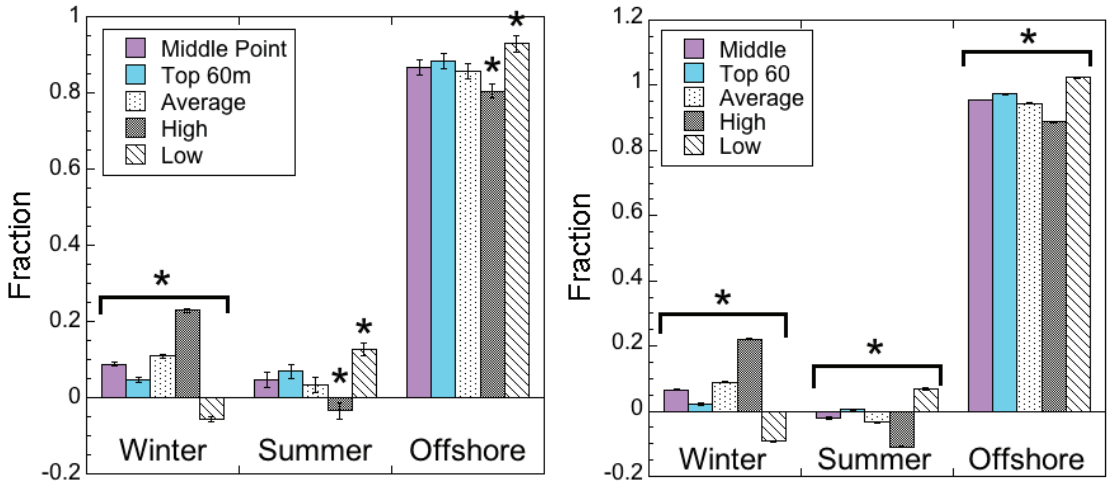

(a) 1 m (b) 60 m

Figure 4.1: Average mass fractions of Bedford Basin water for this study (June 2012 - October 2013) at depths of (a) 1 m and (b) 60 m. Average winter (F_W), summer (F_S), and offshore (F_O) mass fractions (with 95 % CI error bars) are calculated using different offshore end members (Middle Point, Top 60m, Average, High Point, and Low Point). A black "*" indicates that there is a significant difference (p value $<$0.05) between the average mass fraction (i.e. F_W, F_S, or F_O) determined using this offshore end member, and the mass fraction determined by the other four end members. All mass fractions under a bracket (with *) are significantly different from one another.

fractions were calculated with all of the offshore end members (Figure 4.1(a)). The mass fraction calculations for water at 60 m in Bedford Basin found that all of the potential offshore end members calculated significantly different (p value $<$0.05) average mass fractions of average summer precipitation (F_S), winter precipitation (F_W), and offshore water (F_O).

Regardless of depth (Figures 4.1(a) and 4.1(b)), the use of the "High Point" and "Low Point" offshore end members in these mass fraction calculations resulted in statistically different (p value $<$0.05) average mass fraction results (F_S, F_W, and F_O), when compared with the three other potential offshore end members ("Top 60m", "Average", & "Middle"). As discussed in Section 3.2.2, the "High Point" and "Low Point" end members are the least representative of water on the Scotian Shelf entering Halifax Harbour. Therefore, while illustrating the potential range of error associated with offshore end member selection, neither of these two end members will be used as the offshore end member in this study.

Mass fraction calculations were also performed on seasonal groupings of Bedford Basin samples to select the most representative offshore end member as summer and winter precipitation are being used as the two freshwater end members. Bedford Basin samples were divided into three seasonal groupings: summer 2012 (June, July, and August of 2012), winter (December 2012, January and February 2013), and summer 2013 (June, July, and August of 2013) (Figure 4.2). The results of these seasonally-grouped mass fraction calculations should determine whether deviations in the fraction of winter (F_W) and summer (F_S) precipitation correlate with variations in their seasonal input, further illustrating the potential variability associated with the use of different offshore end members.

Figures 4.2(a), 4.2(c), and 4.2(e) present the seasonal mass fraction results for Bedford Basin 1 m samples. At 1 m in summer 2012, calculated mass fractions of winter precipitation (F_W) were found to be significantly different (p value $<$0.05) when the three different offshore end members were used. While, in winter and summer 2012, the "Top 60 m" offshore end member calculated significantly different results from "Middle Point" and "Average", while "Middle Point" and "Average" offshore end member winter mass fractions (F_W) were significantly similar. The average mass fraction results for F_S and F_O at 1 m depth were not found to be significantly different (p value $>$0.05) when using different offshore end members. In comparison, when Bedford Basin samples collected at

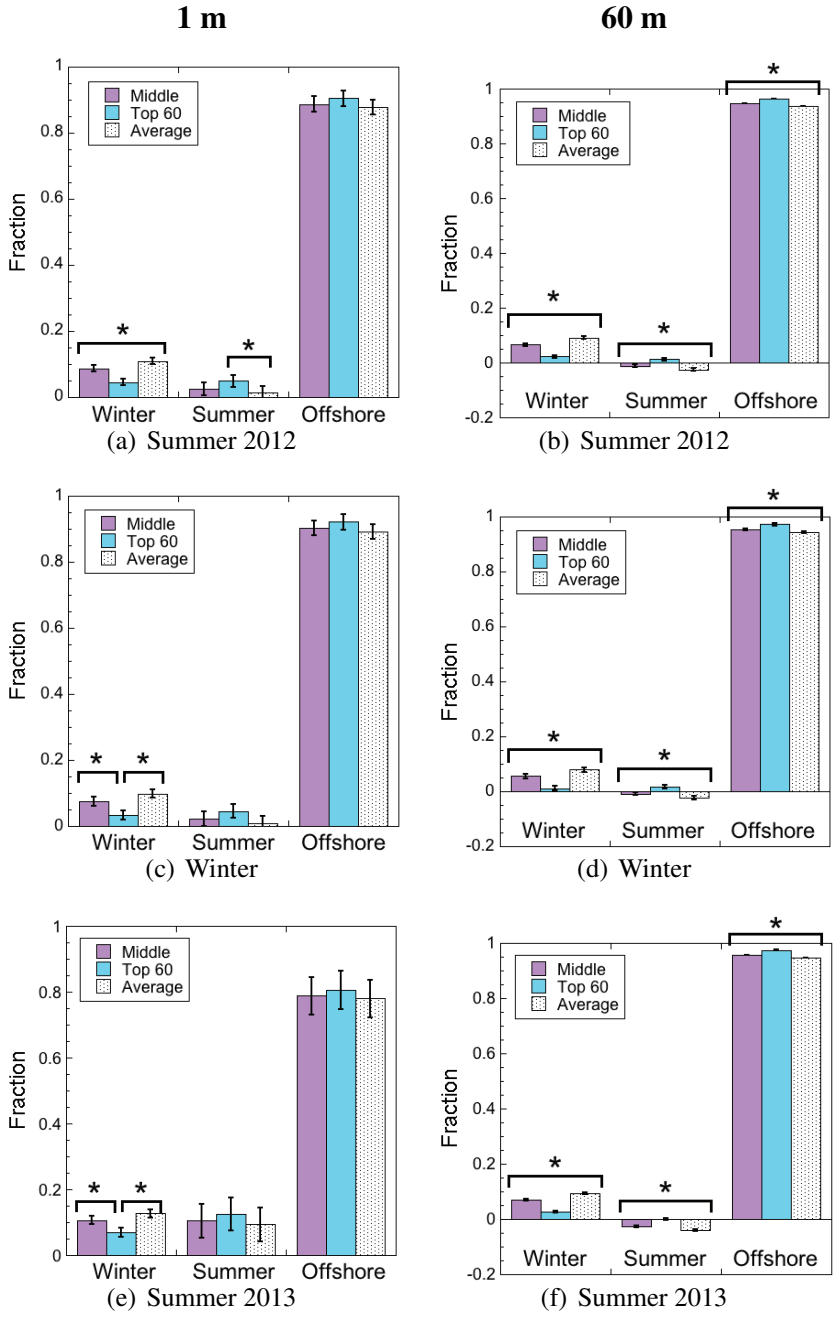

Figure 4.2: Average mass fractions of Bedford Basin water at 1 m (a, c, e) and 60 m (b, d, f) in (a, b) summer 2012 (June, July, Aug 2012), (c, d) winter (Dec 2012, Jan & Feb 2013), and (e, f) summer 2013 (June, July, Aug 2013). Average winter (F_W), summer (F_S), and offshore (F_O) mass fractions (with 95 % CI error bars) are calculated using three potential offshore end members (Middle Point, Top 60m, and Average). A black "*" (p value <0.05) indicates that there is a significant difference between the mass fraction (i.e. F_S, F_W, or F_O) determined using this offshore end member, and the mass fraction determined by the other two end members.

60 m were grouped seasonally (Figures 4.2(b), 4.2(d), and 4.2(f)), all of the end members calculated significantly different mass fractions (p value <0.05).

The significantly different mass fraction results for samples collected at 60 m depth, compared with 1 m, may be due to the stability of bottom waters (*Fader and Buckley*, 1995), and the relatively few renewal events in Bedford Basin throughout the year (*Shan et al.*, 2011). The error bars (95% CI) for the mass fraction results at 60 m are small, particularly when compared to the error bars for the 1 m mass fraction results (Figure 4.2), emphasizing the stability of deep waters compared with frequently-renewed surface waters.

The selection of different offshore end members will result in significantly different mass fraction results, regardless of depth. Therefore, it is necessary to select the end member that best represents water entering Bedford Basin from the Scotian Shelf, while noting that significant differences are possible. It should also be noted that any variability in the δ^{18}O of the winter and summer freshwater end members would also result in an added error. However, as these freshwater inputs were measured throughout the study, we are confident with the selection of these end members.

4.1.2 Selection of the Offshore End Member

4.1.2.1 Selection of an End Member Using Historical Scotian Shelf Data

In addition to defining the variability and error associated with offshore end member selection, mass fraction results can also be used to determine which offshore end member best fits this analysis. When these offshore end members were used to calculate the mass fractions of F_W, F_S, and F_O in Bedford Basin, negative mass fractions were occasionally calculated. The percentages of negative values calculated using different offshore end members are presented in Table 4.1. For each offshore end member, a greater number of negative mass fractions were calculated at 60 m depth, when compared with 1 m (Table 4.1). This may be a result of stable bottom waters in Bedford Basin. However, compared with the mass fraction results for samples collected at 1 m, the percentages calculated for 60 m samples are much smaller, close to zero (Figure 4.2). More negative mass fractions may be calculated at 60 m due to the variability associated with these results. When the "Top 60 m" offshore end member was used in the mass balance calculations, the smallest percentage of negative mass fractions were calculated (Table 4.1).

The fraction of winter precipitation (F_W), summer precipitation (F_S) and offshore (F_O)

Table 4.1: Percentage of negative mass fraction results calculated using different offshore end members. This percentage represents the number of Bedford Basin samples (out of 54) that calculated a negative mass fraction (F_W, F_S, and/or F_O) when this offshore end member was used in the mass balance calculation. This was performed on samples collected at depths of 1 m and 60 m, from June 2012 to October 2013.

Depth	**Offshore End Member**	**Winter (F_W)**	**Summer (F_S)**	**Offshore (F_O)**
1 m	High Point	-	83.3 %	-
	Low Point	96.3 %	-	-
	Mid Point	-	18.5 %	-
	Average	-	35.2 %	-
	Top 60 m	-	1.9 %	-
60 m	High Point	-	100 %	-
	Low Point	100 %	-	-
	Mid Point	-	96.3 %	-
	Average	-	100 %	-
	Top 60 m	1.9 %	35.2 %	-

water in Bedford Basin samples should add up to 1. The first line of the mass balance equation defined in Equation 4.1 presents this relationship:

$$F_W + F_S + F_O = 1$$

This states that (1) there are no additional water inputs to Bedford Basin and (2) the end members are representative of the three inputs, and as such this equation should add up to 1, with no negative mass fractions calculated. If one of these assumptions is not valid, a negative mass fraction would be calculated. Since the only variable that changes in these mass balance calculations is the offshore end member, only the 2^{nd} assumption - that the value of the offshore end member used in this calculation represents the actual input of water to Bedford Basin - can be evaluated with the results from Table 4.1. Therefore, the offshore end member resulting in the fewest negative values should be the most representative of the water entering Bedford Basin from the Scotian Shelf. I have decided to use this constraint on the mass balance results to determine which offshore end member best fits these data.

Figure 4.3 presents schematically a mass balance relationship, illustrating how negative fractions may be calculated. Figure 4.3(a) presents a water mass (identified with a red "x") composed of three inputs (A, B, and C); the mass balance calculation for this water

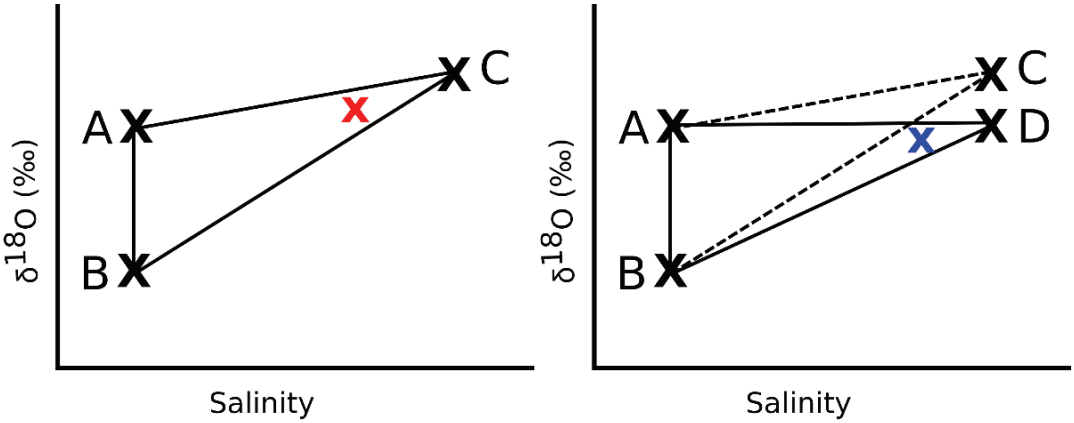

Figure 4.3: (a) Schematic of a mass balance relationship with a water mass (red "x") composed of end members "A", "B", and "C". (b) Illustrates how a negative mass fraction may be calculated for a water mass (blue "x") when using "A", "B", and "C" as end members, but a positive mass fraction would be calculated when using "A", "B", and "D".

mass will result in three positive mass fraction values, all adding up to 1 (Figure 4.3(a)). In comparison, the water mass (identified with a blue "x") presented in Figure 4.3(b) is found outside of the mixing triangle defined by the three inputs (A, B, and C). If the mass balance calculation for this water mass was calculated using "C" as the third end member, a negative mass fraction would result. However, when a different end member ("D") is used, the mass balance calculation will no longer result in negative mass fraction values as this water mass must be composed of water from "D" and not "C". Based on this constraint, the "Top 60m" end member, which resulted in the fewest number of negative values, is the most representative of offshore water entering Bedford Basin (Table 4.1). To better fit these samples, the freshwater end members could have also been adjusted, however it is assumed that these values, which were measured during this study, are representative of the freshwater entering Bedford Basin.

4.1.2.2 Selection of an End Member Using Halifax Harbour Data

The above approach outlines the selection of an offshore end member ("Top 60m") based on Scotian Shelf data (AZMP Halifax Line data: October 2008 & April 2009). Instead of fitting data around a "potential" offshore end member, an offshore end member that encompasses all of the Bedford Basin data into an end member mixing triangle (using the previously selected freshwater end members as the other two points) can be developed. This offshore end member can then be compared to historical measurements of Scotian

Shelf water (salinity and δ^{18}O) to determine if this value is representative of water found on the Scotian Shelf. This should help to determine if negative mass fractions are calculated due to the offshore end member or if changes to the δ^{18}O of freshwater inputs are also driving these changes (Table 4.1).

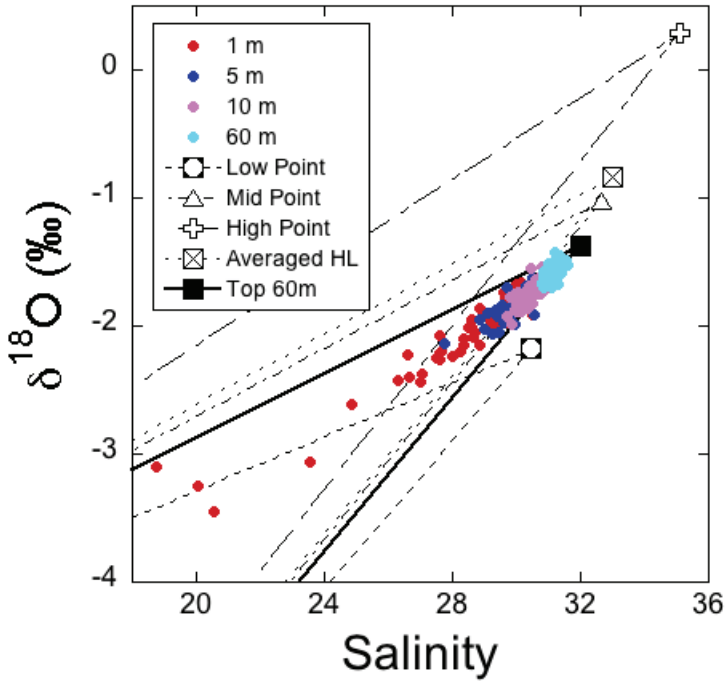

Figure 4.4: Bedford Basin water samples (1, 5, 10, and 60 m) from June 2012 to October 2013, plotted against five different mixing triangles, with the same freshwater end members (not shown), but differing offshore end members.

To develop an end member that fits these data, rather than selecting δ^{18}O and salinity values from Scotian Shelf data, Bedford Basin samples collected at each depth (1, 5, 10, and 60 m) were plotted against the five potential offshore end members (Figure 4.4). The position of the Bedford Basin samples relative to the potential offshore end members helps to determine if a different, more representative, offshore end member is driving the variability in Bedford Basin δ^{18}O and salinity. The majority of the potential offshore end members do not fit the Bedford Basin samples into their mixing triangles (Figure 4.4), also confirmed by negative mass balance results (Table 4.1). When Figure 4.4 is examined, it is evident that "Top 60m" encompasses the most Bedford Basin data, again confirmed by the negative mass balance results (Table 4.1).

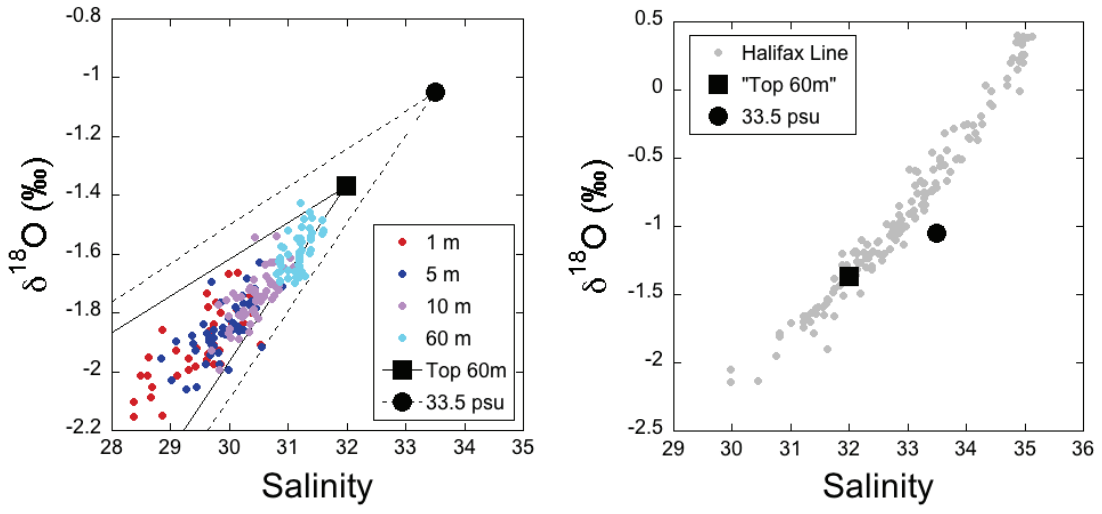

(a) (b)

Figure 4.5: (a) Bedford Basin (1, 5, 10, and 60 m) samples plotted with two mixing triangles with different offshore end members. (b) The "Top 60 m" end member (square) and potential offshore end member at 33.5 (circle), plotted against Halifax Line δ^{18}O and salinity data collected on AZMP cruises in October 2008 and April 2009.

As the majority of the Bedford Basin samples fall inside the "Top 60m" mixing triangle, to develop an offshore end member that fits all of the data, this point will be extended along the same slope until all data points are encompassed. A linear equation was developed using the "Top 60m" end member and a freshwater middle point (-8.18‰), between the winter and summer precipitation end member.

$$y = 0.2129x - 8.18$$

Using this equation of the line, δ^{18}O values were calculated for a number of salinities. All of the Bedford Basin data points collected in this study were encompassed by the mixing triangle when an end member with a salinity of 33.5 was selected (Figure 4.5(a)). As such, this new end member (-1.05‰, 33.5) could now be used as the offshore end member. However, when this end member is plotted alongside Halifax Line data collected in October 2008 & April 2009, this value is not representative of the δ^{18}O-S values recorded on the Scotian Shelf (Figure 4.5(b)). This suggests that a water type of this salinity and δ^{18}O does not exist on the Scotian Shelf, and therefore is not representative of water entering Bedford Basin (Figure 4.5(b)).

In addition to the selection of an offshore end member based on Bedford Basin data,

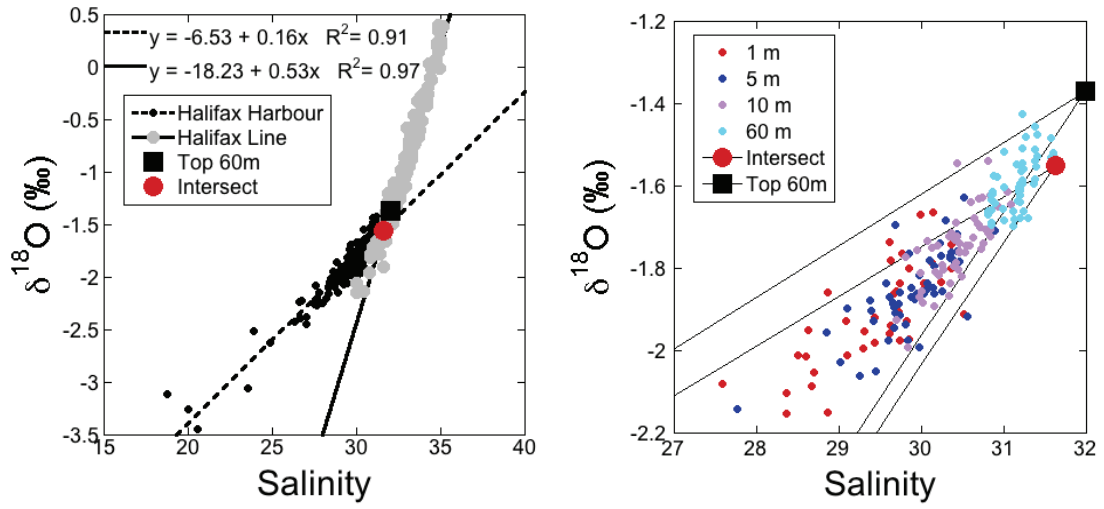

(a) (b)

Figure 4.6: (a) Halifax Line AZMP samples, collected in October 2008 and April 2009, with all Halifax Harbour samples (BB, OH, EP, N, NW), collected between June 2012 and October 2013. The intersect of this relationship (31.63, -1.55‰) (red) and the "Top 60m" end member are added to these regression lines. (b) "Intersect" and "Top 60m" as potential offshore end members, and the fit of all Bedford Basin samples in these mixing triangles.

an offshore end member can be selected by taking the intersect of the regression line calculated for Halifax Line AZMP samples (October 2008 & April 2009), representing Scotian Shelf water, and the regression line for samples collected in Halifax Harbour (including samples from Bedford Basin, the Narrows, Outer Harbour, Eastern Passage, and the Northwest Arm) (Figure 4.6(a)). This intersect identifies the offshore water type influencing the composition of water in Halifax Harbour, and thus may be used as an offshore end member. This "Intersect" offshore end member can be compared to the "Top 60m" end member; where Bedford Basin samples fall with respect to these two mixing triangles should help to illustrate which end member better represents the offshore input of water to Bedford Basin (Figure 4.6(b)). Based on Figure 4.6(a), it is evident that a number of Bedford Basin samples that fall within the "Top 60m" end member mixing triangle are not encompassed by the "Intersect" mixing triangle, with the majority of these samples falling above the mixing triangle. This means that a number of samples collected in Bedford Basin (the majority at 60 m) are more isotopically enriched in δ^{18}O than the "Intersect" end member.

For the purpose of this analysis, we are looking for an offshore end member more isotopically enriched and saline compared with the samples collected in Bedford Basin

Table 4.2: Bedford Basin End Members developed and used in this study.

End Member	Salinity	95% CI	δ^{18}O(‰)	95% CI
Summer	0	-	-5.39	0.96
Winter	0	-	-10.97	2.96
Offshore	31.99	0.18	-1.37	0.08

over this study ($\sim$ 16 months). While the "Intersect" may be representative of what typically enters Halifax Harbour from the Scotian Shelf, due to seasonal differences in offshore input (i.e. April vs. October) there are times in which deep (60 m) Bedford Basin is more isotopically enriched and saline than the water entering from the Scotian Shelf. As such, this "Intersect" end member is not representative of offshore water entering Bedford Basin at all times of the year. For the purpose of this study an idealized δ^{18}O-S value that encompasses all of the samples collected in Bedford Basin over this study will be selected, however the seasonal differences in this offshore input are noted. As such, the "Top 60m" end member is selected due to its better overall fit to the Bedford Basin data, and this conservative value is considered to be the most representative of offshore water entering Bedford Basin throughout the year.

Although the "Top 60m" offshore end member does not encompass all of the data points, it is evident that Bedford Basin samples falling outside of this mixing triangle cannot all be attributed to a differing offshore end member. Bedford Basin samples that fall below this mixing triangle may be influenced by more isotopically depleted meteoric water. This may be due to an additional freshwater input or individual precipitation events not represented by the volume weighted average determined for the winter and summer freshwater end members. Therefore, any points that fall outside of this mixing triangle should be examined individually as there may be a differing saline or freshwater input driving the shift outside of the mixing triangle.

4.1.2.3 Selecting the Offshore End Member

Based on the results of this section, the "Top 60m" offshore end member was selected for this analysis, and this will be referred to as the "offshore" end member for the remainder of this thesis. All mass balance calculations performed on Bedford Basin water collected during this study will employ these three end members (Table 4.2).

4.2 Mass Balance in Bedford Basin

Using the Bedford Basin end members determined in this study (Table 4.2), mass balance calculations (Equation 4.1) can be performed on samples collected in Bedford Basin to determine: (1) the composition of water, (2) the change in this composition over the study period (June 2012 - October 2013), and (3) the δ^{18}O of freshwater inputs to the surface and deep layers of Bedford Basin.

As discussed in Chapter 1, water in Halifax Harbour moves in a typical two-layer estuarine circulation, with seaward flow in the upper layer, and landward flow in the lower (*Fader and Miller*, 2008). This circulation pattern, characteristic of a silled estuary, results in a distinct division between the upper and lower layers of Bedford Basin. *Shan and Sheng* (2012) emphasize this separation, calculating an average flushing rate of $\sim$40 days for upper (0 - 20 m) and $\sim$90 days for lower (20 - 70 m) Bedford Basin using a multi-nested coastal circulation model, developed by *Shan et al.* (2011). Based on the analysis and discussion presented in *Shan et al.* (2011), three different water types can be identified in Bedford Basin: (1) fresh upper layers near Sackville River, (2) salty water in the deep layer, and (3) salty waters introduced from the Scotian Shelf. Freshwater run-off, vertical mixing and sporadic shelf water intrusions throughout the year are the dominant mechanisms controlling the variability of salinity in the deep layers of Bedford Basin (*Punshon and Moore*, 2004; *Shan et al.*, 2011; *Burt et al.*, 2013).

There is a division between the upper (fresher) and lower (saltier) layers of Bedford Basin, leading to the definition of these two layers as different water masses. To determine the composition (i.e. F_W, F_S, and F_O) of the surface and deep layers of Bedford Basin using mass balance calculations, the mixed layer depth (where these two layers are separated) must first be identified.

Throughout the study period (June 2012 - October 2013), samples were collected weekly at 1, 5, 10, and 60 m depth in Bedford Basin. Samples collected at 1 and 60 m can be classified as part of the surface and deep layers respectively, however it is unclear where samples collected at 5 and 10 m should be included. The depth of the mixed layer in Bedford Basin throughout the year can be examined to determine whether samples from these depths belong in the “surface” or “deep” layer, or if the fluctuation of this layer throughout the year means that these two depths cannot be categorized into a single layer (i.e. surface or deep).

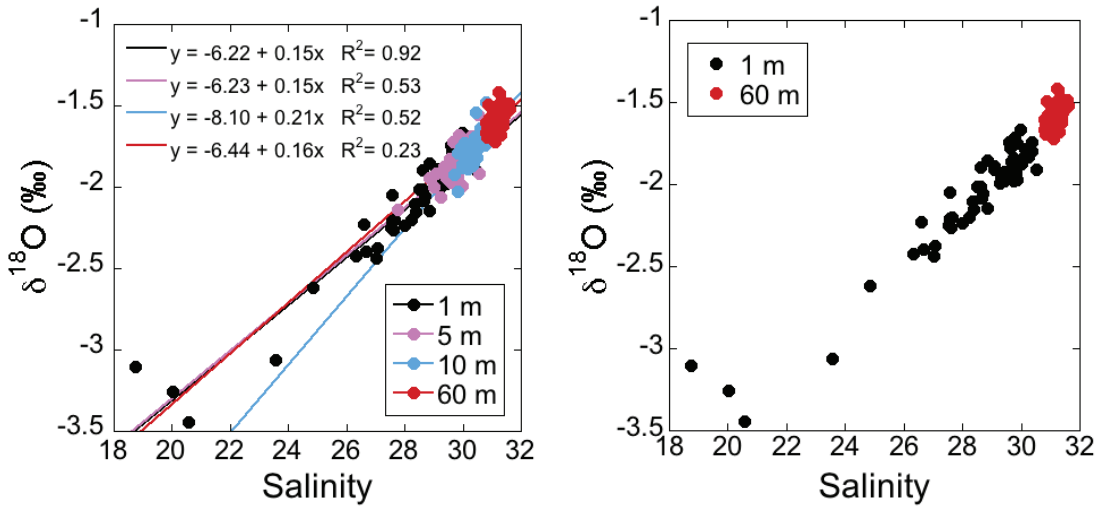

Figure 4.7: δ^{18}O-Salinity plots for (a) 1, 5, 10, and 60 m depth, and (b) 1 and 60 m depth in Bedford Basin, with all samples collected between June 2012 and October 2013.

All of the water samples (1, 5, 10, and 60 m) collected in Bedford Basin over this study period (June 2012 - October 2013) fall along a δ^{18}O-Salinity mixing line, with saltier, more isotopically enriched samples found at depth (60 m), while more isotopically depleted, fresher samples are found at the surface (1 m) (Figure 4.7(a)). By examining Figure 4.7(a), it appears that waters collected at 5 and 10 m depth in Bedford Basin are intermediaries, or mixtures, of water at 1 and 60 m depths. When the δ^{18}O and salinity of samples collected at 1 and 60 m depth are plotted (Figure 4.7(b)), no data points overlap. This emphasizes the fact that the water collected at 1 and 60 m represent distinct water masses.

To examine the shift in the mixed layer and halocline depth throughout the year, and to determine whether samples collected at 5 and 10 m should be included in the surface or deep layer, salinity data (collected by a CTD on the CCGS *Sigma T* alongside our δ^{18}O and salinity sampling) are used. It is evident through the vertical profiles of salinity measured in this study that the depth of the mixed layer is variable (Figure 4.8). Although the salinity typically becomes stable with increasing depth (at $\sim$30 m), there is no defined position of the mixed layer throughout this sample period.

During this study (June 2012 - October 2013), both the depth of the mixed layer and halocline varies in Bedford Basin. To examine the variability in salinity near the surface, Figure 4.9 presents vertical profiles of salinity collected from the fall of 2012 in the top

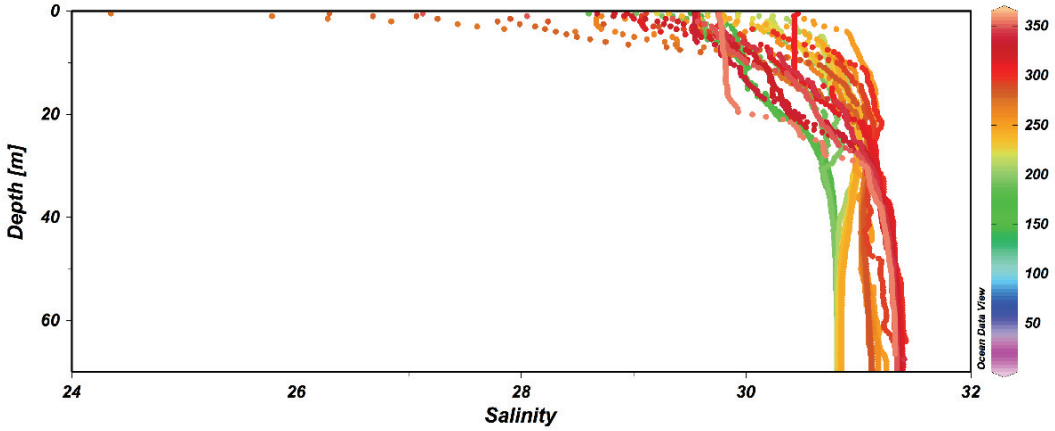

(a) 2012

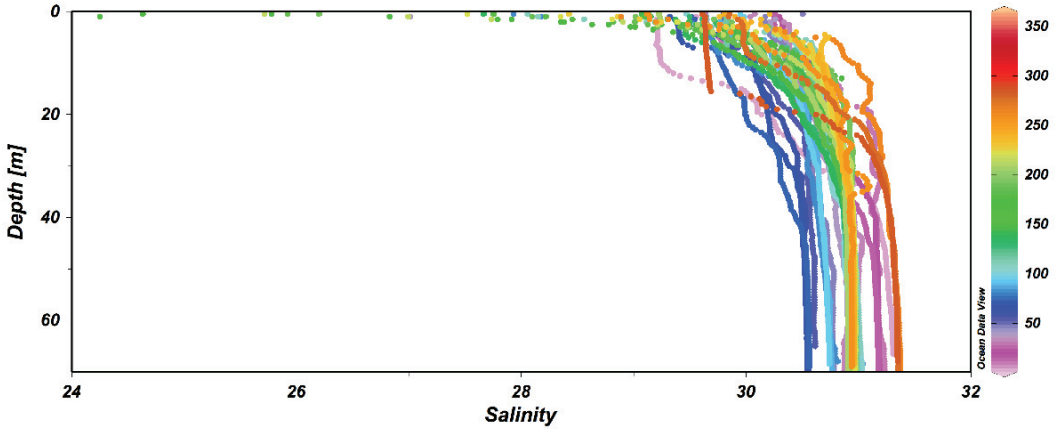

(b) 2013

Figure 4.8: Salinity profiles with depth in Bedford Basin in (a) 2012 and (b) 2013. The colour bar represents the day of the year in which the sample was collected.

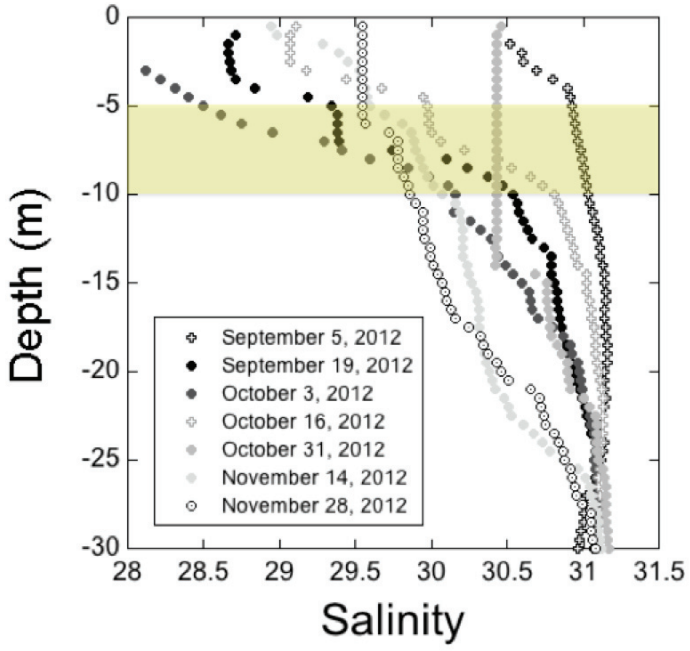

Figure 4.9: Vertical profiles of salinity collected during the fall of 2012 in Bedford Basin. The variability in salinity between 5 and 10 m depth over this period is highlighted in yellow.

30 m of Bedford Basin. Salinity measurements between 5 and 10 m are highlighted to illustrate the fluctuation in the depth of the mixed layer over these depths during this time (Figure 4.9). In the fall of 2012, the mixed layer is found above, between, and below 5 and 10 m, illustrating the need to exclude samples collected at both of these depths from both the "surface" and "deep" layers of Bedford Basin during this analysis. Therefore, due to the distinction in δ^{18}O and salinity between the upper and lower layers of Bedford Basin, the mass fraction analysis of the surface (1 m) and deep (60 m) layers will be performed separately.

4.2.1 Surface Water

The upper layer of Bedford Basin is distinct from bottom waters and freshened by the introduction of precipitation and Sackville River run-off. *Gregory et al.* (1993) found a tidal inflow to freshwater input volume ratio in Bedford Basin of 109.38, illustrating a dominant input of offshore water compared with freshwater inputs (Sackville River, precipitation, and wastewater). By performing mass balance calculations on water collected at 1 m (June 2012 - October 2013), the proportion of inputs, both fresh and saline, to Bedford Basin

surface waters can be constrained.

4.2.1.1 Mass Balance Calculations

Mass balance calculations (Equations 4.2, 4.3, and 4.4) were performed on Bedford Basin samples collected at 1 m depth between June 2012 and October 2013, using the end members established in Section 4.2 (Table 4.2). Figure 4.10(a) presents the average mass balance results for Bedford Basin surface water (1 m), calculated over this time period. These results were averaged, with fractions of 0.047, 0.069, and 0.884 calculated for F_W, F_S, and F_O respectively. A one-way ANOVA with a Tukey's All Pairs Comparison post hoc test found that the average winter and summer mass fractions were significantly similar (p value $>$0.05), while the offshore fraction (F_O) was significantly different (p value $<$0.05) from both F_W and F_S throughout the year (Figure 4.10(a)). Based on these results, at 1 m depth in Bedford Basin offshore water is the dominant input throughout the year, with small inputs of summer and winter precipitation also present.

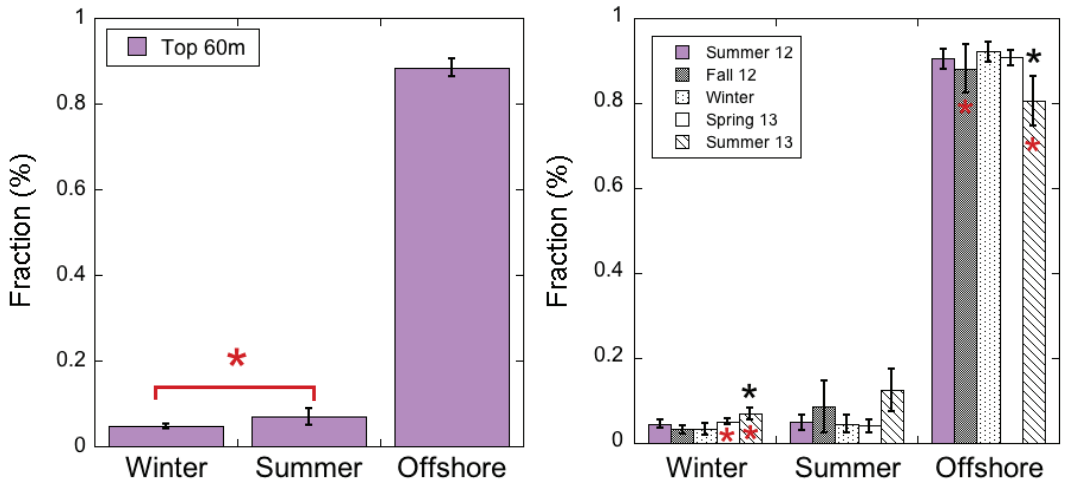

(a) Average (b) Seasonal

Figure 4.10: Bedford Basin 1 m mass fraction results (with 95 % CI error bars) for (a) the total averaged, and (b) seasonal groupings of samples. A black "*" indicates that there is a significant difference (p value $<$0.05), for example: between F_W calculated for "summer 2013" and the other months. A red "*" indicates a significant similarity (p value $>$0.05), for example: the F_W calculated for "summer 2013" and "spring 2013" [in (b)]. All other columns of the same end member (i.e. F_W, F_S, or F_O), and not identified by a "*" are significantly similar to one another. A red bracket indicates that these two mass fractions are not significant different from one another [in (a)].

As winter and summer precipitation are being used as the two freshwater end members in

this analysis, Bedford Basin samples were grouped seasonally to see if the input of summer precipitation (-5.39‰) is driving the freshwater input to Bedford Basin in the summer, and likewise, if the input of winter precipitation (-10.37‰) is driving this freshwater component in the winter. Figure 4.10(b) presents the average mass fraction results for F_W, F_S, and F_O in five different seasonal groupings in Bedford Basin: summer 2012 (June, July, August), fall 2012 (September, October, November), winter 2012/2013 (December, January, February), spring 2013 (March, April, May), and summer 2013 (June, July, August).

In these seasonal groupings (at 1 m), the mass fraction results for F_W and F_S were not found to be significantly different from one another (p value $>$0.05; using a one-way ANOVA test with a Tukey's All Pairs Comparison), with the exception of F_W calculated for "summer 2013", which was found to be significantly different from every seasonal grouping except "spring 2013" (p value $<$0.05) (Figure 4.10(b)). Therefore, with the exception of the mass fraction calculated for F_W in summer 2013, there is no discernible change in F_W or F_S entering Bedford Basin throughout the year when different seasons are compared (June 2012 - August 2013). In addition, the calculated fraction of offshore water did not change significantly throughout the year when different seasonal groupings were compared. With the exception of samples collected in summer 2013, F_O was found to be significantly similar (p value $>$0.05) to these different seasons. The F_O calculated for "summer 2013" is significantly different (p value $<$0.05) from all of the other seasonal groupings, with the exception of "fall 2012" (Figure 4.10(b)). Based on these results, it is evident that there is no significant change in the fractional input of these water sources (offshore water, winter, or summer precipitation) to Bedford Basin throughout the year.

Regardless of the season, the dominant input to Bedford Basin surface waters is offshore water (Figure 4.10). When these data are separated seasonally, the fraction of winter and summer precipitation is variable, with no seasonal shift, contrary to what was expected. The lack of a seasonal shift may suggest that both of these freshwater inputs are present throughout the year (Figure 4.10(b)), or there may be an additional freshwater input to Bedford Basin surface waters. To further investigate the changing precipitation input throughout the year, we can examine where these data fall on a δ^{18}O-S end member mixing triangle (Table 4.2).

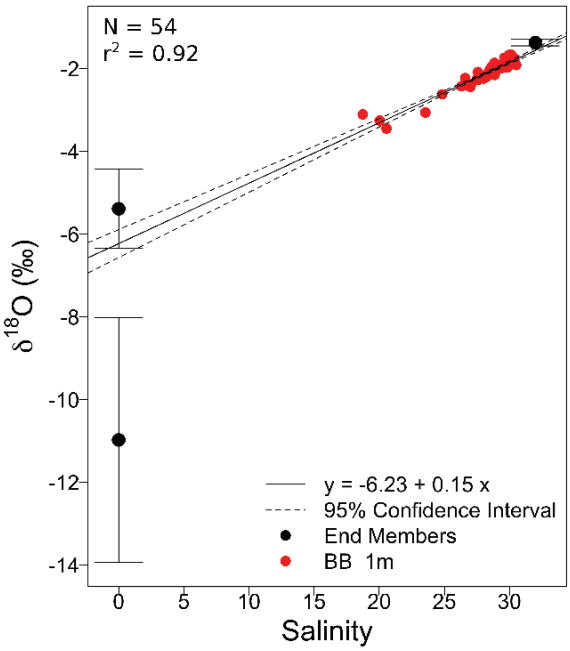

Figure 4.11: δ^{18}O-S relationship for all Bedford Basin 1 m samples collected in this study (June 2012 - October 2013) with BB end members, and their associated error (95% CI).

4.2.1.2 Determining Zero-Salinity Intercepts

As discussed in Section 1.3.2.2, the δ^{18}O-Salinity relationship can be used to determine the zero-salinity, or y-, intercept of the linear regression equation, identifying the δ^{18}O of freshwater present in this water sample. This extrapolation to zero-salinity assumes that the water measured is interacting directly with meteoric water, and not an additional water source(s) (*Fairbanks*, 1982). In addition, the zero-salinity intercept determines only one δ^{18}O value, assuming that there is a single freshwater input. In the mass balance calculations performed throughout this section we are distinguishing between two freshwater inputs (winter and summer precipitation); if the zero-salinity intercept falls between these two end members, then it is likely a mix of both summer (-5.39‰) and winter precipitation (-10.97‰). A zero-salinity intercept that is more isotopically depleted than the winter precipitation end member may indicate a presence of more isotopically depleted precipitation or meteoric water (i.e. Arctic river water: -21‰), entering from the Scotian Shelf.

When all of the Bedford Basin samples collected at 1 m throughout this study were added to a δ^{18}O-S end member mixing triangle, along with the three Bedford Basin end members

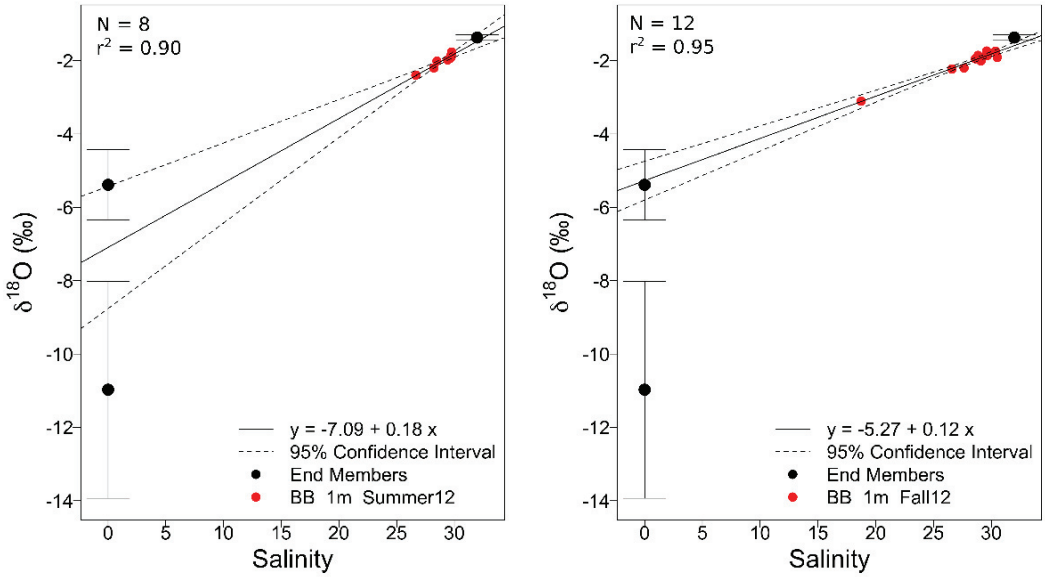

(a) Summer 2012

(b) Fall 2012

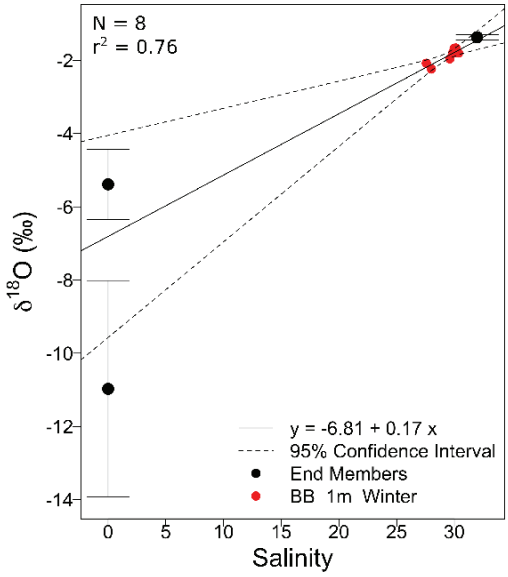

(c) Winter 2012/2013

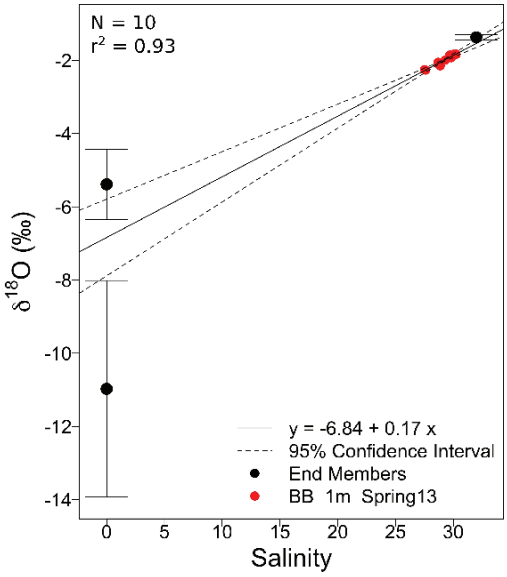

(d) Spring 2013

Figure 4.12: δ^{18}O-S relationship of Bedford Basin 1 m data (red), grouped seasonally, (a) summer 2012, (b) fall 2012, (c) winter 2012/2013, and (d) spring 2013, with Bedford Basin end members included. 95% CIs are added to the linear regression line and end members (black).

(Table 4.2), a zero-salinity intercept of -6.23‰ was determined, indicating the average δ^{18}O of freshwater present in Bedford Basin surface waters throughout this study (Figure 4.11). The average amount-weighted δ^{18}O of precipitation from July 2012 - October 2013 in Halifax, (-6.68‰, 95% CI: 0.74) is within the error of this zero-salinity intercept (-6.23‰, 95% CI: 0.34). This confirms that the freshwater component of Bedford Basin surface waters is driven by the inflow of meteoric water, and precipitation in particular, and that our precipitation and estuarine δ^{18}O values are mostly internally consistent. The zero-salinity intercept (-6.23‰) falls closer to the summer precipitation end member (-5.39‰), than the winter precipitation end member (-10.39‰). Since samples were collected between June 2012 and October 2013, there are two summer seasons in this data-set compared with one winter season, which may partially explain this.

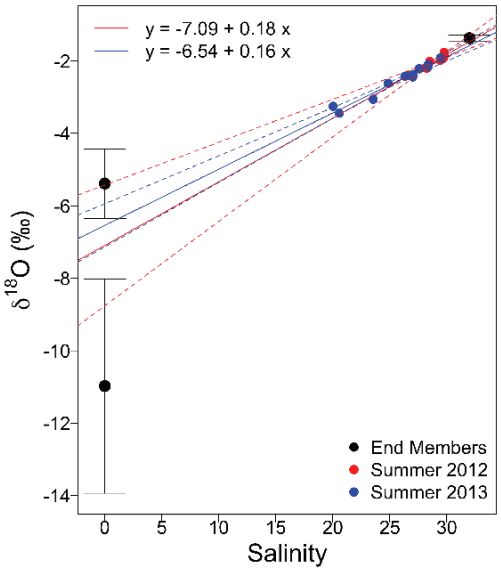

Figure 4.13: δ^{18}O-Salinity relationship of Bedford Basin samples collected at 1 m depth in "summer 2012" (red) and "summer 2013" (blue). Dotted lines indicate the 95% confidence intervals for the linear regression lines.

Figure 4.12 presents the δ^{18}O-S end member mixing triangles for Bedford Basin samples collected at 1 m depth over four different seasons (summer 2012, fall 2012, winter 2012/2013, and spring 2013). There is an apparent variability in the δ^{18}O of freshwater in Bedford Basin, illustrated by the change in the zero-salinity intercept over these seasons. Using the zero-salinity intercepts, the measured δ^{18}O of the freshwater component in Bedford Basin surface waters ranges from -5.27‰ in fall 2012 and -7.09‰ in summer

2012 (Figure 4.12). Despite a shift in the zero-salinity intercepts in these different seasons, the shift does not align with the δ^{18}O measured from precipitation samples over these months (Chapter 3). The zero-salinity intercept calculated for samples collected in "winter 2012/2013" is more isotopically enriched, -6.81‰, when compared with the predicted winter end member, -10.97‰. In addition, the intercept calculated for the "summer 2012" seasonal grouping (-7.09‰) is more isotopically depleted than that of "winter 2012/2103", -6.81‰, contrary to what was expected (Figure 4.12). When the zero-salinity intercepts for the "summer 2012" and "summer 2013" seasonal groupings are compared, both fall outside of the uncertainty associated with the summer freshwater end member (Figure 4.13).

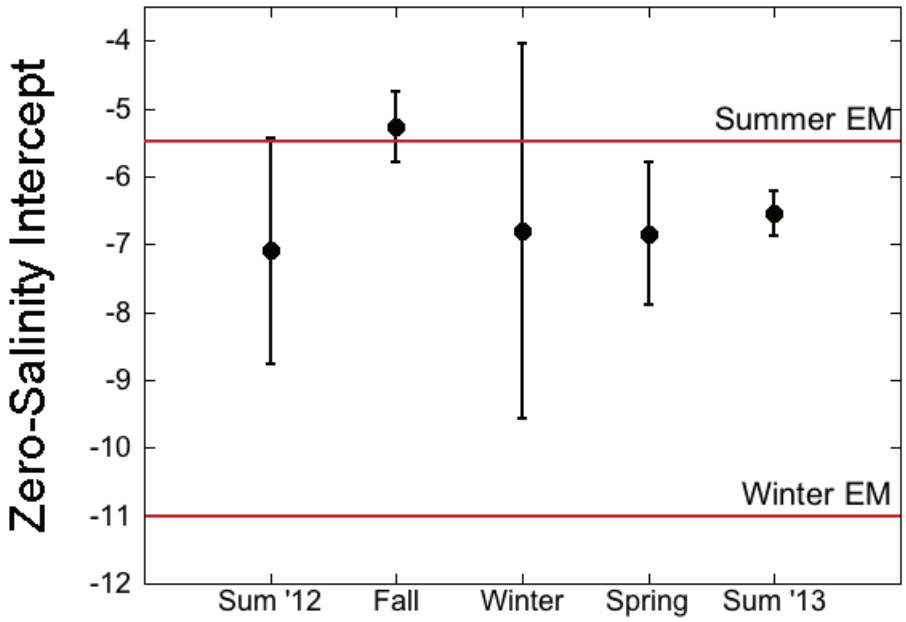

Figure 4.14: Zero-Salinity intercept and associated error (95% CI) calculated for seasonal groupings of the δ^{18}O-S relationship in Bedford Basin 1 m samples. Winter (-10.97‰) and summer (-5.39‰) end members (EM) are included in red.

All of the calculated zero-salinity intercepts, and associated error, for the different seasonal groupings of Bedford Basin surface water (i.e. Figure 4.12 and 4.13) are presented in Figure 4.14. With the exception of the zero-salinity intercepts calculated for "fall" and "summer 2013", there is no significant difference in the intercepts calculated for different seasonal groupings, as illustrated by the 95% CIs (Figure 4.14).

Based on the zero-salinity intercepts observed in the average and seasonal δ^{18}O-S plots

(Figure 4.11 and 4.12), it is evident that the freshwater component of Bedford Basin is isotopically enriched, compared with the winter end member, and more closely related to summer precipitation over the year, regardless of the seasonal grouping. With the exception of the zero-salinity intercept observed for "fall 2012" samples, which is within the range of the summer end member and its associated error (Figure 4.12(b)), the majority of the zero-salinity intercepts calculated for the different seasonal groupings (Figure 4.12) fall somewhere between the winter and summer end members. Despite the fact that there are no zero-salinity intercepts within the uncertainty range of the winter end member, the 95% CIs associated with these regressions are within this uncertainty range in "summer 2012", "winter 2012/2013", and "spring 2013" (Figure 4.12). However, it is notable that little "winter precipitation", or freshwater with a δ^{18}O of $\sim$-10‰, can be identified within Bedford Basin surface waters.

The fact that no zero-salinity intercepts fall within the winter end member (or associated error) may indicate that the winter freshwater end member is not representative of what enters Bedford Basin, rather than the presence (or absence) of "winter precipitation". There is a large range in δ^{18}O associated with winter precipitation, which can be seen in the 95% CI calculated for the winter end member (2.96), in addition to the discussion presented in Chapter 3.

Although "strongly isotopically depleted" samples (defined as: $<$-10‰) were collected over the winter months (10), the majority of the precipitation samples collected throughout this study do not fall in this "more depleted" range (64). It is evident that the winter end member, at -10.97‰, does not encompass the majority of the precipitation samples, and as such, during most times of the year this end member is more isotopically depleted than the freshwater present in Bedford Basin surface waters. This discrepancy in the recorded δ^{18}O of precipitation and freshwater in Bedford Basin surface waters is not related to the amount of precipitation that falls in Halifax, as winter (Dec, Jan, and Feb) precipitation is typically greater than summer (June, July, and Aug) precipitation, 394.9 mm compared with 318.5 mm (*Government of Canada - Climate*, 2014). Sackville River samples, which were not collected in January or February due to ice-cover, could have been used to clarify the δ^{18}O of freshwater entering Bedford Basin over the winter months.

In addition to these potential issues with winter end member definition, δ^{18}O of snowfall may vary with time due to sublimation and melting, leading to discrepancies between the

recorded δ^{18}O of snowfall and what enters Bedford Basin as freshwater run-off. Unlike rainfall, snow often stays on land before melting and run-off can take place, limiting the instantaneous introduction of snowfall into Bedford Basin. In addition to this time lag, the isotopic composition of snow can be modified by (1) sublimation and vapour exchange, and (2) the melting of snow within the snowpack (*Clark and Fritz*, 1997). As snow melts, it undergoes a Rayleigh-like enrichment of meltwater (*Clark and Fritz*, 1997), meaning that the δ^{18}O of what is measured when snow is collected, and what enters Bedford Basin, may be different. Once snow is melted, it becomes more isotopically enriched (compared with its δ^{18}O before melting), due to continuous exchange between meltwater and snow as melting takes place (*Clark and Fritz*, 1997). In addition to melting, sublimation and vapor exchange within the snowpack results in a kinetic isotopic enrichment similar to that of evaporating water, however high humidities within the snowpack lead to a greater degree of equilibrium exchange (*Clark and Fritz*, 1997). Over time the remaining snowpack becomes more isotopically enriched, which may account for some of the discrepancy between measured winter precipitation and the zero-salinity intercepts in Bedford Basin surface waters over the winter months. Therefore, the zero-salinity intercepts calculated for Bedford Basin surface water (Figures 4.11 and 4.12) may more accurately convey the δ^{18}O of precipitation that falls into Bedford Basin, providing additional insight to the input of precipitation to Halifax Harbour.

With further study, it may be possible to compare the δ^{18}O of measured snowfall to the zero-salinity intercept of surface waters to determine the change in δ^{18}O associated with sublimation and melting. However to determine this isotopic variability, a more robust sampling strategy must be established for both snow (snowfall and snowpack) and Bedford Basin surface waters. Although this is beyond the scope of this thesis, this result suggests that we cannot fully close the isotopic mass balance for Bedford Basin, presenting the potential for additional research in this area. It is evident that the use of mass balance calculations and end member mixing triangles can provide insight into the sources and variability of freshwater present in Bedford Basin surface waters.

4.2.1.3 Fitting Data into the Mixing Triangle

Figure 4.11 presents the δ^{18}O-S end member mixing triangle for Bedford Basin samples collected at 1 m. To examine the fit of these Bedford Basin surface samples in the end member mixing triangle, Figure 4.11 is zoomed-in to include all of the samples and the

offshore end member (Figure 4.15(a)). One point - collected on September 5, 2013 - falls outside of this mixing triangle (Figure 4.15(a)). As discussed (Section 4.1.2), a negative mass fraction would be calculated for this sample, and this water must be composed of at least one additional end member not defined in this analysis. When the vertical salinity profiles of the preceding and following weeks are compared with the profile on September 5 (Figure 4.15(b)), the top layer is the saltiest and the depth of the mixed layer is the shallowest on this date. In addition, the salinity on this date does not stabilize with depth, but instead fluctuates down the water column. This may suggest that a vertical intrusion event is taking place in Bedford Basin, bringing saltier, deep water towards the surface.

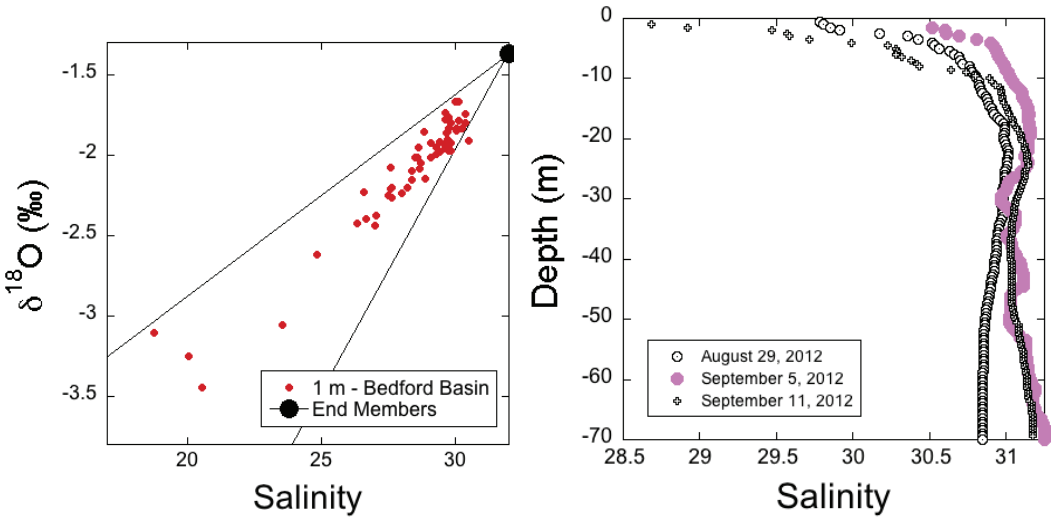

(a) (b)

Figure 4.15: (a) Mixing triangles for Bedford Basin samples at 1 m collected from June 2012 - October 2013, with BB end members. (b) Vertical profiles of salinity measured with a CTD in Bedford Basin, on Aug. 29^{th}, Sept. 5^{th}, and Sept. 11^{th}, 2012.

Shan et al. (2011) found that temperature stratification in Bedford Basin was strongest in September, and this stratification breaks down in the late fall due to increased vertical mixing and heat loss associated with vertical convection. Although *Shan et al.* (2011) found that this breakdown typically begins in late fall, it is likely a saltwater intrusion event, bringing deep (salty) water towards the surface, that is driving this increased salinity in the surface (1 m) sample in early September 2012 (Figure 4.15).

In addition to vertical saltwater intrusion events, changes in precipitation and/or Sackville River input could also be examined to ensure that the increased salinity of this sample is being driven by a vertical intrusion event. On September 5, 2012 a precipitation event

occurred, however the isotopic composition of this rainfall was -3.89‰. If this input of precipitation was causing this point to fall outside of the mixing triangle then this water sample would be fresher and more isotopically depleted, falling above the mixing line. Therefore, this point is likely being influenced by increased vertical mixing, adding stable deep water - dominated by offshore (Scotian Shelf) water with more isotopically depleted freshwater - into the surface layer, causing this point to fall below the mixing triangle.

4.2.1.4 Examining the δ^{18}O-S Relationship

Fluctuations in the δ^{18}O-Salinity relationship over time can be examined in Bedford Basin surface samples. Variations in the salinity of Bedford Basin occur for two reasons: (1) there is a change in salinity as a result of an increase or decrease in freshwater input(s), or (2) there is a change in inputs to Bedford Basin, leading to a differing salinity input, one that does not vary with the defined δ^{18}O-S relationship present in Bedford Basin surface waters. To differentiate between any variations due to the amount of freshwater, compared with a differing input, δ^{18}O-S measurements for all of the samples collected at 1 m depth in Bedford Basin throughout this study (June 2012 - October 2013) are examined (Figure 4.11). Using this relationship, between δ^{18}O and salinity in the surface waters of Bedford Basin, a linear regression equation was developed:

$$\delta^{18}O = 0.146(S) - 6.227$$

We can normalize the δ^{18}O of our samples to salinity using this average δ^{18}O-S relationship in Bedford Basin surface waters; salinity values are input into the above equation to calculate predicted δ^{18}O values. This calculated δ^{18}O value, effectively normalized to salinity, can be compared to the observed δ^{18}O values throughout this study.

$$\frac{\delta^{18}O_{observed}}{\delta^{18}O_{predicted}}$$

The ratio of observed to predicted δ^{18}O values collected at 1 m in Bedford Basin is presented in Figure 4.16. It is notable that samples collected between October and March are often found below the red (1:1) line, while samples collected between April and September are typically found above.

The error associated with δ^{18}O measurements (0.05‰) leads to scatter in the δ^{18}O data,

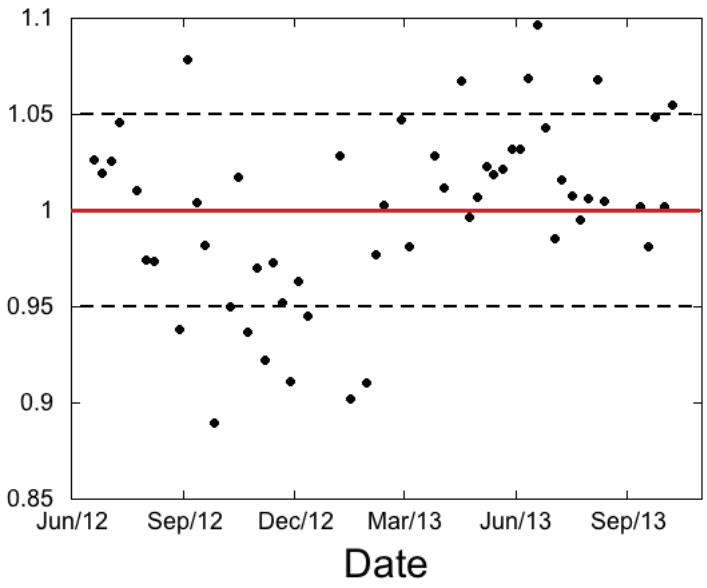

Figure 4.16: The ratio of observed δ^{18}O and δ^{18}O normalized to salinity, using the δ^{18}O-S relationship of Bedford Basin 1 m water, collected from June 2012 to October 2013.

however a number of these points fall outside of the error associated with δ^{18}O measurements, and as such these differences are significant and greater than the instrumental error (Figure 4.16). The variance around the δ^{18}O-S regression line should be equal to the error associated with δ^{18}O measurements. Any variability in δ^{18}O outside the range of this error ($>$0.05) suggests that there is an input of water to the surface carrying a different δ^{18}O-S relationship.

In the fall and winter (October and March), δ^{18}O measured in Bedford Basin surface waters is often more isotopically depleted than the annual average δ^{18}O-S relationship would predict (falling below this 1:1 line, Figure 4.16). This may suggest that an additional (more isotopically depleted) freshwater input is introduced, or that an intrusion or mixing event is taking place, bringing isotopically depleted waters towards the surface from deep Bedford Basin waters or the Scotian Shelf.

To determine if there is a seasonal, or yearly, variation in δ^{18}O normalized to salinity, first these data were grouped monthly and seasonally (fall: Sept, Oct, Nov; winter: Dec, Jan, Feb; spring: Mar, Apr, May; summer: June, July, Aug) (Figure 4.17). The monthly groupings of δ^{18}O normalized to salinity illustrate a decrease in δ^{18}O (relative to the δ^{18}O-S relationship) in the late fall and winter, and an opposing shift in the spring/summer

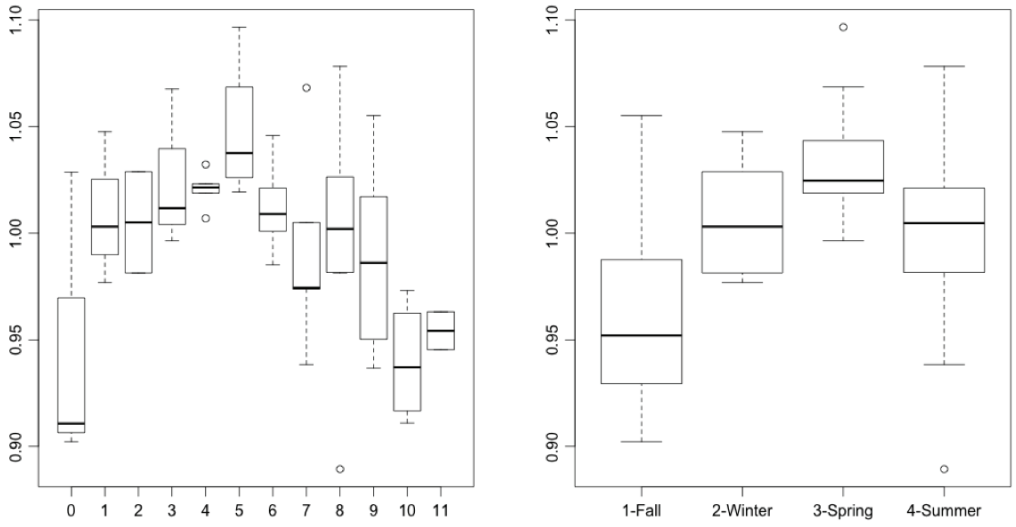

(a) Monthly (b) Seasonally

Figure 4.17: (a) Monthly- (0: January, 11: December) and (b) seasonally-grouped box-plot results for δ^{18}O-normalized to salinity, using the δ^{18}O-S relationship at 1m in Bedford Basin.

(Figure 4.17(a)). However, when an ANOVA is performed on these data, the monthly variability in normalized δ^{18}O is not significant (p value $>$0.05). The seasonally-grouped data (Figure 4.17(b)) show a similar trend, however when an ANOVA is performed on these data it was found that the difference in seasonally normalized δ^{18}O is significant (p value = 0.0003). It should be noted that these seasonal groupings are arbitrarily defined, and different groupings of these data may show that this relationship is or is not significant. However, it is evident that there is a seasonal trend that should be investigated further, particularly with an increased data set over multiple years.

Therefore, in the fall where δ^{18}O is depleted relative to the δ^{18}O-S relationship in surface waters, it is likely that intrusion events are driving this depletion (i.e. $<$1; Figure 4.16). As presented in *Shan et al.* (2011), vertical salinity intrusion events begin in the late fall in Bedford Basin, bringing stable deep waters, with increased salinity and isotopically depleted δ^{18}O values towards the surface. Therefore, these samples collected in the fall, with more isotopically depleted δ^{18}O values than what is predicted (based on normalized δ^{18}O), are likely being driven by intrusion events. A larger data set that incorporates multiple years would confirm this seasonal variability.

4.2.1.5 Summary

By performing linear regressions and mass balance analyses on Bedford Basin surface (1 m) samples, we were able to (1) confirm and quantify freshwater and offshore inputs, (2) compare the calculated zero-salinity intercept with known freshwater inputs, and (3) identify the outliers in the δ^{18}O-S relationship at 1 m depth.

Throughout the year, offshore water dominates Bedford Basin surface waters (Average: 88.4%), while the input of winter and summer precipitation is minimal (Average: 4.7 and 6.9% respectively). There is no seasonality to the winter and summer precipitation end members, contrary to what was expected. Using the δ^{18}O-S relationship to determine the zero-salinity intercept of all Bedford Basin surface samples, the δ^{18}O of freshwater present in Bedford Basin throughout the year (-6.23‰, 95% CI: 0.34) is comparable to the average amount-weighted δ^{18}O of precipitation (-6.68‰, 95% CI: 0.74) measured in Halifax. However, the δ^{18}O of winter precipitation [strongly isotopically depleted (>-10‰)] is never present in surface waters, which may be due to sublimation and melting, causing an isotopic enrichment not represented by precipitation data. Finally, outliers to this δ^{18}O-S relationship may indicate the presence of vertical salinity intrusion events, bringing saltier bottom waters (composed of mainly offshore water) into Bedford Basin surface waters.

4.2.2 Deep Water

Freshwater run-off, vertical mixing and sporadic shelf water intrusions throughout the year are the dominant mechanisms controlling the variability of salinity in deep Bedford Basin waters (*Shan et al.*, 2011). As discussed, the surface and deep waters are separated in Bedford Basin, with stable bottom waters flushing at a slower rate (90 days), compared with the upper water column (40 days) (*Shan and Sheng*, 2012). Below ∼30 m in Bedford Basin the salinity is relatively stable throughout the year, indicating very few flushing events (Figure 4.8). Figure 4.18 presents the general circulation pattern of Bedford Basin, outlining the division of the surface and deep layers. This schematic emphasizes the fact that deep water may originate from only offshore water, avoiding any interaction with the surface waters of Halifax Harbour as it flows inward, leading to no input of freshwater from land (i.e. river run-off, precipitation, wastewater, etc.). Salinity intrusion events may be caused by an increase in offshore water to Bedford Basin, leading to increased vertical mixing and the flushing of surface waters out of Bedford Basin.

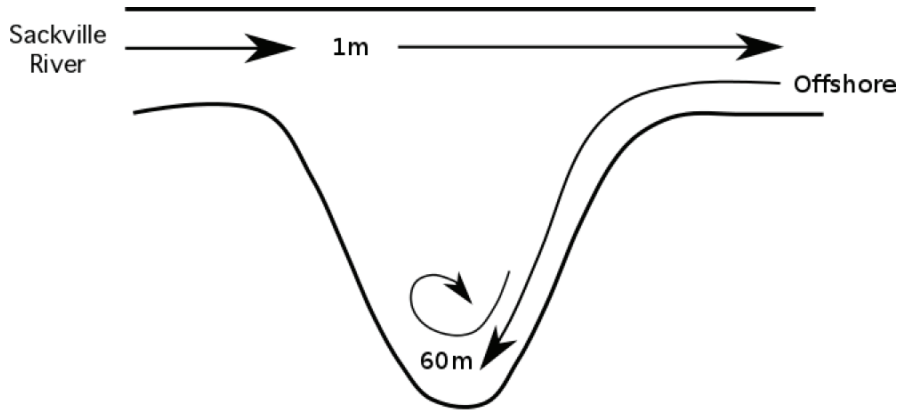

Figure 4.18: Circulation schematic of water flow in Bedford Basin (1 & 60 m).

Due to this division within Bedford Basin, the regression and mass balance analyses performed on Bedford Basin surface data (Section 4.2.1) will be performed additionally on samples collected in the deep waters (60 m) of Bedford Basin. This should help to (1) inform the composition of water at 60 m in Bedford Basin, (2) illustrate how this water is modified throughout the year, and (3) by performing the same analysis on Bedford Basin deep waters as the surface, these results can be directly compared with the analysis performed above (Section 4.2.1).

4.2.2.1 Mass Balance Calculations

Mass balance calculations (Equations 4.2, 4.3, and 4.4) were performed on Bedford Basin samples collected at 60 m depth (June 2012 - October 2013), using the end members established in Section 4.2 (Table 4.2). Figure 4.19(a) presents the average mass balance results calculated over this time period, with average mass fractions of 0.020, 0.006, and 0.974 calculated for F_W, F_S, and F_O respectively. A one-way ANOVA with a Tukey's All Pairs Comparison post hoc test found that these average mass fractions were all significantly different from one another (p value $<$0.05) (Figure 4.19(a)). Like surface waters, bottom waters are dominated by offshore water input throughout the year. However, as a result of stagnant bottom waters and relatively few flushing events over this time period, the calculated fractions of winter and summer precipitation are very small ($<$3% in total). It should also be noted that unlike the water at 1 m, which was dominated by summer precipitation, with δ^{18}O values around -6‰, a higher fraction of winter precipitation was found in this analysis, suggesting that more isotopically depleted freshwater ($<$-6‰) enters the deep waters of Bedford Basin.

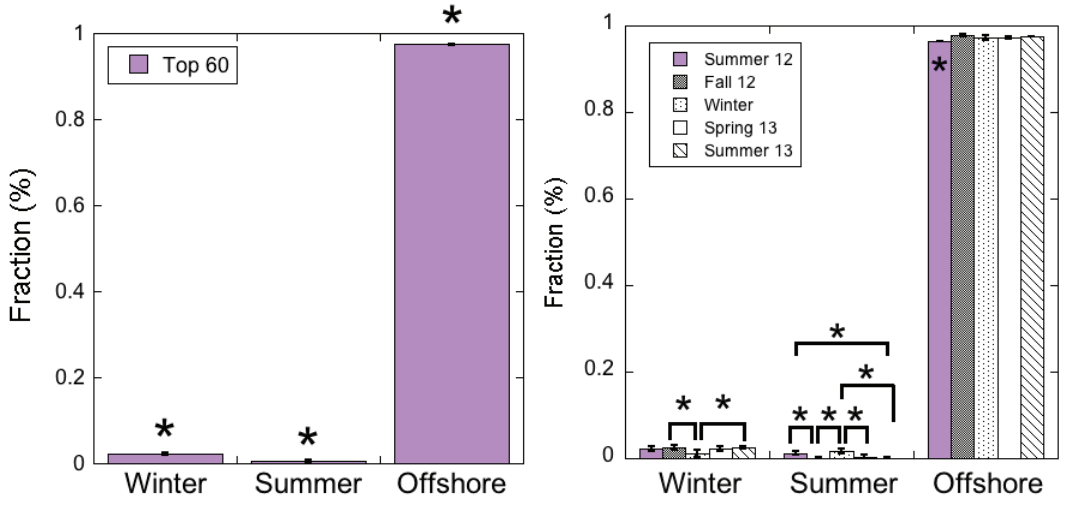

(a) Average (b) Seasons

Figure 4.19: Bedford Basin 60 m mass fraction results (with 95 % CI) for (a) the total averaged, and (b) seasonal groupings of samples. A black "*" (p value <0.05) indicates that mass fractions are significantly different, for example: between the mass fraction (i.e. F_S, F_W, or F_O) determined in a seasonal grouping (i.e. summer 2012), and the mass fraction determined by the other four seasons (i.e. fall 2012, winter 2012/2013, spring 2013, or summer 2013).

Like the analysis performed for 1 m Bedford Basin water, samples collected at 60 m were grouped seasonally to see if there is any indication that more summer or winter precipitation is influencing Bedford Basin water composition in different seasons. The fraction of offshore water calculated in different seasons is only significantly different (p value <0.05) from the other months in the summer of 2012 (Figure 4.19(b)). F_S and F_W were both found to be significantly different from other seasons (Figure 4.19(b)), when a one-way ANOVA test with a Tukey's All Pair Comparison was performed on the data, however it is evident that the input of precipitation (or any freshwater) is minimal throughout the year. It should also be noted that the 95% CIs associated with these averaged mass fractions are much smaller than those associated with the 1 m results (Figure 4.10(b)). This is related to the stability of Bedford Basin deep water, and the little variability associated with δ^{18}O and salinity at 60 m over this study.

4.2.2.2 Determining Zero-Salinity Intercepts

When the δ^{18}O-S end member mixing triangle for all of the samples collected at 60 m in Bedford Basin is plotted, the zero-salinity intercept was found to be -7.47‰ (95% CI: 2.17). Despite the fact that this value is comparable to the zero-salinity intercept

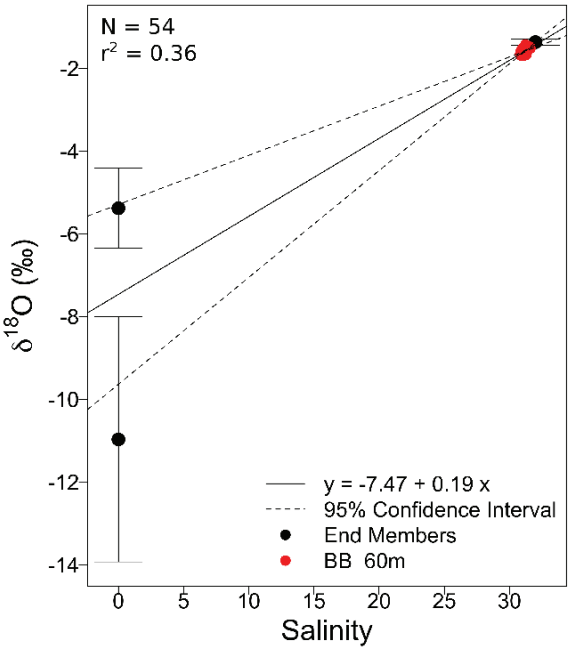

Figure 4.20: δ^{18}O-S relationship for all Bedford Basin 60 m samples collected in this study (June 2012 - October 2013) with Bedford Basin end members, and their associated error (95% CI).

presented for Bedford Basin 1 m data over this study (-6.23‰, 95% CI: 0.34) and the δ^{18}O of precipitation collected in Halifax (-6.68‰, 95% CI: 0.74), the r^2 associated with this measurement is very weak, 0.36, and the 95% CI associated with the zero-salinity intercept is large, 2.17. There is a weak relationship between δ^{18}O and salinity measurements collected at 60 m depth, illustrated through the uncertainty associated with this zero-salinity intercept (Figure 4.20).

Like the samples collected at 1 m (Figure 4.12), these δ^{18}O-S regressions were grouped seasonally to illustrate (1) the shift in the zero-salinity intercept over time and, (2) which freshwater end member is present in deep Bedford Basin waters (Figure 4.21). First, the zero-salinity intercepts calculated for these seasonal groupings are variable (-10.9 to -68.9‰), and far more isotopically depleted than the seasonally grouped zero-salinity intercepts determined for water at 1 m depth in Bedford Basin (-5.27 to -7.09‰). In addition, the r^2 values associated with the δ^{18}O-S relationship in all of these seasonal groupings are poor (0.25 - 0.72), indicating little to no relationship between δ^{18}O and salinity measurements at 60 m depth. This is evident when the seasonal grouping of "summer 2012" is examined; this grouping has the weakest r^2 value (0.25) as well as a calculated zero-salinity intercept of -68.91‰, more isotopically depleted than any freshwater input measured over the time of this study (Figure 4.21(a)). In this case, it is evident that the poor relationship between δ^{18}O and salinity (r^2: 0.25) leads to a zero-salinity intercept not representative of the freshwater input to this water. In addition, the variability and error (95% CI) associated with these calculated zero-salinity intercepts ranges between 6.6 (winter) and 121.2 (summer 2013).

For the 1 m seasonal groupings, the r^2 values ranged from 0.76 to 0.95, illustrating a strong relationship between δ^{18}O and salinity, and as a result, a confidence in the calculated zero-salinity intercept values. Therefore, despite the fact that we can calculate zero-salinity intercepts for 60 m, based on the weak relationship (r^2) between δ^{18}O and salinity at 60 m depth, a better technique must be used to determine the freshwater end member(s) present in deep Bedford Basin waters.

4.2.2.3 Fitting Data into the Mixing Triangle

A dominant input of offshore water, and minimal input of freshwater to Bedford Basin deep water throughout the year is evident through the mass balance results. Negative mass fraction results can tell us what samples fall outside of the Bedford Basin mixing

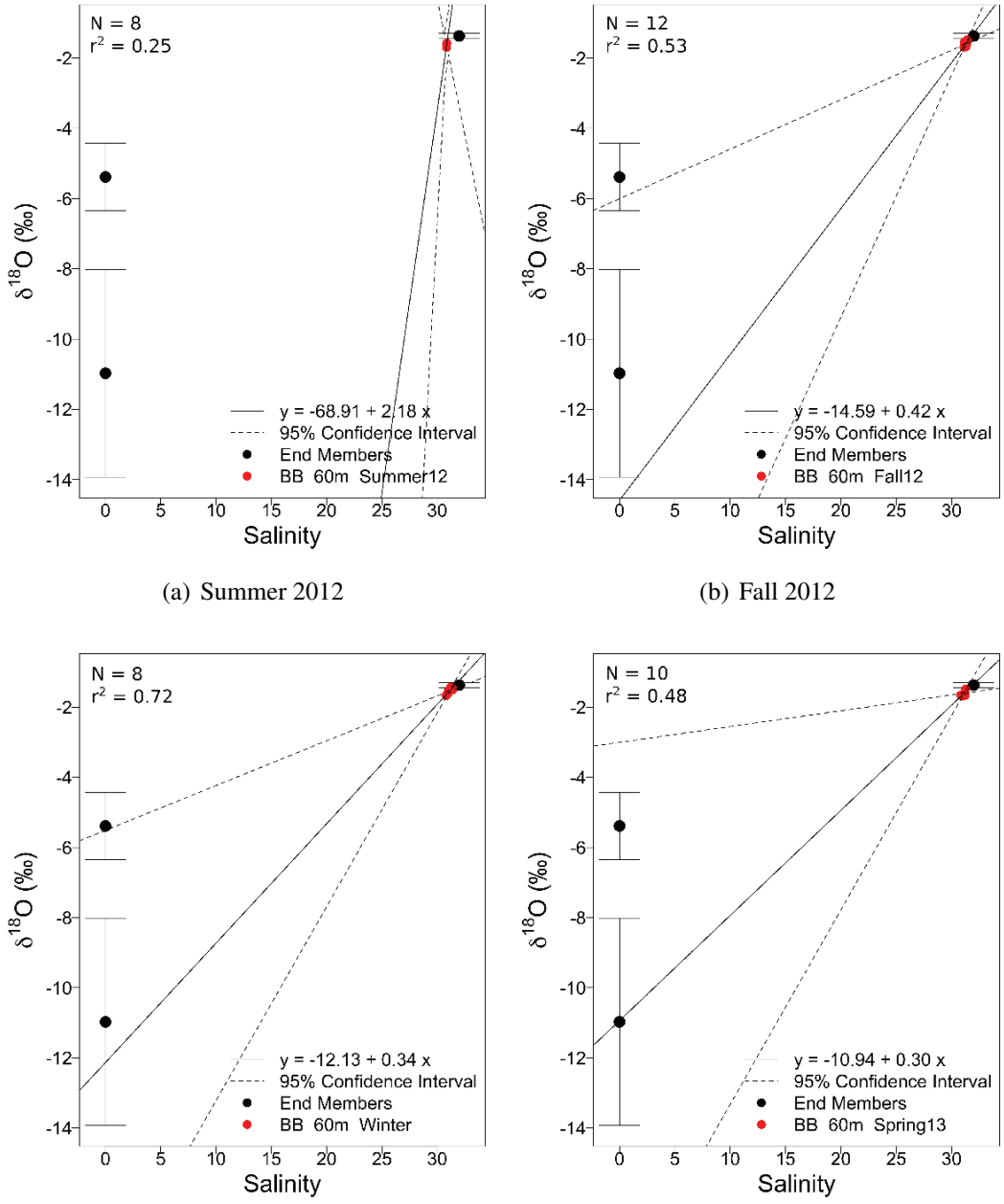

(a) Summer 2012

(b) Fall 2012

(c) Winter 2012/2013

(d) Spring 2013

Figure 4.21: δ^{18}O-S relationship of Bedford Basin 60 m data (red), grouped seasonally (a) summer 2012, (b) fall 2012, (c) winter 2012/2013, and (d) spring 2013, with Bedford Basin end members included. 95% CIs are added to the linear regression line and end members (black).

triangle, and therefore must be composed of a different water source(s). The number of negative mass fractions calculated for Bedford Basin 60 m water is presented in Table 4.1. Although the use of the "Top 60m" end member results in the fewest number of negative mass fractions calculated with the 60 m samples, this number is much higher compared with the samples collected at 1 m depth (19 samples out of 54, compared with 1).

At 60 m depth, 1.9% of F_W and 35.2% of F_S mass fraction results (out of 54 samples) were calculated to have negative mass fractions, indicating that these samples do not fit within the defined mixing triangle. To look at what points are falling outside of this mixing triangle and where, all of the samples collected at 60 m were plotted on the Bedford Basin end member mixing triangle (Figure 4.22). Since these samples all fall close to the offshore end member, this plot was zoomed-in so all of the Bedford Basin 60 m points were encompassed. The freshwater end members cannot be seen in Figure 4.22, however the end member mixing lines are presented.

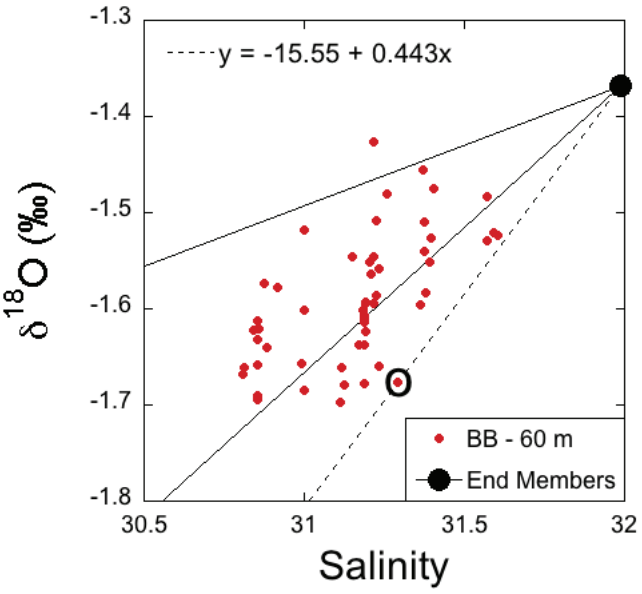

Figure 4.22: Mixing triangle for all Bedford Basin 60 m water samples (red) during the time of this study (May 2012 - Oct 2013). The offshore end member is presented (black). The solid lines (mixing lines) connect to the summer (-5.39‰) and winter precipitation (-10.97‰) end members (not shown). The dashed line represents the slope developed to encompass all of the points that fall below the mixing triangle, done by taking the slope of the circled point and the offshore end member.

The majority of the Bedford Basin 60 m samples that fall outside of the mixing triangle

are below the offshore end member and winter precipitation end member mixing line (Figure 4.22). Only one sample, collected on January 16, 2013, falls above the mixing triangle, with a more isotopically enriched δ^{18}O value than other samples with a similar salinity. A negative F_W value was calculated for this sample; in comparison, all of the samples that fall below the line were found to have positive F_W values but negative F_S values (Table 4.1). Samples falling below the winter precipitation-offshore mixing line are likely being influenced by a more isotopically depleted freshwater input, illustrating the presence of another freshwater end member in deep Bedford Basin.

As discussed in Chapter 1, freshwater originating from higher latitudes is progressively depleted in δ^{18}O. *Fairbanks* (1982) identified the freshwater end member present in offshore Scotian Slope/Labrador Sea water to be -21‰, as this value is associated with a dominant input of river water from the Arctic, present in the North Atlantic (*Fairbanks*, 1982). Through oxygen isotope analysis of waters in and around the Scotian Shelf, it was found that the dominant freshwater inputs must originate at high-latitudes, rather than locally (*Khatiwala et al.*, 1999; *Fairbanks*, 1982). As illustrated in Figure 4.18, water found at 60 m originates from offshore (Scotian Shelf), isolated from the surface waters of Bedford Basin and any freshwater inputs from land (i.e. river run-off, precipitation, or wastewater). As such, it is possible that the freshwater end member present in Bedford Basin 60 m water is not composed of winter or summer precipitation, but rather high-latitude freshwater inputs found on the Scotian Shelf.

Fairbanks (1982) determined a linear regression line for Scotian Shelf surface and nearshore samples; this equation was found to be δ^{18}O = 0.422(S) - 15.55 (r = 0.99, n = 4), identifying a freshwater end member of -15.55‰ for the Scotian Shelf. It should be noted that the zero-salinity intercept is not well constrained ($\pm$5.38), with only four samples, but meteoric water with a δ^{18}O composition comparable to this end member (-15.55‰) has been found north of the Gulf of Lawrence (*Tan and Strain*, 1980; *Fairbanks*, 1982).

To calculate an additional freshwater end member for 60 m water that fits all of the samples collected into the mixing triangle (Figure 4.22), a new mixing line that encompasses all of the data was developed. A linear equation was developed using the offshore end member (-1.37‰, 31.99) and the Bedford Basin 60 m sample that falls the furthest below the mixing triangle. This point (-1.68‰, 31.29) is circled in Figure 4.22, and when this line is added to the mixing triangle (dashed line: Figure 4.22), all of the Bedford Basin

60 m samples that fall below the original mixing triangle are now encompassed into this "new" mixing triangle (for the purpose of this analysis we are ignoring the one point that falls above). Using these two points, the following linear equation was developed:

$$\delta^{18}O = 0.443(S) - 15.55$$

The zero-salinity intercept of this line (-15.55‰) represents the freshwater end member present in deep Bedford Basin water. This zero-salinity intercept matches the Scotian Shelf end member established by *Fairbanks* (1982) (-15.55‰), illustrating the fact that this zero-salinity intercept is comparable to freshwater present on the Scotian Shelf. This freshwater end member is more isotopically depleted than the meteoric input entering Bedford Basin from land. Therefore, based on the location of these samples below the mixing line, it is evident that ∼35.2% (or more) of Bedford Basin samples over this study period are being influenced by freshwater entering from the Scotian Shelf, rather than freshwater inputs from land.

At 60 m depth, offshore water, carrying its own freshwater signature, introduces an additional freshwater end member to Bedford Basin not present in surface waters. Therefore, instead of using summer and winter precipitation as freshwater end members at 60 m depth, two more realistic end members would be "precipitation", an average of Halifax yearly precipitation, and "offshore freshwater", with a δ^{18}O of -15.55‰.

4.2.2.4 Examining the δ^{18}O-S Relationship

When fluctuations in δ^{18}O and salinity with time at 60 m depth are examined, there is a weak relationship between δ^{18}O and salinity (r^2 = 0.36) (Figure 4.23). To investigate this weak relationship further, and determine why there is a comparably stronger relationship between δ^{18}O and salinity in surface waters, the change in salinity and δ^{18}O with time was examined in both the deep and surface waters of Bedford Basin (Figure 4.23). When the relationship of δ^{18}O and salinity with time at 60 m depth is examined, it is evident that these two variables do not co-vary with time. Salinity at 60 m depth has periods of stability over time, while δ^{18}O is variable over the same periods (e.g. April - August 2013).

The stability of salinity at 60 m depth, compared with the variability in δ^{18}O, is a result of differences in the analytical precision of these measurements. The analytical precision associated with δ^{18}O measurements is 0.05‰ (cavity ring-down spectrometer) compared with 0.002 psu for salinity (salinometer) (Chapter 2). Bottom waters (60 m)

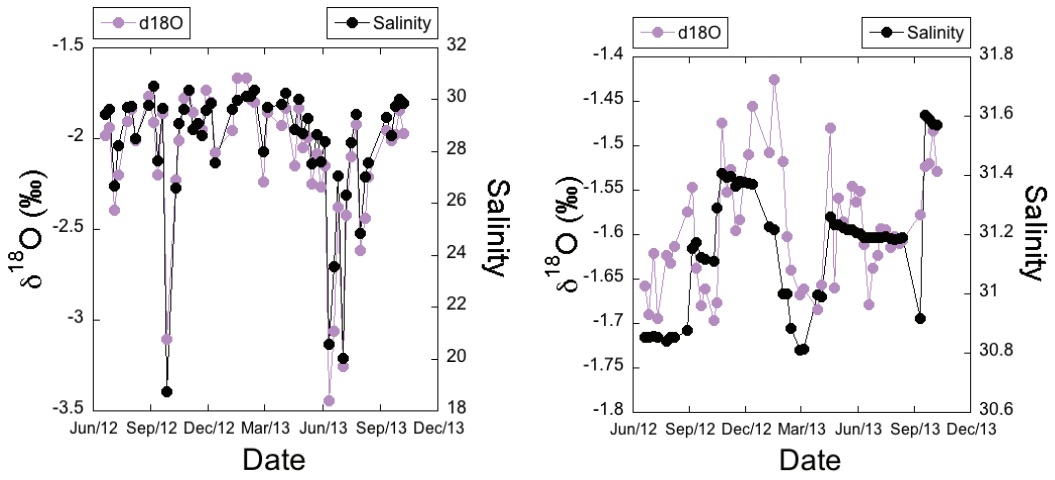

(a) 1 m (b) 60 m

Figure 4.23: Change in δ^{18}O (purple) and salinity (black) of (a) 1 m and (b) 60 m Bedford Basin water over the time of this study (June 2012 - October 2013).

in Bedford Basin are well-mixed, well-stratified and only occasionally renewed (*Shan and Sheng*, 2012). As such, these waters are stable, with a well-defined salinity and δ^{18}O until a vertical intrusion or mixing event takes place. The error associated with δ^{18}O measurements (0.05‰) leads to scatter in the δ^{18}O data, while the precision associated with the salinity measurements (0.002 psu) leads to stable and accurate salinity values recorded for water at 60 m depth. Therefore, any variance around the δ^{18}O-S regression line greater than the analytical error associated with δ^{18}O measurements (0.05‰) would suggest that there is an additional input of water, altering the δ^{18}O-S relationship.

To examine the variability in δ^{18}O around this regression line, δ^{18}O at 60 m was normalized to the δ^{18}O-S regression line (Figure 4.24), using the same method presented in Section 4.2.1.4 for 1 m samples. The predicted δ^{18}O is divided by the observed δ^{18}O to determine where samples are falling off this 1:1 line. Based on the analytical precision of δ^{18}O measurements, it is assumed that a calculated ratio between 1 and $\pm$ 0.05‰ would be associated with instrumental error; any error greater than this may indicate that there is an additional factor, such as an intrusion event, resulting in a deviation away from the regression line.

Dashed black lines establish the boundaries of the analytical precision ($\pm$ 0.05‰). In the fall of 2012, three samples fall outside of this analytical boundary, with observed δ^{18}O values greater than predicted (Figure 4.24). This variability may be associated with

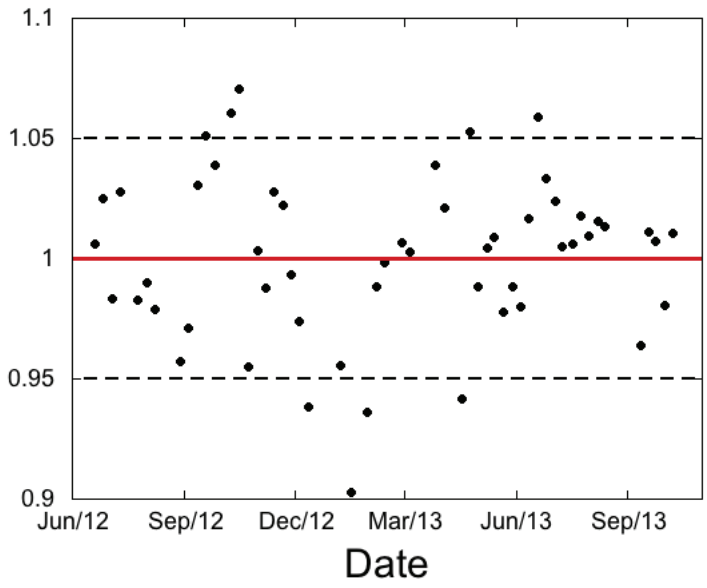

Figure 4.24: The ratio of observed δ^{18}O and δ^{18}O normalized to salinity, using the δ^{18}O-S relationship of Bedford Basin 60 m water, collected from June 2012 to October 2013.

increased vertical intrusion events and overturning occurring in the late fall, as discussed in *Shan et al.* (2011). Samples collected in December of 2012 and January of 2013 are also outside of this analytical boundary, with predicted δ^{18}O values greater than what is observed in deep Bedford Basin waters. Although some variability in δ^{18}O can be attributed to the analytical uncertainty associated with measurements, significant deviations ($>$0.05) away from the δ^{18}O-S relationship may be a result of intrusion events, introducing new water, with a different δ^{18}O-S relationship, to Bedford Basin.

4.2.2.5 Scotian Shelf Mass Balance

As discussed in Section 4.2.2.4, bottom waters are often stable with little variability in the δ^{18}O-S relationship; a vertical intrusion event in Bedford Basin allows deep, stable bottom waters to mix with the surface layer, resulting in a shift in the δ^{18}O-S relationship. These stable bottom waters are dominated by offshore water, with little to no input of freshwater from land. The mass balance equation developed for Bedford Basin (Section 4.2) will only work when deep waters are well-mixed and there is an input of freshwater (i.e. F_W and/or F_S) from the surface. When only Scotian Shelf water is contributing to the deep Bedford Basin layer, and there is no exchange with surface waters or inland freshwater inputs, a different mass balance equation must be considered.

A Scotian Shelf mass balance equation can be developed by assuming that this stable, deep Bedford Basin water is only composed of offshore water originating from the Scotian Shelf. By examining the end members present on the Scotian Shelf, classified by *Shadwick and Thomas* (2011), a mass balance calculation using St. Lawrence Estuary Water (SLEW), Warm Slope Water (WSW), and Labrador Shelf Water (LShW) can be used to determine the fraction of these three source waters present in Bedford Basin 60 m water (Equation 4.5). This assumes that no mixing of Bedford Basin 60 m water occurred between leaving the Scotian Shelf and entering Halifax Harbour (i.e. no inland freshwater inputs).

$$\begin{aligned} F_{SLEW} + F_{LShW} + F_{WSW} &= 1 \\ F_{SLEW}S_{SLEW} + F_{LShW}S_{LShW} + F_{WSW}S_{WSW} &= S_{BB} \\ F_{SLEW}X_{SLEW} + F_{LShW}X_{LShW} + F_{WSW}X_{WSW} &= X_{BB} \end{aligned} \tag{4.5}$$

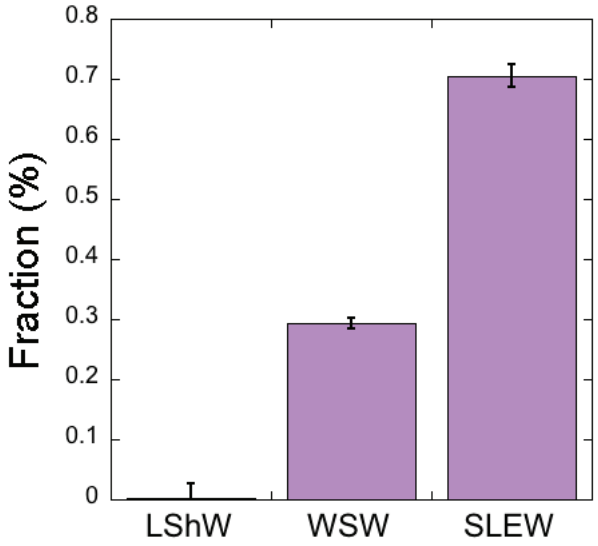

Figure 4.25: Bedford Basin 60 m total averaged mass fraction results (with 95% CI) for samples collected between June 2012 and October 2013, using Scotian Shelf end members (LShW, WSW, and SLEW). All mass fractions are significantly different from one another (p value <0.05) using a Tukey's All Pairs Comparison.

Using Equation 4.5, the mass fractions of Scotian Shelf source waters present in Bedford Basin 60 m water can be quantified. Based on this calculation, it was determined that the majority of Bedford Basin 60 m water is composed of SLEW and WSW, with little to

no input of LShW (Figure 4.25). However, like the mass fraction results using Bedford Basin end members, this does not take into account where these samples fall with respect to the Scotian Shelf end member mixing triangle. In addition, like the Bedford Basin mass balance calculation performed on 60 m water, a number of these mass fractions result in negative values. To examine where these Bedford Basin 60 m samples fall with respect to these two mixing triangles and why negative values are calculated, Figure 4.26 can be examined.

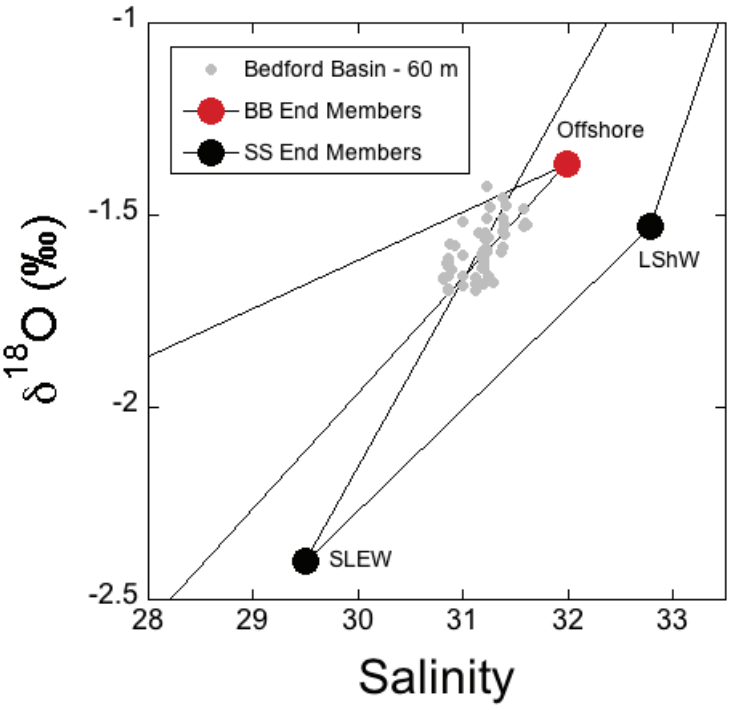

Figure 4.26: Bedford Basin 60 m δ^{18}O-S relationship and the fit of these samples with respect to the Bedford Basin (offshore, summer, and winter) and Scotian Shelf (SLEW, LShW, and WSW) mixing triangles. WSW, summer, and winter end members are located outside the boundaries of this plot.

With the exception of the one sample that falls above the Bedford Basin mixing triangle (collected on January 16, 2013), all of the Bedford Basin 60 m samples either fall into the Bedford Basin mixing triangle, the Scotian Shelf mixing triangle, or both (Figure 4.26). This supports the fact that the water in Bedford Basin is composed of water from these six different source waters, and emphasizes, with the shift in the mixing triangle, the change in water mass origin that occurs over different times of the year. Where these samples fall with respect to the end member mixing triangles may define the composition of Bedford

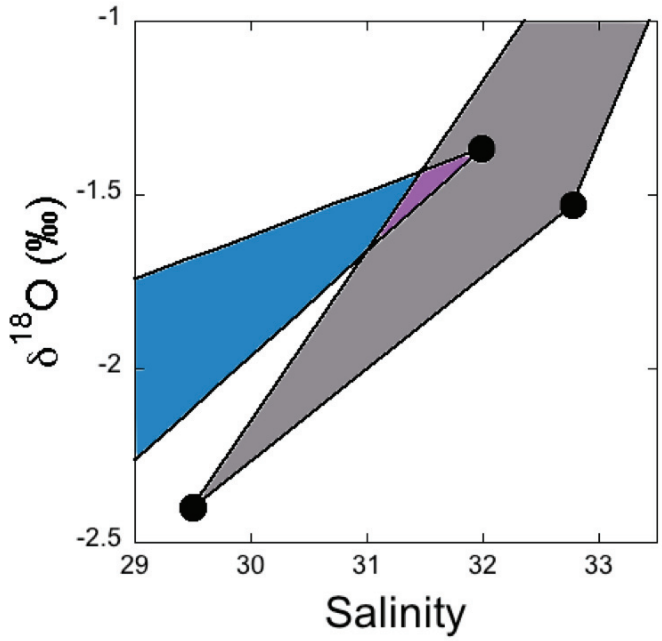

(a)

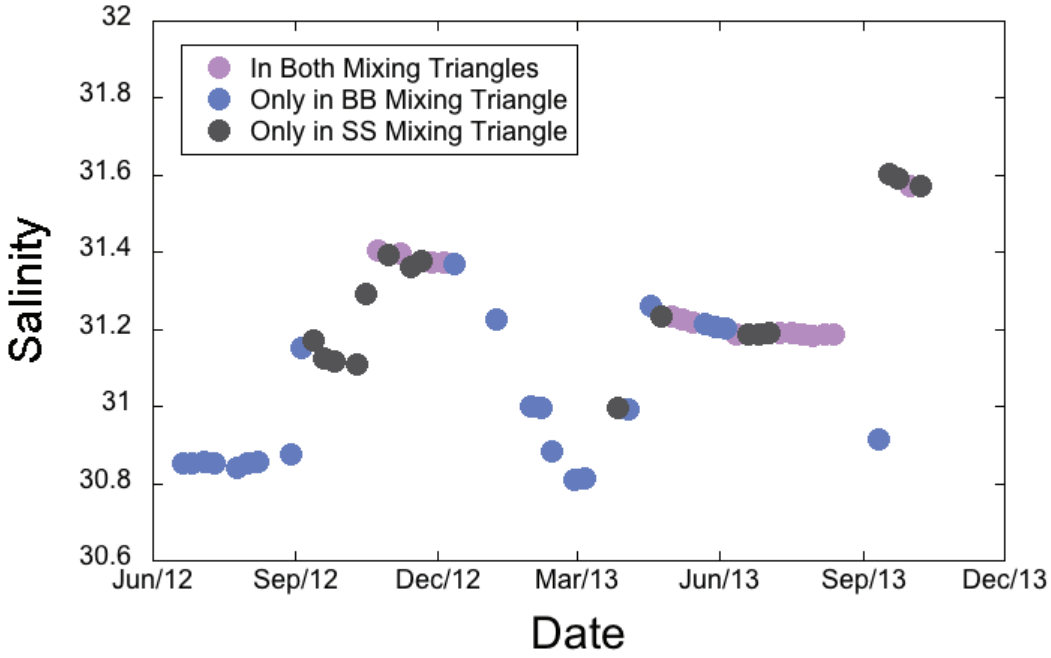

(b)

Figure 4.27: (a) Mixing triangles for Bedford Basin and Scotian Shelf grouped into three categories, (1) both mixing triangles (purple), (2) only in BB (blue), and (3) only in SS (gray), based on their positions in these mixing triangles. (b) Bedford Basin 60 m δ^{18}O and salinity measurements plotted against the time (June 2012 - October 2013) in this study, with data grouped into these categories.

Basin bottom water; water composed of only offshore inputs may be associated with the Scotian Shelf mixing triangle, while water with an introduction of freshwater from the surface following a flushing or vertical intrusion event may be found in the Bedford Basin mixing triangle.

To further determine whether a "shift" in these mixing triangles exists in Bedford Basin deep water, the 60 m samples were divided into three categories depending on whether these values fall: (1) in the Bedford Basin mixing triangle, (2) in the Scotian Shelf mixing triangle, or (3) in both mixing triangles. To look at these shifts, changes in salinity that correspond with changes in the position of samples in the mixing triangles can be used. In Figure 4.27 these three categories are separated into three colours to illustrate where Bedford Basin 60 m samples fall with respect to these two mixing triangles.

Based on Figure 4.27(b), samples that fall in the Bedford Basin mixing triangle (blue) seem to be associated with times of varying salinity, or before a change in salinity occurs. One exception to this can be seen in the summer of 2013, during a period of stability. Samples found in the Scotian Shelf mixing triangle (gray) and in both (purple), seem to be associated with more stable periods, emphasizing a dominant input of offshore water in deep Bedford Basin that is not mixing with freshwater inputs from land.

Therefore, the position of samples on these two mixing triangles and the variability in salinity may help to inform us as to whether Bedford Basin bottom waters are well-mixed, suggesting a vertical intrusion event, or stable, with a dominant input of offshore water. In periods of stable salinity, with no input of freshwater from land, it may be possible to look at the contribution of Scotian Shelf water within samples collected from Bedford Basin, providing us with additional insight into the composition of water on the Scotian Shelf, without leaving Halifax Harbour.

4.2.2.6 Summary

By performing linear regressions and mass balance analyses on Bedford Basin deep (60 m) water, we were able to (1) illustrate the dominance of offshore water, (2) establish a new freshwater end member, (3) identify changes to the δ^{18}O-S relationship, and (4) establish two mixing triangles for deep Bedford Basin.

Throughout the year, the input of offshore water to deep Bedford Basin dominates (Average: 97.4%) with very little freshwater inputs (summer or winter precipitation). The weak relationship between δ^{18}O and salinity in these deep waters leads to an uncertainty

in the zero-salinity intercepts calculated from this relationship. No seasonal zero-salinity intercepts can be considered due to this poor relationship, however the average δ^{18}O of freshwater at 60 m (-7.47‰) is comparable to the average δ^{18}O of freshwater determined at 1 m (-6.23‰). A new freshwater end member (-15.55‰), representative of offshore freshwater was determined, comparable to the Scotian Shelf freshwater end member established by *Fairbanks* (1982). The Scotian Shelf mixing triangle best fits 60 m data composed of only Scotian Shelf water with no introduction of freshwater from land; bottom waters associated with vertical intrusion events and the introduction of meteoric water from Halifax in comparison, fit into the Bedford Basin mixing triangle.

CHAPTER 5

CONCLUSIONS

Annual variability in the δ^{18}O-S relationship of Bedford Basin and its approaches (e.g. precipitation, offshore water, Sackville River, etc.) has been examined for the first time in this North Atlantic estuary. The use of a Picarro L2301-i isotopic water analyzer has allowed for the first detailed study of annual δ^{18}O variability in Halifax Harbour. A number of major conclusions can be drawn.

The main freshwater inputs to Bedford Basin were defined as Sackville River, precipitation, and wastewater. However, these three inputs were not found to be isotopically (δ^{18}O) distinct from one another and therefore cannot be defined as separate end members to Bedford Basin, as all freshwater inputs co-vary throughout the year. Due to considerable variability in the δ^{18}O of precipitation between seasons (winter: -10.37‰; summer: -5.39‰), winter and summer precipitation were separated and used as the two freshwater end members to Bedford Basin. An offshore end member, representative of water entering Halifax Harbour, was selected with the use of AZMP Halifax Line data (October 2008 & April 2009). This offshore end member, which represents a more saline and isotopically depleted input compared with Bedford Basin 60 m water, was selected using past literature on water circulation, while noting the uncertainty in mass balance results based on this selection.

Mass balance calculations were performed on Bedford Basin surface (1 m) and deep (60 m) water samples, collected from June 2012 to October 2013. Surface samples confirm a dominant input of offshore water (average: 88.4%), and minimal freshwater inputs. Summer precipitation dominates throughout the year (6.9%) compared with winter precipitation (4.7%), as this end member only represents a small amount of strongly

isotopically depleted (-δ^{18}O) precipitation occurring over a few months (December - March). The lack of strongly isotopically depleted precipitation in Bedford Basin surface waters may be due in part to the input of snow and increases in δ^{18}O associated with sublimation within a snowpack. This may lead to a freshwater input entering Bedford Basin that differs isotopically from the value recorded during the original precipitation event. The zero-salinity intercept calculated for all Bedford Basin surface waters (-6.23‰, 95% CI: 0.34), is comparable to the average amount-weighted δ^{18}O of precipitation measured in Halifax (-6.68‰, 95% CI: 0.74), indicating that this input is influencing the freshwater composition of surface waters. Seasonality of δ^{18}O in surface waters exists but it seems to be related to saltwater intrusion events rather than seasonal variability in precipitation.

Deep water samples indicate little input of freshwater from onshore, with the majority of this water originating from offshore (ranging from $\sim$96 to 99% over this study). A more dominant input of winter precipitation is present in bottom waters when compared to summer precipitation, with averages of 2.1 and 0.4% respectively. The zero-salinity intercept calculated using the offshore end member and the sample that falls the furthest below the winter precipitation-offshore mixing line establishes a new freshwater end member in stable bottom waters, representing the δ^{18}O of offshore freshwater. This offshore freshwater end member ($\sim$ -15.55‰) is directly comparable to the Scotian Shelf freshwater end member established by *Fairbanks* (1982), -15.55‰. The zero-salinity intercept calculated for all Bedford Basin 60 m samples (-7.47‰) was comparable to the zero-salinity input calculated for 1 m and the δ^{18}O of precipitation in Halifax. However, the weak relationship between δ^{18}O and salinity at depth means that no seasonal zero-salinity intercepts could be considered. When intrusion events occur between the deep and surface layers, a mass balance calculation using the "Bedford Basin" end members will best fit this relationship at 60 m depth, while bottom waters composed entirely of offshore water, fit into a "Scotian Shelf" mixing triangle.

Through this study, the δ^{18}O and salinity of Bedford Basin and its approaches have been quantified for the first time. This allows us to use these data in additional studies, comparing the results to past (and future) studies of Bedford Basin water mixing and for comparison with future model analyses. In addition, it provides us with "baseline" measurements of δ^{18}O, beneficial as changes to the freshwater balance of the North Atlantic (with increased

ice-melt, river run-off, or sea-level rise) may alter the freshwater composition and δ^{18}O of these inputs. By identifying the current composition of these inputs, and illustrating the dominant presence of offshore (Scotian Shelf) water to Bedford Basin, it is possible to identify how changes to the freshwater balance of the North Atlantic may impact the water composition of this coastal estuary in the future.

BIBLIOGRAPHY

AMEC Earth and Environmental, Halifax Harbour water quality monitoring program final summary report, *Tech. rep.*, Dartmouth, Nova Scotia, Canada, 2011.

Bass, A. M., N. C. Munksgaard, D. OGrady, M. J. Williams, H. C. Bostock, S. R. Rintoul, and M. I. Bird, Continuous shipboard measurements of oceanic δ^{18}O, δD and $\delta^{18}C_{DIC}$ along a transect from New Zealand to Antarctica using cavity ring-down isotope spectrometry, *Journal of Marine Systems*, *137*, 21–27, 2014.

Bedard, P., C. Hillaire-Marcel, and P. Pagé, ^{18}O modelling of freshwater inputs in Baffin Bay and Canadian Arctic coastal waters, 1981.

Bigg, G. R., and E. J. Rohling, An oxygen isotope data set for marine waters, *Journal of Geophysical Research*, *104(C4)*, 8527–8535, 2000.

Blasch, K. W., and J. R. Bryson, Distinguishing sources of ground water recharge by using δ^2H and δ^{18}O, *Groundwater*, *45*, 294–308, 2007.

Brand, W. A., and T. B. Coplen, Stable isotope deltas: tiny, yet robust signatures in nature, *Isotopes in environmental and health studies*, *48*, 393–409, 2012.

Buckley, D., Historical perspective of metal contamination in Halifax Harbour, in *Preserving the Environment of Halifax Harbour Workshop # 2*, edited by A. Ducharme and G. Turner, pp. 18 – 25, 2001.

Buckley, D. E., and G. V. Winters, Geochemical characteristics of contaminated surficial sediments in Halifax Harbour: impact of waste discharge, *Canadian Journal of Earth Sciences*, *29*, 2617–2639, 1992.

Buckley, D. E., J. N. Smith, and G. V. Winters, Accumulation of contaminant metals in marine sediments of Halifax Harbour, Nova Scotia: environmental factors and historical trends, *Applied Geochemistry*, *10*, 175–195, 1995.

Burt, W., H. Thomas, K. Fennel, and E. Horne, Sediment-water column fluxes of carbon, oxygen and nutrients in Bedford Basin, Nova Scotia, inferred from 224 ra measurements, *Biogeosciences*, *10*, 53–66, 2013.

Cappa, C. D., M. B. Hendricks, D. J. DePaolo, and R. C. Cohen, Isotopic fractionation of water during evaporation, *Journal of Geophysical Research*, *108*, 4525, 2003.

Clark, I., and P. Fritz, *Environmental Isotopes in Hydrology*, first ed., Lewis Publishers, 1997.

Cooper, L. W., *Isotopic fractionation in snow cover*, Elsevier: Amsterdam, 1998.

Coplen, T. B., New guidelines for reporting stable hydrogen, carbon, and oxygen isotope-ratio data, *Geochimica et Cosmochimica Acta*, *60*, 3359–3360, 1996.

Corlis, N. J., H. Herbert Veeh, J. C. Dighton, and A. L. Herczeg, Mixing and evaporation processes in an inverse estuary inferred from δ^2H and δ^{18}O, *Continental shelf research*, *23*, 835–846, 2003.

Craig, H., Isotopic variations in meteoric waters, *Science*, *133*, 1702–1703, 1961.

Craig, H., and L. I. Gordon, Deuterium and oxygen 18 variations in the ocean and the marine atmosphere, in *Stable Isotopes in Oceanographic Studies and Paleotemperatures*, edited by E. Tongiorgi, pp. 9–130, Consiglio nazionale delle ricerche, 1965.

Craig, H., L. I. Gordon, and Y. Horibe, Isotopic exchange effects in the evaporation of water, *Journal of Geophysical Research*, *68*, 5079–5087, 1963.

Curry, R., B. Dickson, and I. Yashayaev, A change in the freshwater balance of the Atlantic Ocean over the past four decades, *Nature*, *426*, 826–829, 2003.

Dansgaard, W., Stable isotopes in precipitation, *Tellus XVI*, *4*, 436–468, 1964.

Environment Canada, Sackville River at Bedford [NS], http://www.wateroffice.ec.gc.ca, 2013, online; accessed on July 12, 2013.

Epstein, S., and T. Mayeda, Variation of O^{18} content of waters from natural sources, *Geochimica et Cosmochimica Acta*, *4*, 213–224, 1953.

Fader, G. B. J., and D. E. Buckley, Environmental geology of Halifax Harbour, *Geoscience Canada*, *22(4)*, 152–171, 1995.

Fader, G. B. J., and R. O. Miller, Surface geology, Halifax Harbour, Nova Scotia, *Geological Survey of Canada*, *Bulletin 590*, 1–177, 2008.

Fairbanks, R. G., The origin of continental shelf and slope water in the New York Bight and Gulf of Maine: Evidence from $H_2^{18}O/H_2^{16}O$ ratio measurements, *Journal of Geophysical Research*, *87(C8)*, 5796–5808, 1982.

Fournier, R. O., Final report of the Halifax Harbour task force, *Tech. rep.*, 1990.

Frew, R. D., P. F. Dennis, K. J. Heywood, M. P. Meredith, and S. M. Boswell, The oxygen isotope composition of water masses in the northern North Atlantic, *Deep-Sea Research I*, *47*, 2265–2286, 2000.

Fritz, P., R. J. Drimmie, S. K. Frape, and K. O'Shea, The isotopic composition of precipitation and groundwater in Canada, in *Isotope Techniques in Water Resources Development*, pp. 539–551, IAEA, 1987.

Gardner Pinfold Consulting Economists Ltd., Economic potential of HRM and Halifax Harbour, *Tech. rep.*, Halifax Regional Municipality, 2004.

Gat, J. R., Oxygen and hydrogen isotopes in the hydrologic cycle, *Annual Review of Earth and Planetary Sciences*, *24*, 225–262, 1996.

Gat, J. R., *Isotope Hydrology: A Study of the Water Cycle*, Imperial College Press, London, 2010.

Gearing, J. N., D. E. Buckley, and J. N. Smith, Hydrocarbon and metal contents in a sediment core from Halifax Harbour: a chronology of contamination, *Canadian Journal of Fisheries and Aquatic Sciences*, *48*, 2344–2354, 1991.

Government of Canada - Climate, Canadian climate normals 1981 - 2010: Halifax Citadel, http://climate.weather.gc.ca/climate_normals/results_1981_2010_e.html?stnID=6357&lang=e&StationName=halifax&SearchType=Contains&stnNameSubmit=go&dCode=0, 2014, online; accessed on April 11, 2014.

Government of Canada - Climate, Daily data report for October 2014: Halifax International Airpoit, http://climate.weather.gc.ca/climateData/dailydata_e.html?timeframe=2&Prov=NS&StationID=50620&dlyRange=2012-09-10|2014-10-23&Year=2014&Month=10&Day=01, 2014, online; accessed on October 24, 2014.

Gregory, D., B. Petrie, F. Jordan, and P. Langille, Oceanographic, geographic, and hydrological parameters of Scotia-Fundy and Southern Gulf of St. Lawrence inlets, *Tech. rep.*, Bedford Institute of Oceanography, 1993.

Gupta, P., D. Noone, J. Galewsky, C. Sweeney, and B. H. Vaughn, Demonstration of high-precision continuous measurements of water vapor isotopologues in laboratory and remote field deployments using wavelength-scanned cavity ring-down spectroscopy (WS-CRDS) technology, *Rapid communications in mass spectrometry*, *23*, 2534–2542, 2009.

Halifax Regional Municipality, Regional planning - Halifax Regional Municipality: Summary of research, *Tech. rep.*, 2004.

Halifax Water, Halifax water 16th annual report, *Tech. rep.*, Halifax Water, 2012.

Hoefs, J., *Stable isotope geochemistry*, Springer, 1997.

Huntsman, A. G., Circulation and pollution of water near and around Halifax Harbour, *Contributions to Canadian Biology and Fisheries*, *2*, 71–81, 1924.

Jouzel, J., and L. Merlivat, Deuterium and oxygen 18 in precipitation: Modeling of the isotopic effects during snow formation, *Journal of Geophysical Research: Atmospheres (1984–2012)*, *89*, 11749–11757, 1984.

Jupia Consultants Ltd., Halifax: Becoming a shipbuilding centre of excellence, *Tech. rep.*, The Greater Halifax Partnership, 2011.

Karim, A., and J. Veizer, Water balance of the Indus River Basin and moisture source in the Karakoram and western Himalayas: Implications from hydrogen and oxygen isotopes in river water, *Journal of Geophysical Research: Atmospheres (1984–2012)*, *107*, ACH–9, 2002.

Kendall, C., and J. J. MacDonnell, *Isotope tracers in catchment hydrology*, Access Online via Elsevier, 1998.

Khatiwala, S. P., R. G. Fairbanks, and R. W. Houghton, Freshwater sources to the coastal ocean off northeastern North America: Evidence from $H_2{}^{18}O/H_2{}^{16}O$, *Journal of Geophysical Research*, *104(C8)*, 18241–18255, 1999.

Loder, J. W., G. Han, C. G. Hannah, D. A. Greenberg, and P. C. Smith, Hydrography and baroclinic circulation in the Scotian Shelf region: Winter versus summer, *Canadian Journal of Fisheries and Aquatic Sciences*, *54*, 40–56, 1997.

MacLachlan, S. E., F. R. Cottier, W. E. Austin, and J. A. Howe, The salinity: δ18O water relationship in Kongsfjorden, western Spitsbergen, *Polar Research*, *26*, 160–167, 2007.

Manabe, S., and R. J. Stouffer, Simulation of abrupt climate change induced by freshwater input to the North Atlantic Ocean, *Nature*, *378*, 165–167, 1995.

Martin, J. M., and R. Letolle, Oxygen 18 in estuaries, *Nature*, *282*, 292 – 294, 1979.

Masson-Delmotte, V., S. Hou, A. Ekaykin, J. Jouzel, A. Aristarain, R. Bernardo, D. Bromwich, O. Cattani, M. Delmotte, S. Falourd, et al., A review of Antarctic surface snow isotopic composition: Observations, atmospheric circulation, and isotopic modeling, *Journal of Climate*, *21*, 3359–3387, 2008.

Merlivat, L., and J. Jouzel, Global climatic interpretation of the deuterium-oxygen 18 relationship for precipitation, *Journal of Geophysical Research: Oceans (1978–2012)*, *84*, 5029–5033, 1979.

Mook, W. G., The oxygen-18 content of rivers, *SCOPE*, *52*, 565 – 570, 1982.

Morgan, V. I., Antarctic ice sheet surface oxygen isotope values, *Journal of Glaciology*, *28*, 315 – 323, 1982.

Motoyama, H., N. Hirasawa, K. Satow, and O. Watanabe, Seasonal variations in oxygen isotope ratios of daily collected precipitation and wind drift samples and in the final snow cover at Dome Fuji Station, Antarctica, *Journal of Geophysical Research: Atmospheres (1984–2012)*, *110*, 2005.

Munksgaard, N., C. Wurster, A. Bass, I. Zagorskis, and M. Bird, First continuous shipboard δ18O and δD measurements in sea water by diffusion sampling cavity ring-down spectrometry, *Environmental Chemistry Letters*, *10*, 301–307, 2012.

Munksgaard, N. C., C. M. Wurster, and M. I. Bird, Continuous analysis of δ18O and δD values of water by diffusion sampling cavity ring-down spectrometry: a novel sampling device for unattended field monitoring of precipitation, ground and surface waters, *Rapid Communications in Mass Spectrometry*, *25*, 3706–3712, 2011.

Nicholls, H. B., Investigations of marine environmental water quality in Halifax Harbour, *Tech. rep.*, Canadian Technical Report of Fisheries and Aquatic Sciences No. 1693, 1989.

Östlund, H. G., and G. Hut, Arctic Ocean water mass balance from isotope data, *Journal of Geophysical Research*, *89(C4)*, 6373–6381, 1984.

OKeefe, A., and D. A. Deacon, Cavity ring-down optical spectrometer for absorption measurements using pulsed laser sources, *Review of Scientific Instruments*, *59*, 2544–2551, 1988.

Peng, H., B. Mayer, S. Harris, and H. R. Krouse, A 10-yr record of stable isotope ratios of hydrogen and oxygen in precipitation at Calgary, Alberta, Canada, *Tellus*, *56B*, 147–159, 2004.

Picarro, Cavity ring-down spectroscopy (CRDS), http://www.picarro.com/technology/cavity_ring_down_spectroscopy, 2014, online; accessed on January 28, 2015.

Pilsen, M. E. Q., *An Introduction to the Chemistry of the Sea*, Prentice-Hall Inc., 1998.

Punshon, S., and R. M. Moore, Nitrous oxide production and consumption in a eutrophic coastal embayment, *Marine chemistry*, *91*, 37–51, 2004.

Rozanski, K., L. Araguàs-Araguàs, and R. Gonfiantini, Isotopic patterns in modern global precipitation, in *Climate Change in Continental Isotopic Records*, edited by P. K. Swart, K. C. Lohmann, J. McKenzie, and S. Savin, pp. 1–36, American Geophysical Union, 1993.

Shadwick, E., and H. Thomas, Carbon dioxide in the coastal ocean: a case study in the Scotian Shelf region, *Ocean Year Book*, *25*, 171–204, 2011.

Shan, S., Numerical study of three-dimensional circulation and hydrography in Halifax Harbour using a nested-grid ocean circulation model, Master's thesis, Dalhousie University, Halifax, Nova Scotia, 2010.

Shan, S., and J. Sheng, Examination of circulation, flushing time and dispersion in Halifax Harbour of Nova Scotia, *Water Quality Research Journal of Canada*, *47*, 353–374, 2012.

Shan, S., J. Sheng, K. R. Thompson, and D. A. Greenberg, Simulating the three-dimensional circulation and hydrography of Halifax Harbour using a multi-nested coastal ocean circulation model, *Ocean Dynamics*, *61*, 951–976, 2011.

Stalker, J. C., R. M. Price, and P. K. Swart, Determining spatial and temporal inputs of freshwater, including submarine groundwater discharge, to a subtropical estuary using geochemical tracers, Biscayne Bay, South Florida, *Estuaries and coasts*, *32*, 694–708, 2009.

Tan, F., and P. Strain, The distribution of sea ice meltwater in the eastern Canadian Arctic, *Journal of Geophysical Research: Oceans (1978–2012)*, *85*, 1925–1932, 1980.

Taylor, S., X. Feng, J. W. Kirchner, R. Osterhuber, B. Klaue, and C. E. Renshaw, Isotopic evolution of a seasonal snowpack and its melt, *Water Resources Research*, *37*, 759–769, 2001.

University of Colorado: Institute of Arctic and Alpine Research, Stable isotope lab - O: Liquid water and ice, http://instaar.colorado.edu/sil/analyses/analysis_detail.php?analysis_ID=5, 2005, online; accessed on October 27, 2014.

Urey, H. C., The thermodynamic properties of isotopic substances, *Journal of the Chemical Society (Resumed)*, pp. 562 – 581, 1947.

Visser, J., Halifax wins $25 billion shipbuilding contract, http://www.ctvnews.ca/halifax-wins-25-billion-shipbuilding-contract-1.713515, 2011, online; accessed on October 23, 2014.

Walker, S. A., K. Azetsu-Scott, C. Normandeau, E. Kerrigan, J. McKay, R. Friedrich, S. E. Craig, B. Newman, and D. W. R. Wallace, Oxygen isotope measurements in natural seawater using cavity ring-down spectroscopy (CRDS), in prep.

Zhou, S., M. Nakawo, S. Hashimoto, and A. Sakai, The effect of refreezing on the isotopic composition of melting snowpack, *Hydrological processes*, *22*, 873–882, 2008.